Behaviour of compacted bentonite at elevated temperatures

Panagiotis Stratos

Geoenvironmental Research Centre

Cardiff School of Engineering

Cardiff University

Thesis submitted in candidature for the degree of Doctor of Philosophy at Cardiff University

March 2017

ACKNOWLEDGEMENTS

I would like to sincerely thank my supervisors Professor Hywel Rhys Thomas and Dr Snehasis Tripathy for their continuous support, guidance and motivation throughout this research. I am also extremely grateful to the Radioactive Waste Management (former Nuclear Decommissioning Authority) and Engineering and Physical Sciences Research Council for their financial support without which this work would not have been possible.

I would like to thank Dr. Sivachidambaram Sadasivam for his invaluable help with my chemical and mineralogical tests. I would also like to thank the technical staff of the School of Engineering, in particular Harry, Steph, Ian without for their enormous support during my experimental work.

I would like to thank my GRC colleagues, including Alex, Sanjana, Jamie, Lee, Manju, Jack, Irfan, Renato and Alejandro for their continuous support and encouragement during this work.

This work wouldn't be completed without the continuous support of my friends. At first I would like to thank my "family" in Cardiff - Nadine, George, Iliana, Peri, Christina for always being there for me. Also I would like to thank Claire and Shakil for their encouragement during this work. Then I would also like to thank Manos Katerina, George, Kostas, Kuriakos, Koula, Aris, Vasilis, Eleni, Socrates, Nikos, Efthymia, Marko and Giorgis for their support and good thoughts. I would like to thank Andriana for supporting me in one of the most difficult periods of my life.

I would like to express my gratitude to my friend and flatmate Amalia for her continuous support, motivation and patience that she exhibited during my write up period.

I would like to thank my "brothers" from Nafpaktos, Dimitris, Lampros, Thanos, Antreas, Giorgos, Vasilis and Christos for their friendship all these years.

Last but not least I want to thank my family for their support. My father Panagiotis for always advising me and pushing me to get better, my mother Ioanna who was always there for me sending me her positive energy, my sister Afroditi for always caring and thinking of me and all the rest of my family who supported me with all of their strengths and made me feel special from day one.

I would like to dedicate this work to my parents for their sacrifices all these years and my baby nephew/godson Nasos to whom I wish to surpass me one day.

DECLARATION

This work has not been submitted in substance for any other degree or award at this or any other university or place of learning, nor is being submitted concurrently in candidature for any degree or other award.

Signed …… (candidate) Date …31/03/2017……

STATEMENT 1

This thesis is being submitted in partial fulfillment of the requirements for the degree of ……(insert MCh, MD, MPhil, PhD etc, as appropriate)

Signed …… (candidate) Date …31/03/2017……

STATEMENT 2

This thesis is the result of my own independent work/investigation, except where otherwise stated, and the thesis has not been edited by a third party beyond what is permitted by Cardiff University's Policy on the Use of Third Party Editors by Research Degree Students. Other sources are acknowledged by explicit references. The views expressed are my own.

Signed …… (candidate) Date …31/03/2017……

STATEMENT 3

I hereby give consent for my thesis, if accepted, to be available online in the University's Open Access repository and for inter-library loan, and for the title and summary to be made available to outside organisations.

Signed …… (candidate) Date …31/03/2017……

STATEMENT 4: PREVIOUSLY APPROVED BAR ON ACCESS

I hereby give consent for my thesis, if accepted, to be available online in the University's Open Access repository and for inter-library loans **after expiry of a bar on access previously approved by the Academic Standards & Quality Committee.**

Signed …… (candidate) Date …31/03/2017……

ABSTRACT

Compacted bentonites are proposed to be used as the barrier and backfilling materials in underground disposal of high-level nuclear waste. The in-situ boundary conditions in this case dictate exposure of compacted unsaturated bentonites to elevated temperature from the waste containers and hydration upon fluid uptake from the surrounding host rock.

In the past, small- and medium-scale laboratory tests and in situ tests in prototype repositories have been considered by several research organizations. Most of the earlier studies have focussed in studying the thermo-hydraulic-mechanical-chemical behaviour of compacted bentonites when subjected to temperatures below 100 °C.

In this thesis laboratory test results of several non-isothermal and non-isothermal hydraulic tests on compacted MX80 bentonite are presented. Compacted bentonite specimens were subjected to temperatures of either 85 or 150 °C at one end, whereas the temperature at the opposite end was maintained at 25 °C. A hydraulic pressure of 600 kPa was applied during the non-isothermal hydraulic tests. The temperature and the relative humidity were monitored along predetermined depths of the specimens. The axial stress was monitored at the opposite end of the high temperature source. The influences of thermal and thermo-hydraulic gradients on the water content, volume-mass properties, suction, chemical composition and mineralogy were studied in detail.

The test results showed that thermal gradients caused redistribution of water content (soil suction), whereas thermo-hydraulic gradients caused both redistribution and an increase in the water content within compacted bentonites, leading to development of axial stresses at the opposite end of the heat source. An increase in the water content and degree of saturation towards the opposite end of heat source indicated development of a low permeability zone at the interface between the restraint and unsaturated bentonites. Under the applied thermal and thermo-hydraulic gradients, the dry density increased near the high temperature source end, whereas it decreased at the opposite end. A variation in the dry density is attributed to the combined influence of shrinkage of bentonite at and near the heat source, relaxation of confinement at the opposite end of heat source and macro and micro structural changes within compacted bentonites. Mineralogical transformation (montmorillonite to illite) did not occur under the applications of both thermal and thermo-hydraulic gradients. A variation of the water content however caused shifting of c-axis spacing indicating hydration and dehydration of elementary layers of montmorillonite.

TABLE OF CONTENTS

LIST OF TABLES

LIST OF FIGURES

CHAPTER 1.
INTRODUCTION

1.1 Introduction

The safe disposal of radioactive wastes requires a well-planned long term solution. The isolation and the secure packing of the waste canister is very important to avoid any ecological disasters. Thomas et al. (1998) stated that the geoengineered barriers can be used in the safe disposal of high level radioactive wastes. The deep geological repositories have been considered as the most suitable method for the high level disposal high-level waste. The underground repositories are designed as a tunnel system located at a minimum depth of 500 m below the surface (Pusch, 1982). The nuclear waste canisters will be placed in deposition holes at regular intervals along the tunnel network (Bucher and Müller-Vonmoos, 1989).

The engineered barriers system will be used to encapsulate the nuclear waste canisters. The engineered barriers are fabricated by highly compacted swelling clays (Sun et al., 2009). According to Villar and Lloret (2007) the bentonite is an ideal clay to serve as the buffer and backfill materials in the engineered barrier system due to its low permeability, high swelling and retention capacities. With this attributes compacted bentonite would manage to hold the waste canisters structurally in place by preventing any possible collapse of the excavation and also will ensure the water tightness of the system by retaining the water coming from the saturated host rock away from the canister (Tripathy et al., 2004).

During the operational period of the deep geological repository, compacted bentonites are expected to experience thermal and hydraulic loadings. The section of the bentonite in contact with the waste canister will be subjected to elevated temperatures due to the thermal dissipation of the nuclear waste, whereas the section in contact with the host rock will be subjected to hydraulic loading due to the water infiltration from the saturated host rock. Pusch et al. (2010) stated that for temperatures above the 100 °C the smectite minerals may get transformed to illite. Thus, a majority of the deep geological concept avoid the direct disposal of the nuclear waste and adopt a period of cooling down prior the final disposal. A better understanding of the long term behaviour of the compacted bentonites as the barrier and backfilling materials is essential for efficient design of the deep geological repository.

The thermal and hydraulic loadings applied on the bentonite buffer can cause the localised shrinkage / swelling of the material. Also, the applied gradients would cause changes in the temperature, water content, dry density, suction and anion concentrations with elapsed time along the full length of the buffer. Several studies in

the past have focused on testing of compacted bentonites under potential deep geological repository conditions (application of thermal and hydraulic gradients) in laboratory scale experiments (Martın et al., 2000; Samper et al., 2000; Börgesson et al., 2001; Cuevas et al., 2002; Pintado et al., 2002; Gatabin and Billaud, 2005; Villar et al., 2005; Singh, 2007; Mishra et al., 2008; Villar et al., 2008; Åkesson et al., 2009; Fernández and Villar, 2010; Gómez-Espina and Villar, 2010; R Bag, 2010; Cleall et al., 2011; Schanz et al., 2013; Gómez-Espina and Villar, 2015; Tripathy et al., 2015).

A very limited number of tests were conducted for temperatures above the 100 °C (Gatabin and Billaud, 2005; Åkesson et al., 2009; Gómez-Espina and Villar, 2010; Gómez-Espina and Villar, 2015). The studies concerning the behaviour of compacted bentonites when it is subjected solely to thermal loading is scarce in literature (Singh, 2007; Åkesson et al., 2009; Bag, 2011). The potential changes in the mineralogy of the compacted bentonite due to the thermal and hydraulic gradients is scarce in the literature (Gómez-Espina and Villar, 2010; Dohrmann and Kaufhold, 2014; Gómez-Espina and Villar, 2015).

1.2 Scope and objectives of the research

According to Wersin et al. (2007) allowing disposal of high-level waste at temperatures above the 100 °C while still maintaining the performance of the engineered barrier system is economically highly beneficial. Further reasearch is also needed to explore the uncertainties that surrounds the effectes of temperatures up to 150 °C on phase transformation from smectite to illite and the associated processes.

This work is a part of the Systems Approach For Engineered Barrieres (SAFE Barriers) project, which is a multidisciplinary research into the thermo-hydro-mechanical-chemical (THMC) evolution of Engineered Barrier Systems (EBS) under the full range of environmental conditions (Fig. 1.1).

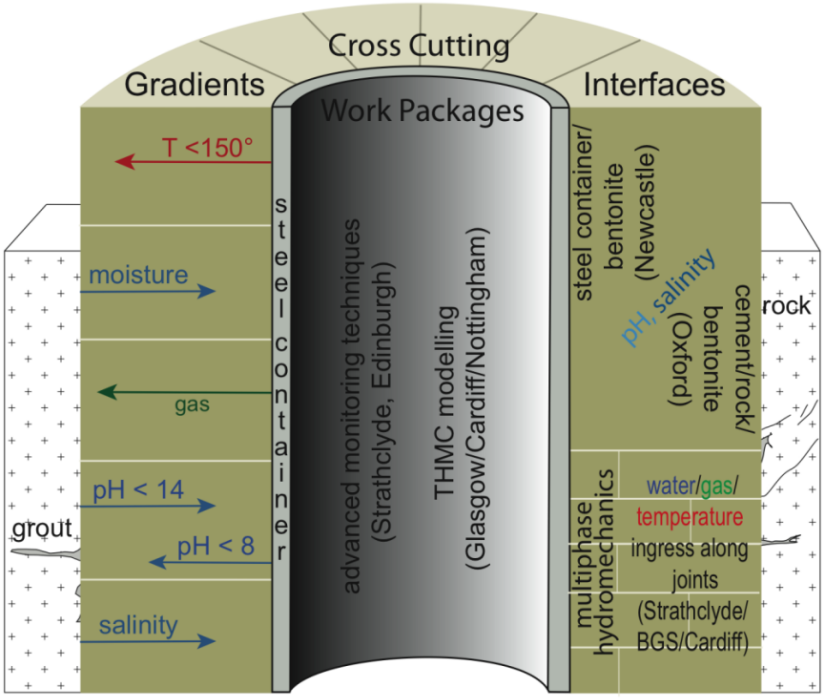

Figure 1.1 Operational structure of the SAFE Barriers project

This research focuses on the thermo-hydro-mechanical, chemical and mineralogical behaviour of compacted MX80 bentonites acting as a host for the nuclear waste canister. The main objectives of this research were to study the following aspects:

1) To design and fabricate a testing device which will be capable of applying temperatures up to 200 °C and high fluid injection pressures on compacted bentonites while facilitating measurement of changes in the temperature,

relative humidity and axial stress, and to study the thermo-hydraulic response of compacted bentonites using the device.

2) To investigate the influence of thermal and thermo-hydraulic gradients on the hydro-mechanical behaviour of compacted bentonites for a temperature of 85 °C.
3) To investigate the influence of thermal and thermo-hydraulic gradients on the changes in the cations concentrations along the full length of compacted bentonite specimens for applied temperatures of 85 and 150 °C.
4) To investigate the influence of thermal and thermo-hydraulic gradients on the mineralogy along the full length of compacted bentonite specimens for applied temperatures of 85 and 150 °C.
5) To investigate the influence of thermal and thermo-hydraulic gradients on the development of axial stress from the compacted bentonite for temperatures above the 100 ℃.
6) To investigate the influence of thermal and thermo-hydraulic gradients on the cations concentrations along the full length of the compacted bentonite specimen for temperature above the 100 ℃.

Experimental studies concerning the concentrations of anions and the usage of numerical model to assess the thermo-hydro-mechanical and chemical behaviour of compacted bentonites are beyond the scope of this study.

1.3 Thesis outline

The thesis is divided into seven consecutive chapters.

Chapter 1 presents the background of the research, the main objectives of this research and outline of the thesis.

Chapter 2 presents a review of literature related to this study. The structure of the montmorillonite and the micro-structure of compacted bentonites are presented. The mechanisms governing the swelling in compacted bentonites and the effects of thermo-hydraulic gradients and solute transports are discussed. A detailed review on previous studies on the thermo-hydro-mechanical-chemical behaviour are reviewed. The mechanisms governing the heat water and solute transport are presented along with various devices used in the past to carry out non-isothermal tests.

Chapter 3 presents the physical and chemical properties of the MX80 bentonite used in this study. The testing devices used, their components are presented. The procedure adopted for preparing compacted specimens, testing methods, verification of the functionalities of the device accessories, the types of tests performed, and the procedure adopted for extracting specimens from the specimen mould after completion of the tests are presented. The post-mortem analyses (mineralogical and chemical tests) that were carried out on the extracted specimens are described.

Chapter 4 presents the influence of the thermal gradients on the variation of temperature, relative humidity and axial stress in compacted bentonite specimens. The experimental program that followed is presented. The temperature, relative humidity variations measured at predetermined levels along the length of the bentonite

specimens, the monitored axial stress generated at the opposite end of the heat source and the profiles of the water content, dry density, degree of saturation and suction after termination of the thermal tests are presented. The temperatures used were 25 °C at the top of the specimens and either 85 or 150 °C at the bottom of the specimens.

Chapter 5 presents the influence of the thermo-hydraulic gradients on the variations of the temperature, relative humidity and axial stress in compacted bentonite specimens. The experimental program that was followed is stated. The temperature, relative humidity variations measured at predetermined levels along the length of the bentonite specimens, the monitored axial stress generated at the opposite end of the heat source and the profiles of the water content, dry density, degree of saturation and suction after termination of the thermo-hydraulic tests are presented. The temperatures used were 25 °C at the bottom of the specimens and either 85 or 150 °C at the bottom of the specimens. The applied water pressure at the top of the specimens was either 5 or 600 kPa.

Chapter 6 presents the influence of the thermal and thermo-hydraulic gradients on the concentration of the cations and the mineralogy along the full depth of the specimen after the completion of the tests. A brief literature review concerning the influence of thermal loading and chemical changes in compacted bentonites is presented. The experimental program for the mineralogical and chemical analyses undertaken in this study are presented in detail. The main results and of the chemical and mineralogical tests are presented.

The main conclusions drawn from this research are presented in **Chapter 7**.

CHAPTER 2.
LITERATURE REVIEW

2.1 Introduction

Compacted bentonites have been considered as suitable barrier and backfilling materials in the deep geological repository concepts (Thomas et al., 1998). The waste canisters are planned to be placed at depths greater than 500 m below the ground surface (Pusch, 1982). In some geographical locations, the canisters will be placed in deposition holes excavated in crystalline rock, whereas in other cases over-consolidated deposits of soils and salt rocks may surround the disposal facilities.

Compacted bentonite rings positioned surrounding the waste canisters is expected to create a barrier between the copper/steel canister and the host rock. Compacted bentonite will be used as a backfill to seal the excavated tunnels and the access galleries after the waste canisters put in place. In engineered barrier systems, the waste canister may high temperatures. Thus, the bentonite buffer is subjected to thermal gradients. On the other hand, the saturated host rock in some instances may allow supply of water/saline fluid to the barrier and backfilling materials.

This chapter presents a review of the literature pertaining to the fundamental understanding of the various process (physical, chemical) that are expected to occur in the engineered barriers conditions which in turn will affect the long term behaviour of compacted bentonites as buffer material.

Sections 2.2 and 2.3 present the structure of the montmorillonite and the micro-structure of the compacted bentonites respectively. Section 2.4 presents the mechanism governing the swelling in compacted bentonites. The effects of thermal and hydraulic gradients and solute transport are demonstrated in this section. The compressibility of bentonite is demonstrated in section 2.5. In section 2.6, a detail review on previous studies on the thermo-hydro-mechanical-chemical behaviour of bentonite is presented. A review of the literature on the mechanisms governing the heat water and solute transport are covered in section 2.7. The influence of thermal and hydraulic gradients on the aspects associated with the mineralogical phase transformation and ion redistribution are presented in Chapter 6. A summary of this chapter is presented in section 2.8.

2.2 Structure of montmorillonite

Bentonites are clays that primarily contain the mineral montmorillonite. The mineral montmorillonite is one of three-sheet minerals classified under the smectite group of minerals. Upon exposed to water (either liquid or vapour form), montmorillonite expands. The volumetric expansion of clays occurs due to the mineralogical composition of their structural units. The unit layer of montmorillonite composed of an alumina octahedral sheet sandwiched by two silica tetrahedral sheets (Fig. 2.1) (Mitchell and Soga, 2005). A silicon atom at the centre and four oxygen atoms at each corner of a tetrahedron form the silica tetrahedral sheets, whereas an aluminium atom at the centre of an octahedral and six hydroxyls at each corner form the alumina octahedral sheet.

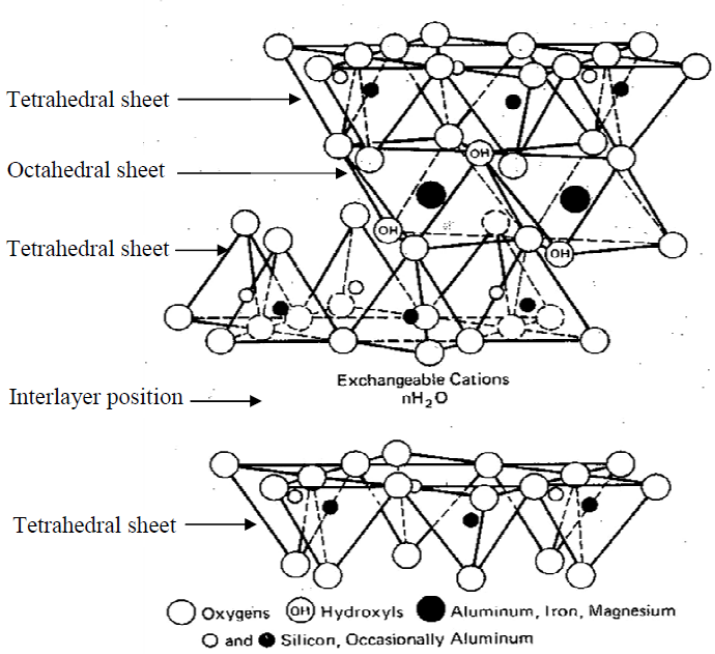

Figure 2.1 Structure of montmorillonite mineral (Mitchell and Soga, 2005)

Several stacks of the clay mineral (clay particle) arranged in matrix form an aggregate of clay. The isomorphous substitution in the crystal lattice is responsible for the negative charges on the surfaces of the clay minerals (Mitchell and Soga, 2005). The negative charged surface attracts the exchangeable cations present in the clay media. According to Mitchell and Soga (2005) the physico-chemical interaction between montmorillonite mineral and water molecules is considered as the basis of analysis of the behaviour of bentonites in contact with water or electrolytes.

2.3 Structure of compacted bentonite

The number of elementary layers that form a bentonite particle depends on the water content and the exchangeable cations present in the montmorillonite (Pusch et al., 1990; Mitchell, 1993; Pusch, 2001; Schanz and Tripathy, 2009; Fredlund et al., 2012). Compacted bentonites are formed from aggregates with closely spaced mineral particles (Delage et al., 2006). The energy used during the compaction process influences the spaces between the bentonite aggregates (Dixon et al., 1999). The porosity of the bentonite varies due to the simultaneous presence of structural units, particles and aggregates. In particular there are two type of pores, namely the micro-pores and the macro-pores. (Pusch, 1982; Gens and Alonso, 1992; Yong, 1999; Lu and Likos, 2004; Delage et al., 2006; Montes-Hernandez et al., 2006). Delage et al. (2006) defines the micro-pores as the pores within the aggregates (i.e., intra – aggregate pores) which are the pores between the elementary layers and between the particles. As macro-pores or interaggregate pores are defined the pores between the aggregates. The pores between the particles some times are also named as interparticle or meso-pores (Delage et al., 2006).

The pore size distribution for clay specimens is determined by Mercury Intrusion Porosimetry (MIP) (Dixon et al., 1999; Lloret Morancho et al., 2003; Montes-h et al., 2003; Delage et al., 2006; Montes-Hernandez et al., 2006). According to Laird (2006), compacted bentonites can be described to possess 'dual porosity' due to the contribution of both micro- and macro-pores to the pore size distribution.

According to Delage et al. (2006) a change in the water content affects the number of elementary elements in the bentonite aggregate, thus a change in the water content changes the microstructure of the compacted bentonite (Lloret Morancho et al., 2003). Figure 2.2 shows a schematic representation of microstructure of an expansive clay at very high water contents (Nagaraj and Murthy 1985). The elementary layers stacked form the clay particles. The interlayer or 'absorbed water' is located between the elementary elements in the micro-pores. Clay clusters are formed from the arrangement of several aggregates. The void between particles and cluster is called macro-pores and the water contained in them is referred as the bulk water.

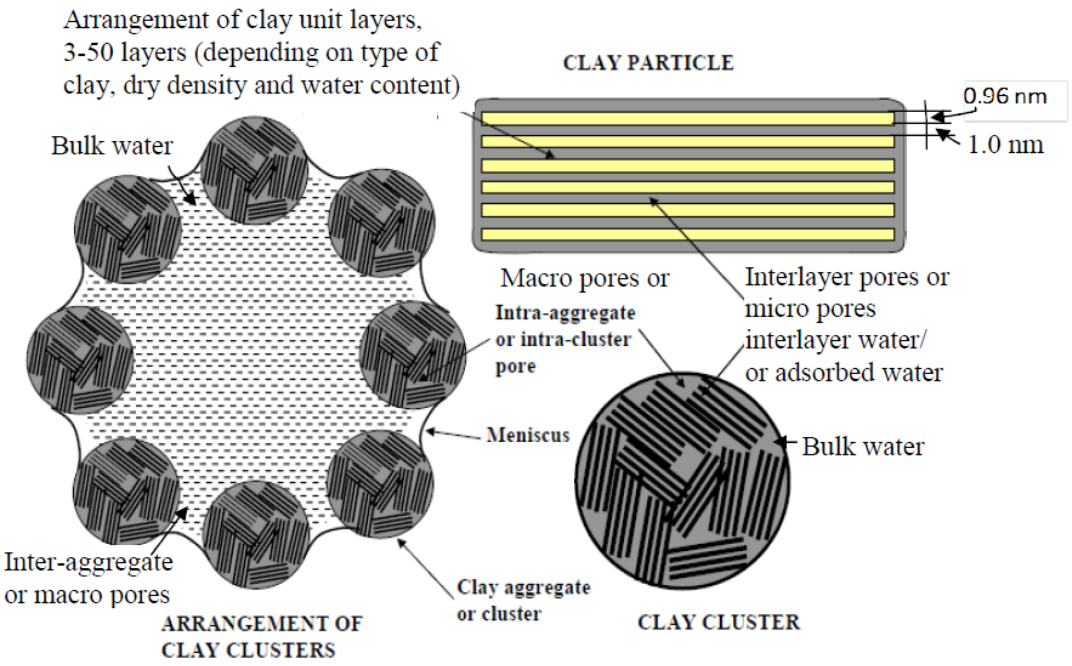

Figure 2.2 Representation of micro structure of expansive clays (Nagaraj and Murthy, 1985)

Pusch et al. (2001) stated that any potential changes in the microstructure of compacted bentonites immediately affects the hydraulic conductivity, swelling pressure and cations / anion diffusion capacities. The macro – porosity of the compacted bentonite reduces with the increase of the water content (Lloret Morancho et al., 2003; Lloret and Villar, 2007). The hydraulic conductivity of compacted bentonite decreases with the increase of the water content (Thomas et al., 2003).

2.4 Mechanisms governing swelling of bentonite

When bentonites are exposed to water or electrolyte, swelling occurs and in unrestrained conditions their volume increases. The hydration of bentonites under volume restrained conditions lead to the development of swelling pressure. According

to Sridharan et al. (1986), swelling pressure is the pressure required to maintain the void ratio of the specimens constant during the hydration process of unsaturated expansive soils. Two distinct mechanism govern the swelling pressure of bentonites: the crystalline and the osmotic swelling (Olphen, 1977).

The hydration of the bentonite leads to the hydration of the ions and mineral surfaces (Pusch, 1982; Alther, 2004). The infiltration of water between the unit layers, changes the c axis spacing. The water molecules entered between the layers are formed in layers called the hydrate layers. Up to four hydrate layers are intercalated between unit layers in a smectite particle (Olphen, 1977). The above process is called crystalline swelling (Grim, 1968; Saiyouri et al., 2000; Lu and Likos, 2004). Yong (1999) stated that, the crystalline swelling is controlled by the particle size, properties of absorbed liquid, layer charge, interlayer cations and temperature. The potential energies in between the elementary layers during the crystalline swelling are balanced by the Columbic and van der Waals attraction and Born's repulsion forces (Laird, 2006).

Beyond the crystalline swelling osmotic swelling is significant (Olphen, 1977). The osmotic swelling occurs due to the formation of electrical diffuse double layers between the unit layers and in between the elementary particles (Mitchell, 1993; Delage et al., 1998; Bradbury and Baeyens, 2003; Delage et al., 2006; Laird, 2006). As stated by Mitchell and Soga (2005), during the hydration of the bentonite, the cations on the platelet surfaces tend to diffuse away from the mineral surfaces towards the water present away from the minerals in order to equalise concentration. This action is countered by the electrostatic attraction between the cations and the mineral surface, as the mineral is still governed by a charge deficit. Figure 2.3 shows, the distribution of ions adjacent to the clay surface for clays with very high water contents.

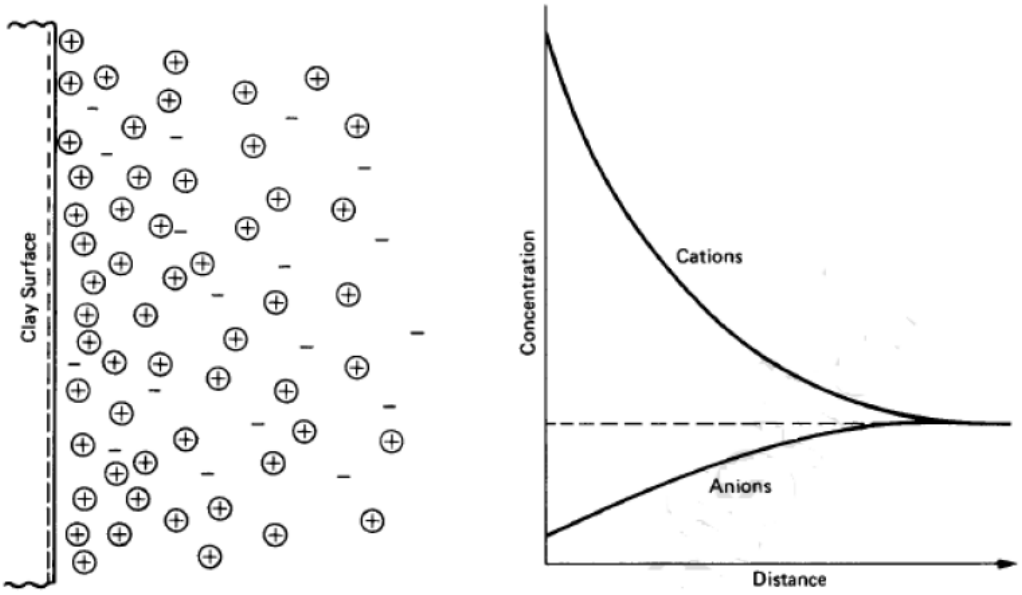

Figure 2.3 Distribution of ions adjacent to a clay surface according to the concept of the diffuse double layer (Mitchell and Soga, 2005)

The swelling pressure of bentonites can be determined by the Gouy-Chapman diffuse double layer theory (Olphen, 1977; Tripathy et al., 2004; Schanz et al., 2013). The experimental data show an agreement with the diffuse double layer theory when the distances between the surface platelets were large enough for the diffuse double layers to form (Shainberg and Kemper, 1966). However, the repulsive forces formed from the close distances of the clay platelets doesn't allow the formation of the double diffusion layers (Swartzen-Allen and Matijevic, 1974; Olphen, 1977; Tripathy et al., 2006).

2.4.1 Effects of temperature on the swelling pressure

Pusch (1980) performed laboratory tests in which bentonite specimens were hydrated with distilled water and different electrolytes under two different temperatures (20 and 90 °C). The swelling pressure of the specimens subjected to 90°C

was significantly lower than the specimens treated with 20 °C. The presence of unstable interlayer and interparticle water due to the increased temperature lead to the reduction of the swelling pressure (Pusch, 1980). Pusch et al. (1990) stated that the increase in temperature decreases the swelling pressure of Ca-bentonite. The results of Villar and Lloret (2004) on FEBEX bentonite (i.e., Ca-Mg bentonite), Romero et al. (2003) on Boom clay and Bag (2011) on MX80 bentonite also showed a decrease of the swelling pressure of at higher temperatures.

2.4.2 Effects of electrolyte concentration on the swelling pressure

Bentonites that are proposed to be used as barrier and backfilling materials in the deep geological disposal concepts are expected to be exposed to groundwater or electrolytes migrated from the subsurface and host rock. (Karnland et al., 2007) investigated the swelling behaviour of compacted MX80 bentonite in saline environment. The specimens were hydrated with 0.1 M, 0.3 M and 1.0 M NaOH solutions. The swelling pressure significantly reduced when the specimens were treated with 0.3 M and 1.0 M solutions. According to Karnland et al. (2007) the reduction in the swelling pressure occurs due to an immediate osmotic effect and a continuous dissolution of silica minerals leading to the loss of mass and consequently the decrease of the bentonite specimen.

Castellanos et al. (2008) noted that highly compacted FEBEX bentonite (above 1.60 Mg/m^3) experiences minimum reduction of swelling capacity when treated with saline solutions. On the other hand, the swelling capacity of bentonite with lower dry density decreases significantly in saline environments. Similar findings reported also for Na^+ and Ca^{2+} bentonites by Komine et al. (2009).

Bag (2011) reported that compacted bentonites with dry densities in the range of 1.25 to 1.60 Mg/m^3 and under the influence of post compaction residual stress exhibit less swelling pressures (8 to 15%) as compared to their stress released counterparts. As a result, the potential swelling pressures for compacted bentonites in the repositories conditions may reduce since compacted bentonites are placed without any post compaction lateral residual effects.

The swelling potential of compacted bentonites is affected by the high concentration of NaCl. Compacted bentonite specimens exhibited a reduction in their exerted swelling pressure for dry densities between the 1.20 to 1.50 Mg/m^3. For higher dry densities the effect was negligible due to the mechanisms governing the swelling pressure (hydration of cations and overlapping of the Stern layers (Olphen, 1977; Bag, 2011).

2.5 Compressibility behaviour of bentonite

In deep geological repositories, compacted bentonites exhibit swelling when exposed to fluids. Upon completion of swelling, the swollen bentonite is expected to be in contact with host rock. The stress convergence of the host rock is an important issue and the pressure-void ratio relationship of the compacted bentonites (Schanz and Tripathy, 2005). Numerous studies have been carried out on the compressibility of compacted bentonites, covering a wide range of void ratios (Bolt, 1956; Mesri and Olson, 1971; Sridharan et al., 1986; Al-Mukhtar et al., 1999; Marcial et al., 2002; Tripathy and Schanz, 2007; Baille et al., 2010). Initially saturated bentonites with water content greater than their liquid limits used to access their compressibility

behaviour. Similarly, some of these studies have explored in detail the compressibility behaviour of compacted saturated bentonites (Baille et al. 2010).

Sridharan et al. (1986) treated homo-ionised bentonites with pressures between 6.25 and 300 kPa. Mesri and Olson (1971) subjected Na- and Ca-bentonites to pressures up to 4000 kPa. Tripathy and Schanz (2007), showed that the compressibility behaviour of bentonites at large pressures can be established based on the Gouy-Chapman diffuse double layer theory. Baille et al. (2010) studied the compressibility behaviour of compacted bentonites at large applied pressures (up to 25 MPa). Baille et al. (2010) calculated the hydraulic conductivity of the compacted bentonites for void ratio between 0.5 and 2. The hydraulic conductivity for a void ratio of 0.5 was 5×10^{-13} m/s, whereas for the void ratio of 2, it increased to about 6×10^{-12} m/s.

2.6 Thermo-hydro-mechanical-chemical tests on compacted bentonites

Compacted bentonites used as buffer and backfill materials in the deep geological repository concepts for the high-level wastes (HLW) will be subjected to elevated temperatures and hydraulic gradients. The thermal and hydraulic gradients are expected to trigger several physical processes in the bentonite (Pusch and Yong, 2006). In order to understand the behaviour of compacted bentonites in the HLW disposal repositories the understanding of the heat and water flow processes is essential. The following processes may occur due to the exposure of the compacted bentonite to thermal and hydraulic gradients (Martın et al., 2000; Samper et al., 2000; Börgesson et al., 2001; Cuevas et al., 2002; Pintado et al., 2002; Gatabin and Billaud, 2005; Villar et al., 2005; Singh, 2007; Mishra et al., 2008; Villar et al., 2008; Åkesson

et al., 2009; Fernández and Villar, 2010; Gómez-Espina and Villar, 2010; Bag, 2011; Cleall et al., 2011; Schanz et al., 2013; Gómez-Espina and Villar, 2015; Tripathy et al., 2015): (*i*) swelling and shrinkage of the material, (*ii*) possible alteration of the initial water content, degree of saturation, suction and dry density values, (*iii*) diffusion and advection processes could change the cations and anions concentrations along the full length of the compacted bentonite and (*iv*) possible changes of the mineralogical composition of the compacted bentonite.

2.6.1 Thermo-hydro-mechanical testing conditions

Several experimental studies were conducted in the past to investigate the thermo-hydro-mechanical behaviour of compacted bentonites in the engineered barrier systems conditions. Table 2.1 presents the initial and testing conditions of the laboratory scale thermal and thermo-hydraulic tests carried out using several bentonites. The dry density of the compacted bentonite specimens varied between 1.40 and 1.72 Mg/m^3 and the maximum applied temperature varied between 70 and 140 ℃. For the thermo-hydraulic tests, the hydrating fluid injected with a maximum pressure of 1.5 MPa. The duration of the testing periods varied from 1 day up to 8 years.

Most off the previous studies subjected the compacted bentonite specimens to thermal and hydraulic loading simultaneously at opposite ends. However, the impact of thermal loading on the hydro-mechanical behaviour of compacted bentonites, particularly under the influence of high temperature has not been explored in detail in the past. This aspect is of interest particularly for understanding the early-life phase of deep geological disposal facilities. Very high temperatures of spent fuel, radioactive decay of wastes, and formation of high thermal zones at and near the interface of waste

canisters and compacted bentonite buffer are some of the in situ conditions which demand detailed investigations concerning the thermo-hydraulic behaviour of compacted bentonites at high temperatures.

Applications of thermal and thermo-hydraulic gradients may cause development of stresses within compacted bentonite systems (Tripathy et al. 2015). The impact of magnitude of the applied temperature is crucial for the development of thermal gradients within compacted bentonites. The thermal gradient depends upon various factors, such as water content, dry density, and thermal conductivity of the confinement. The impact of different temperature and characteristics of the physical boundary on the response of compacted bentonites has not been explored in the past.

Up to now, most HLW concepts are based on a design criterion of a maximum temperature of 100 °C. Most of the studies based on the above design criteria led to the exploring of the effects for temperatures up to 100 °C. The implementation of this criteria may not be cost-effective in some cases. Therefore, understanding of the physical and chemical processes occurring in compacted bentonites for temperatures above the 100 ℃ is essential for the design of future HLW repositories.

Table 2.1 Summary of the thermal and thermo-hydraulic tests in this study

Type of test	Material used (bentonite)	Specimen size		Initial compaction condition		Temperature (°C)	Fluid injection pressure	Reference
		Ht (mm)	Dia. (mm)	ρ_d (Mg/m^3)	w (%)			
TH	FEBEX	146	150	1.65	11.23	100	1.0 MPa	Samper et al. (2000)
TH	Bentonite OT-9607	100	50	1.65	16	70, 25	--	Börgesson et al. (2001)
TH	FEBEX	76	38	1.63	15.33	80, 30	--	Pintado et al. (2002)
TH	FEBEX	25	50	1.65	14.1	100, 60, 35	1.0 MPa	Martın et al. (2000); Cuevas et al. (2002)
	MX80	202.7	203	1.79	13.2	150, 25	--	Gatabin and Billaud (2005)
THM	Calcigel	300	150	1.65	13.5	80	--	Mishra et al. (2008)
TH	FEBEX	202.5	202	1.7	13.3	120, 84	--	Åkesson et al. (2009)
TH	MX80	--	--	1.65	17.7	130, 90	1.5 MPa	Pusch et al. (2009)
TH	FEBEX	600	70	1.65	13.6	100	1.2 MPa	Villar et al. (2005), Villar et al. (2008); Fernández and Villar (2010)
TH	MX80	100	100	1.63	16 / 22	85, 25	600 kPa	Cleall et al. (2011)
TH	Calcigel	300	150	1.40	9.7	80, 20	15 kPa	Schanz et al. (2013)
TH	MX80	80	100	1.60	9.6	85, 25	--	Tripathy et al. (2015)
TH	MX80	200	70	1.72	16	140, 30	10 kPa	Gómez-Espina and Villar (2010); Gómez-Espina and Villar (2015)

* T-Thermal, TH-Thermo-hydraulic

2.6.2 Thermo-hydro-mechanical testing devices for testing compacted bentonite at temperatures less than 100°C

Several devices have been used to study the thermal, hydraulic and mechanical responses of compacted bentonites. Börgesson et al. (2001) fabricated a twin cell apparatus called KID-BEN (Fig. 2.4). Each cell was made out of Bakelite with an insulating air layer. The dimensions of it are 5cm internal diameter and 10 cm height. The material that was used for these tests was a compacted sodium bentonite (OT-9607) with density 1.65 Mg/m3 which was placed in the cell. The cell had temperature regulators at the two ends. The temperature regulators were connected to a thermostat to circulate water at a constant specified temperature. The cold end of the cell had a constant temperature of 25 °C while the temperature at the hot end was varied from 35-70 °C. Each cell served different purposes. The first one was used to measure the distribution of the water in the sample and the second to monitor the temperature distribution with the aid of six thermocouples.

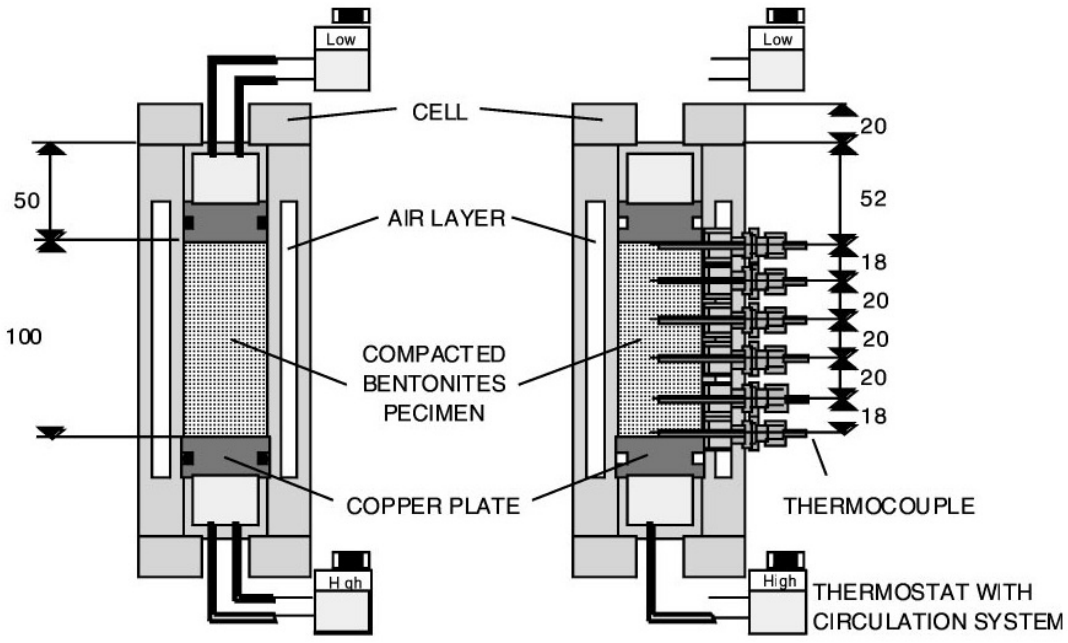

Figure 2.4 A schematic representation of Börgesson et al. (2001)'s experimental device

Pintado et al. (2002) used an apparatus that facilitated monitoring of the deformation during the Thermo-Hydraulic (TH) test in order to back analyse the thermo-hydraulic properties of the bentonite (Fig. 2.5). For the tests they used FEBEX bentonite, originated from the South East of Spain. The compacted bentonite samples had a dry density of 1.63 Mg/m^3 and water content of 15.33%. The dimensions of the cylindrical specimen were: 38 mm diameter and 76 mm height. The apparatus was made up of a perpex tube that contained a 55 mm thick insulation which covered the deformable latex membrane that carried the sample. In order to obtain the information of the heat flux, two specimens were used in the tests. The heater was a copper cylinder which contained five electrical resistances with 38mm diameter and 50 mm height. In order to improve the insulation of the soil and the durability of the membrane which was in contact with the heater, a liquid silicon that solidified in a few hours was used. During the tests, the hot side of the specimen was in the range of 70-80 °C, whereas the cold side was maintained at a constant temperature of 30 °C with the aid of circulating water in the stainless steel face, which in turn was in contact with the soil. Temperature measurements were carried out from the top specimen. Temperature measurements at the bottom of the specimen was undertaken only at the middle point to ensure the symmetry of the heat flux.

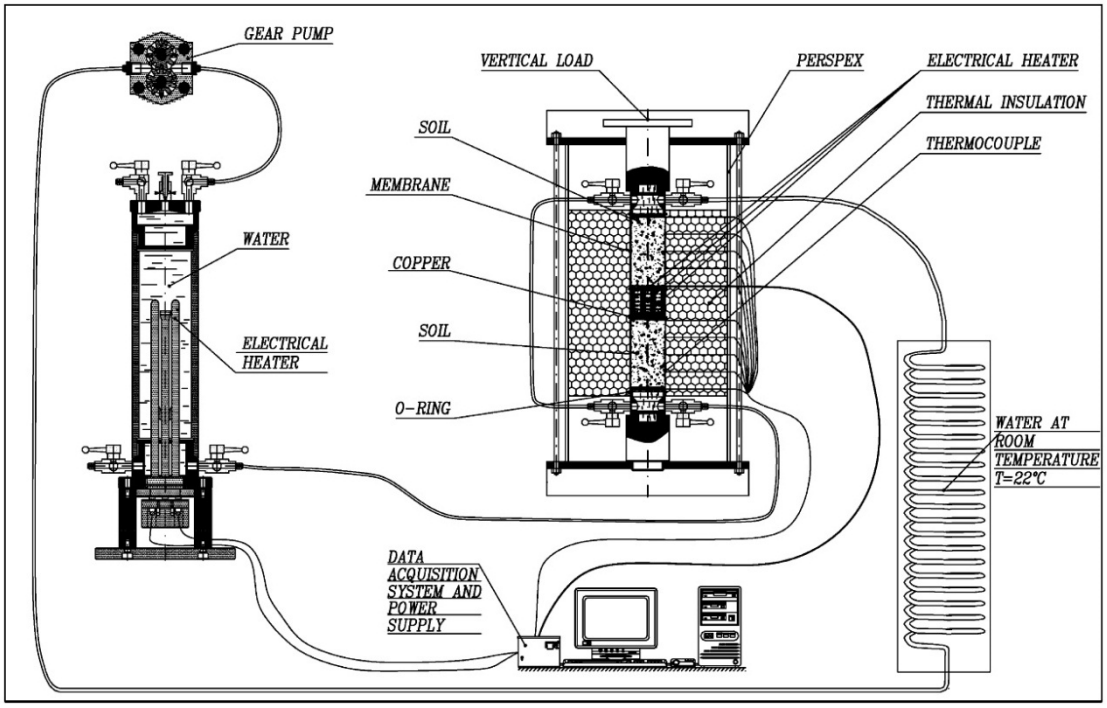

Figure 2.5 A schematic representation of Pintado et al. (2002)'s experimental device

Mishra et al. (2008) carried out thermal and thermo-hydraulic tests on compacted Calcigel bentonite. The length of the specimens used was 300 mm. In order to minimise the density variation instead of compacting the whole specimen in a single lift, they dynamically compacted 3 blocks of 100 mm thick bentonite. In this way, a constant dry density of 1.65 Mg/m^3 could be achieved. Schanz et al. (2013) used a similar apparatus to conduct tests on Calcigel bentonite specimens with dry density 1.40 Mg/m^3. The cell was made out of stainless steel with an internal liner from PTFE in order to avoid the heat dissipation. The thicknesses of the stainless steel and PTFE sleeves were 25 and 17 mm, respectively. The internal dimensions of the cell were: 150 mm diameter and 410 mm height. The cell has the ability to host thirteen sensors which measure temperature, relative humidity, water content and axial pressure. A total of eight sensors were bored into the specimen (5 nos. of temperature sensors and 3 nos. of water content sensors), two load cells were placed at top and bottom of the column cell. Three nos. of relative

humidity sensors were used which were placed in external chambers. The maximum applied temperature during the test was 80 ℃.

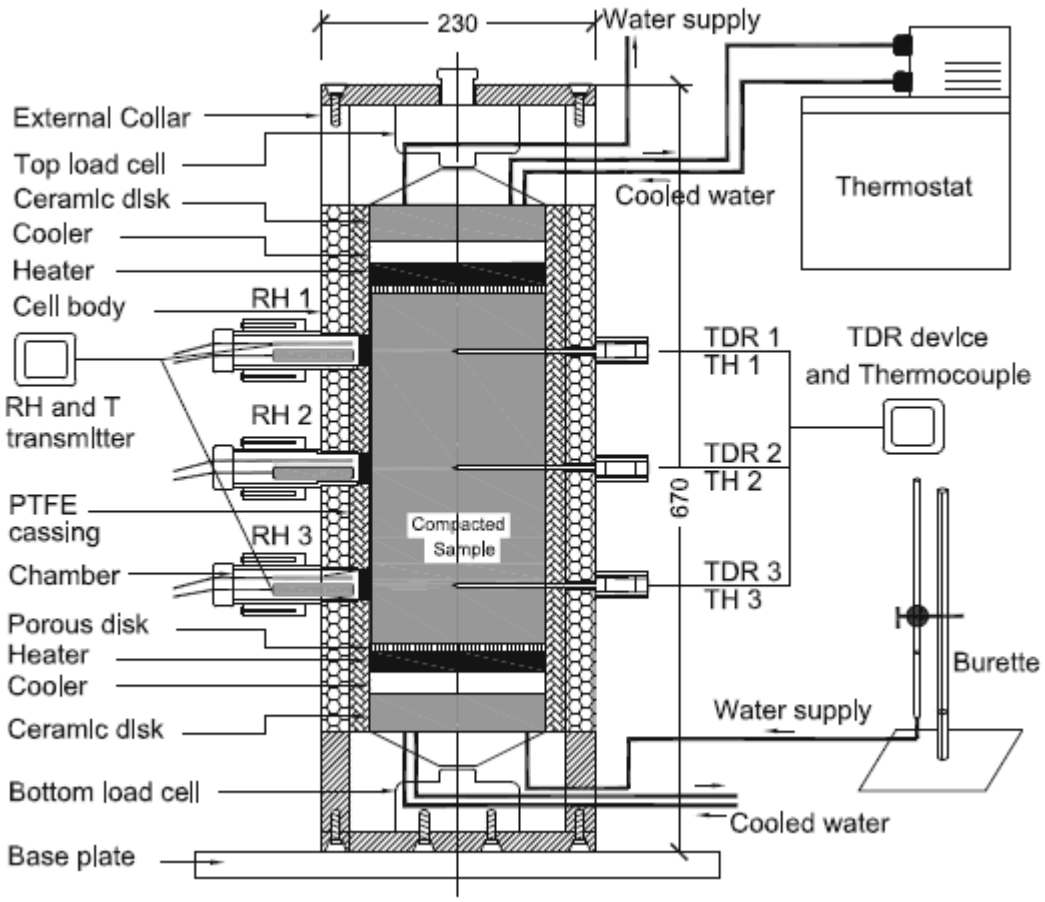

Figure 2.6 A schematic layout of THM Cell (Mishra et al., 2008; Schanz et al., 2013)

Singh (2007) conducted thermo-hydraulic tests using a TH cell. Compacted MX80 bentonite with a dry density of 1.63 Mg/m^3 was considered for the tests. The cell consisted of four parts (*i)* the top section, (*ii*) the interconnecting ring, (*iii*) the central section and (*iv*) the bottom part. The top section is made out of a sand blasted austenitic stainless steel cylinder with outer diameter of 142 mm, wall thickness of 10 mm and height of 100 mm. On top of the cylinder, a cylinder made from the same material (250 mm diameter and 15mm thick) was welded. The main function of the cylinder was to

maintain a constant temperature and facilitate supplying pressurised water at the top end (cold end) of the sample. The interconnecting stainless steel bars connect the top and the central sections and limit any leakage. An O-ring was used at top of the ring and two O-rings were used at the bottom. The central section is a chamber that hosts bentonite sample (100 mm diameter and 100 mm high). It is made out of a stainless steel cylinder with outer diameter of 142 mm, a wall thickness of 10 mm and a height of 140 mm. The steel cylinder is lined with a PTFE sleeve which has characteristics of low friction and thermal conductivity. The dimensions of the PTFE sleeve are: 124 mm outer dia., 12 mm - wall thickness and a height of 140 mm. The central section of the cell has three holes staggered at 120° along the full height of the section, which served as the access points for the relative humidity and temperature probes. Prior the test, the relative humidity and temperature probes were needed to be bored into the bentonite sample. After the insertion of the probes the central part was wrapped with an insulating material to minimise the radial heat loss. The bottom section is a stainless steel cylinder with a dia. Of 250 mm and a thickness of 30 mm. The water tightness of the cell was achieved due to the use of two O-rings where the central and the bottom sections are connected.

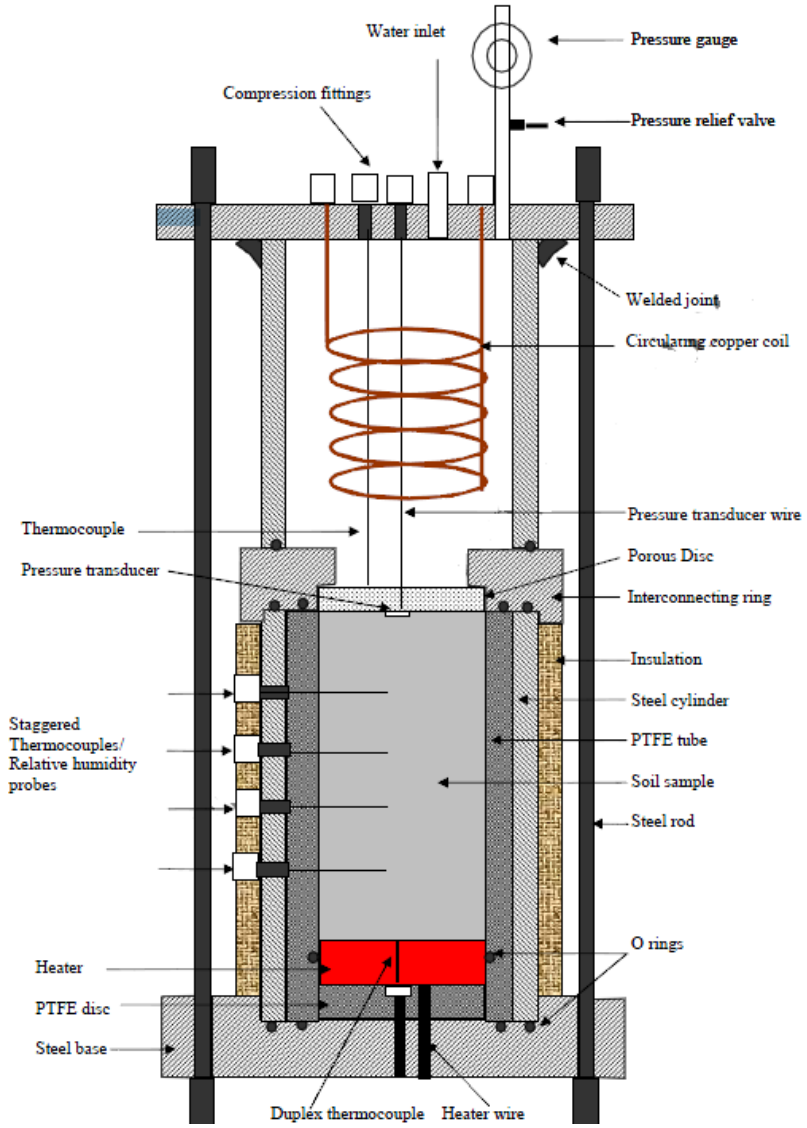

Figure 2.7 A schematic representation of Cardiff University TH Cell (Singh 2007)

Following to Singh's (2007) work, Bag (2011) modified the Cardiff TH cell (Fig. 2.8) to measure the axial pressure generated from compacted bentonite during the tests. This was achieved by adding a loading plunger and a load cell on top of the bentonite sample. The load cell was placed with the top part of the load plunger to record the axial force. The dimensions of compacted bentonites tested using the device were: 100 mm dia. and 80mm height.

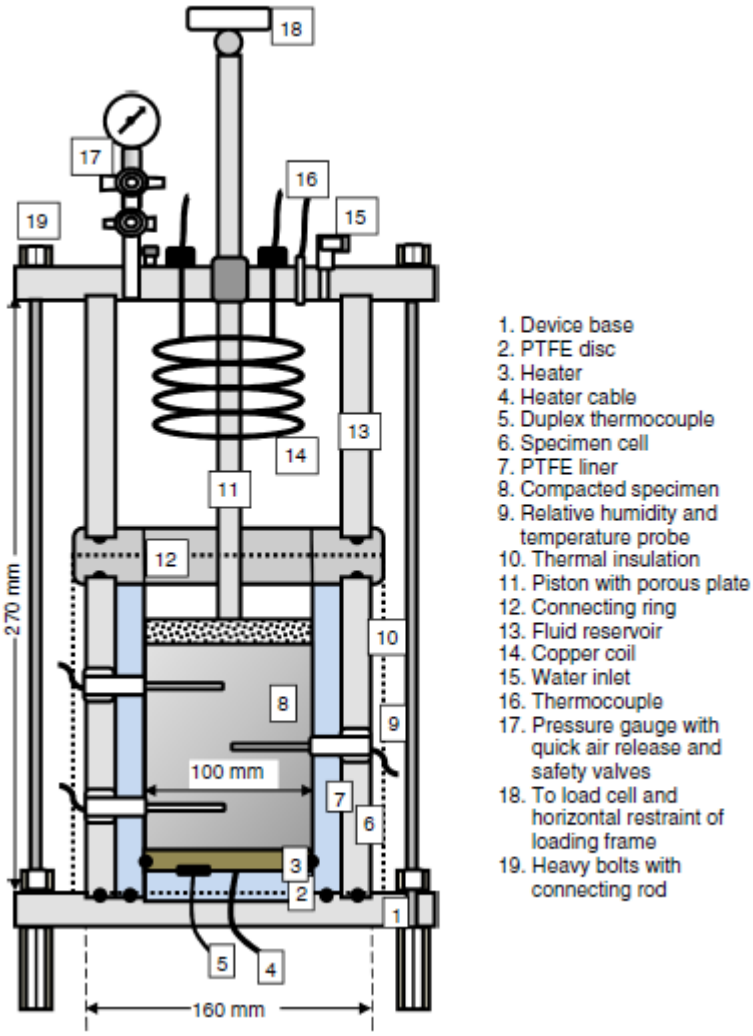

Figure 2.8 A schematic representation of Cardiff University THM Cell. (Tripathy et al., 2015)

2.6.3 Thermo-hydro-mechanical-chemical testing devices for testing compacted bentonites at temperatures greater than 100℃

Gatabin and Billaud (2005) conducted THM tests on compacted MX80 bentonites. The dry density of the bentonite specimens was 1.79 Mg/m^3. The applied temperature during the tests was 150 °C. A PTFE tube was used to fabricate the cell with a PTFE lining to avoid any heat dissipation during testing. The heater was placed (Fig. 2.9) at the bottom of the cell (hot side) and the hydration unit at the top (cold side). Twenty nine sensors were used in total in order to investigate the thermo-hydraulic behaviour of

the compacted bentonites. Nine sensors measured the axial and radial stresses. A force sensor at the top of the specimen and eight pressure sensors were used to measure the axial and the radial stresses respectively. The temperature and relative humidity along the length of the bentonite specimen were measured with thirteen thermocouples and seven relative humidity sensors. The size of the specimen used were: 202.7 mm dia. and 203 mm height.

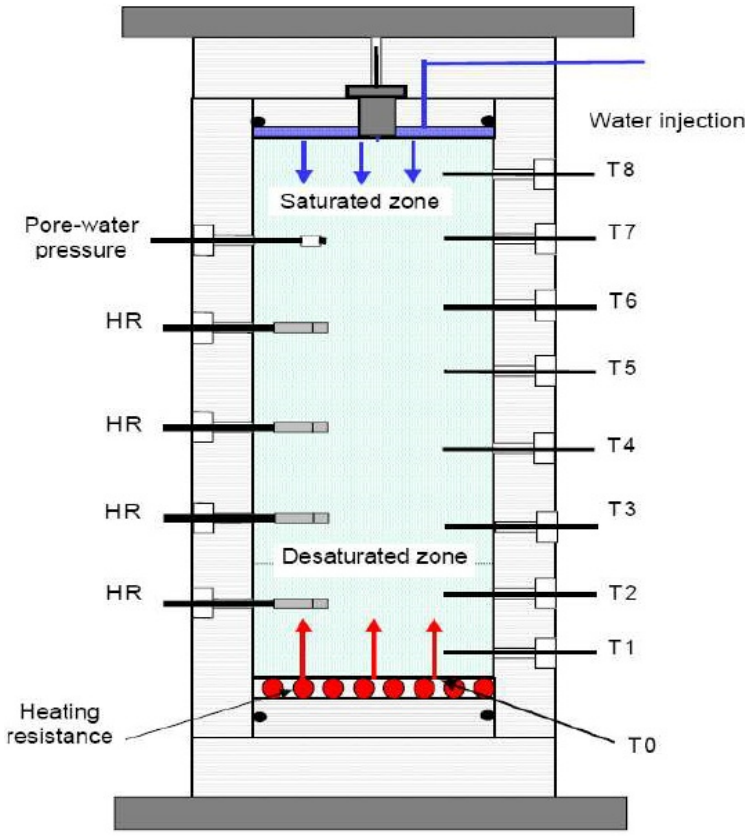

Figure 2.9 A schematic representation of Gatabin and Billaud (2005)'s THM cell

Villar et al. (2005) conducted thermo-hydraulic tests on FEBEX bentonite. The dry density and water content of the specimens tested were 1.65 Mg/m^3 and 14 %, respectively. The cell used (Fig. 2.10) was made out of Teflon with internal diameter 7 cm and length 20 cm. On top of the cell, a stainless steel plug was used to hydrate the specimen and circulate water into it in order to keep the temperature at the top of the

specimen constant at 30 °C. The bottom part of the cell was a stainless steel heater to apply a temperature of 100 °C. Three relative humidity and temperature probes were used to measure the temperature and relative humidity variations along the length of the specimen. A large number of studies were conducted at later stage using the cell for both FEBEX and MX80 bentonites. FEBEX bentonite samples were treated with 100 °C (Villar et al., 2008; Fernández and Villar, 2010). Gómez-Espina and Villar (2010, 2015) used the cell to conduct thermo-hydraulic tests on compacted MX80 bentonites. According to their experimental program a temperature of 140 °C was applied at the bottom of the bentonite samples during the tests. In order to facilitate the above testing conditions a different set of relative humidity and temperature probes were used that enabled measuring temperatures up to 180 °C. The cell described above couldn't record the axial pressure but an indicative value could be taken after the completion of the test by measuring the deformation of the cell.

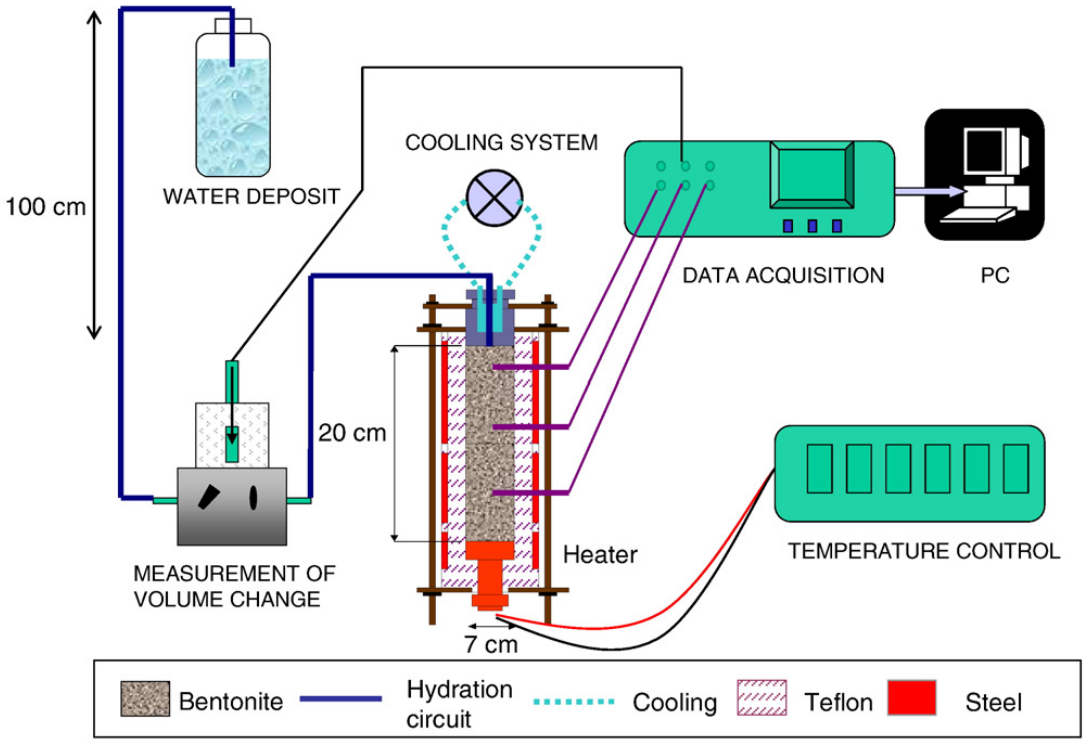

Figure 2.10 A schematic representation of the FEBEX TH cell (Villar et al., 2008)

Åkesson et al. (2009) fabricated a cell to conduct THM tests on compacted MX80 bentonites. Similarly to Gatabin and Billaud (2005), the cell was fabricated by using a stainless steel tube with a PTFE sleeve inside it. Two hollow copper plates wounded with the heating cables were used to maintain the desired temperature, both at the top and the bottom ends of the specimen. The dimensions of MX80 bentonite used were: 202.5 mm dia. and 202 mm height. For the compaction a pressure of 32 MPa applied during the sample preparation process. The achieved dry density was 1.70 kg/m^3. Twenty nine sensors were fitted in the bentonite specimen. Fourteen resistance temperature probes, eleven relative humidity sensors and four pore pressure sensors were used to measure the temperatures, relative humidity and pore water pressure along the length of the specimen. A load cell was used at top of the specimen and three strain gauge total pressure sensors were installed in the cell body to monitor the axial and radial stresses. The whole cell was enveloped with 50 mm thick rock-wool strips to thermally isolate it. It has to be mentioned that a cylindrical zone 50 mm in diameter along the vertical axis of the specimen left intact without any sensors so that it could be cored at the end of the test for analysis purposes.

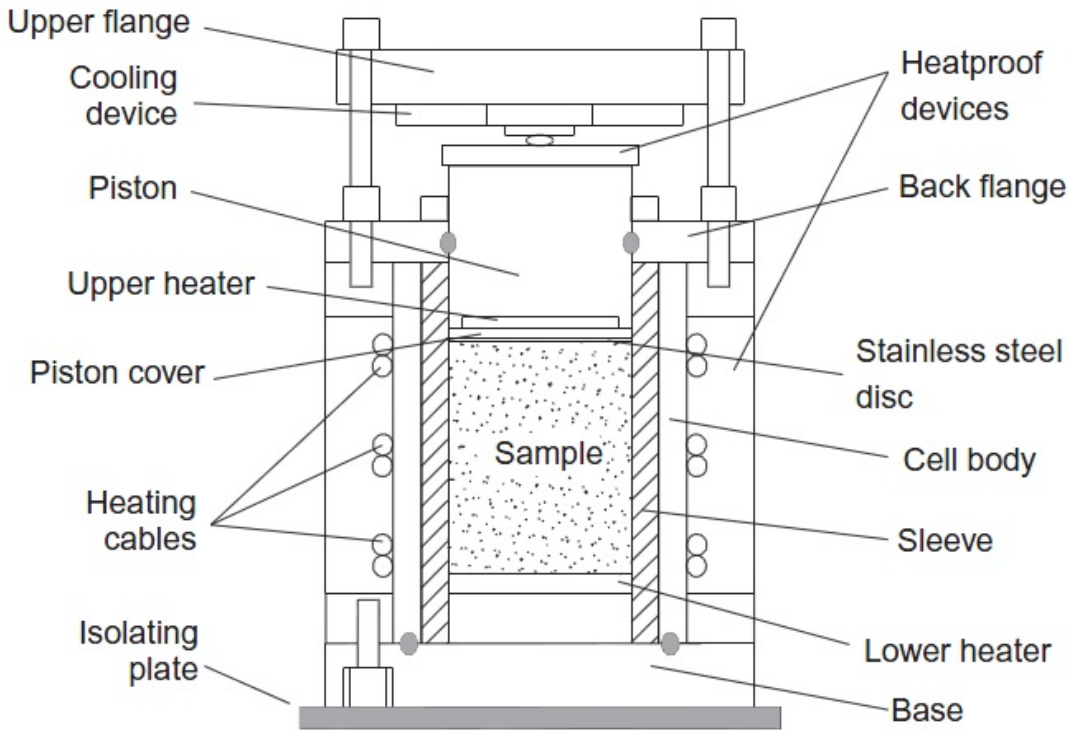

Figure 2.11 A schematic diagram of Akesson et al (2009)'s cell

2.7 Full scale tests for high level nuclear waste disposal

Except of the laboratory tests that investigate the behaviour of compacted bentonites as buffer material for nuclear waste disposal repositories many groups around the world are working on large scale tests in repository conditions. There are several restraints governing the large scale tests with the most important being the funding that in needed to cover the construction of laboratories that can host this type of tests and the time that it needs to be dedicated for a full scale test to reach equilibrium. The following section covers a few large scale experiments conducted by several teams around the world.

Table 2.2 Summary of large scale THM tests

Type of test	Material used (bentonite)	Specimen size		Initial compaction condition		Temperature (°C)	Fluid injection pressure	Reference
		Ht (m)	Dia. (m)	ρ_d (Mg/m^3)	w (%)			
THM	50:50 (by dry weight) mixture of quartz sand and sodium rich bentonite	5.0	1.24	1.28	18.3	85	1.0 MPa	Dixon et al. (2002)
THM	FEBEX	5.1	0.30	1.8	-	100	-ATM	Goebel et al. (2006)
THM	FEBEX	7.92	2.28	1.6	14.4	100	1.0 MPa	Gens et al. (2009)
THM	Kyungju	1.36	0.75	1.5	13	90	0.5 MPa	Cho et al (2010)
THM	FEBEX	6.0	1.62	1.65	17.1	100	0.5 MPa	Villar et al. (2012)

Dixon et al. (2002) reports the buffer-container experiment (BCE) which conducted at the Atomic Energy of Canada Limited's Underground Research Laboratory at Lac du Bonnet, Manitoba. The BCE examined the influence of heat on the performance of a large mass of buffer. Temperatures, water contents, and total and hydraulic pressures within and surrounding the installation were monitored for approximately 2.5 years.

The BCE fabricated in granite boreholes with 5.0 m depth and 1.24 m diameter. The buffer material was dynamically compacted in 50 mm thick lifts, directly into the boreholes using a dynamic impact hammer. During the buffer installations, various instruments were installed within the buffer. Vertical restraint against swelling achieved with the inclusion of a rigid steel cap.

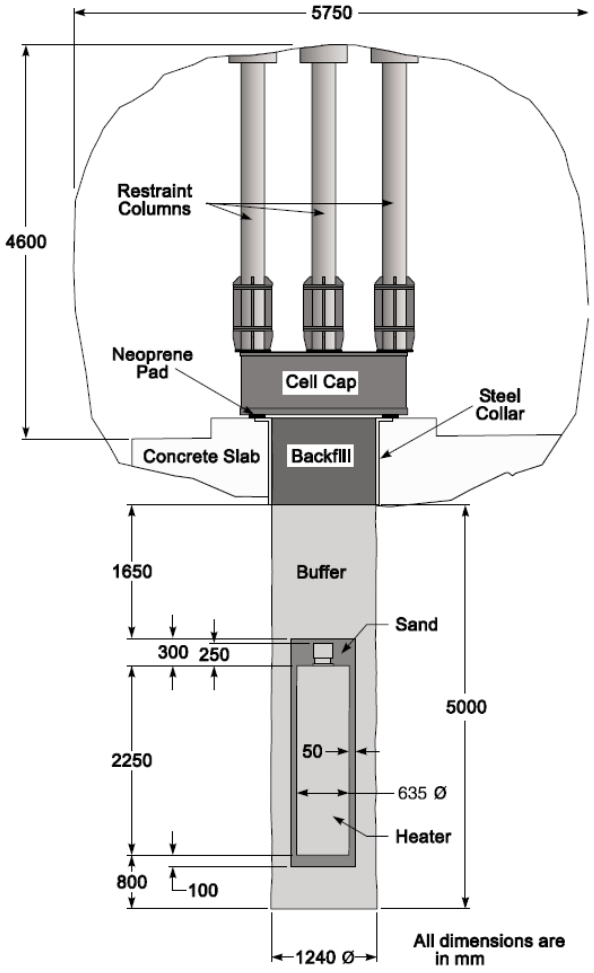

Figure 2.12. General Layout of the buffer-container experiment (Dixon et al. 2002)

A total of 511 instruments (Temperature sensors – 298, Total pressure – 56, Hydraulic pressure – 38, Water content – 41, Strain displacement – 81) were installed in the BCE to provide data for experiment analysis and to conduct field trials on the durability and reliability of the instruments. The instruments provided continuous record of the pressures and temperatures and a general indication of the water content within the buffer.

Goebel et al. (2006) describe the HE experiment which performed in the Mont Terri Rock Laboratory in Canton Jura in the north-west of Switzerland. For the purposes of the experiment a niche was built in the shaly facies of the Opalinus Clay formation. A central vertical borehole 7.5m long and 300mm in diameter was drilled in the niche floor. A 2.0m long heater was introduced in the borehole and surrounded by a bentonite buffer 5.1m in height made of ring-shaped compacted FEBEX bentonite blocks with a dry density of 1.8 g/cm3. 34 sensors were installed in the bentonite buffer to monitor humidity, temperature, total pressure and pore pressure.

Due to the virtual absence of free water in the host rock formation, an artificial hydration system was needed to accelerate the hydration process in the buffer prior to the heating phase. A cylindrical ceramic filter was fixed to the outer part of the heater tube and connected to the niche equipment by means of four tubes for water injection. The artificial saturation of the system was under atmospheric pressure condition and lasted for 35 months before the heating phase (duration 18 months) began. A total of 150.51 litres were injected into the system. The gap between the bentonite buffer and the rock, as well as the upper part of the borehole, were filled with sand.

The heater borehole was covered with a steel lid anchored to the rock to support the potential thrust caused by bentonite swelling. A sealing plug basically made of epoxy resin was installed in the upper part of the borehole, to provide gas and water tightness. Two pass-through pipes with a valve were installed across this plug to allow gas and water sampling and pressure monitoring.

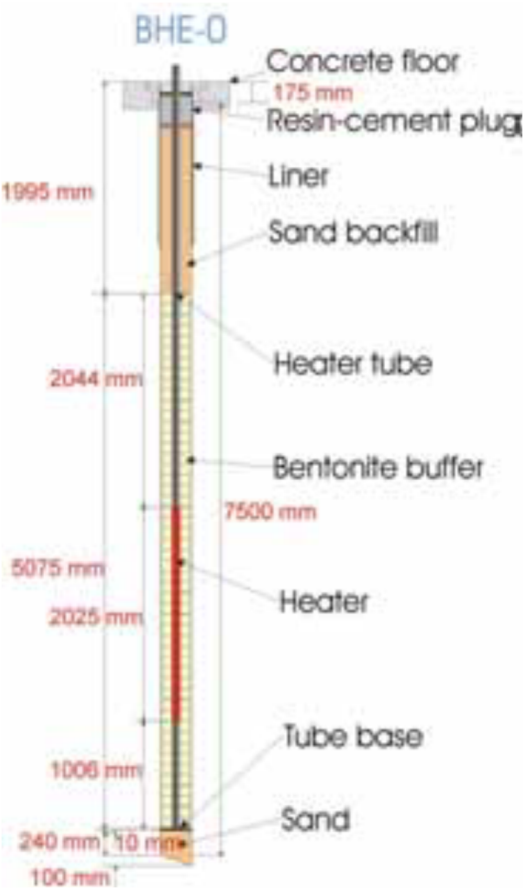

Figure 2.13 Layout of the HE experiment central borehole BHE-0. (Geobel et al. 2006)

Gens et al. (2009) demonstrates the FEBEX (full-scale engineered barrier experiment) in situ test. The FEBEX in situ test simulates, at full scale, the Spanish repository concept for high level wastes, which envisages placing the waste-containing canisters in horizontal drifts surrounded by an engineered barrier made up of compacted bentonite.

The test carried out at the Grimsel test site (GTS) an underground laboratory excavated in granite rock in the Swiss Alps. A circular tunnel with 2.28m diameter and 70.4 m length excavated for the needs of the test. The last 17.4m selected to perform the test. Two 4.54 m long and 0.90 m in diameter heaters used to simulate the heat generated by the high level wastes. The space between the rock surface and the heaters was backfilled using blocks of compacted bentonite. The bentonite is obtained from a quarry in the volcanic zone of Serrata de Nıjar in Southern Spain. Its smectite content is in the range of 88-96%. The bentonite blocks were compacted to a dry density of 1.7 Mg/m^3 at an average water content of 14.4%. Due to the existence of several small gaps between blocks, the clay barrier and the rock, the overall dry density of the emplaced barrier was 1.6 Mg/m^3. The test is heavily instrumented with a total of 632 sensors to be installed in the engineered barrier and in the rock. The sensors are used to measure the following parameters: temperatures, relative humidity (total suction), pore water pressures, total pressures and displacements. The heating stage of the test lasted five years.

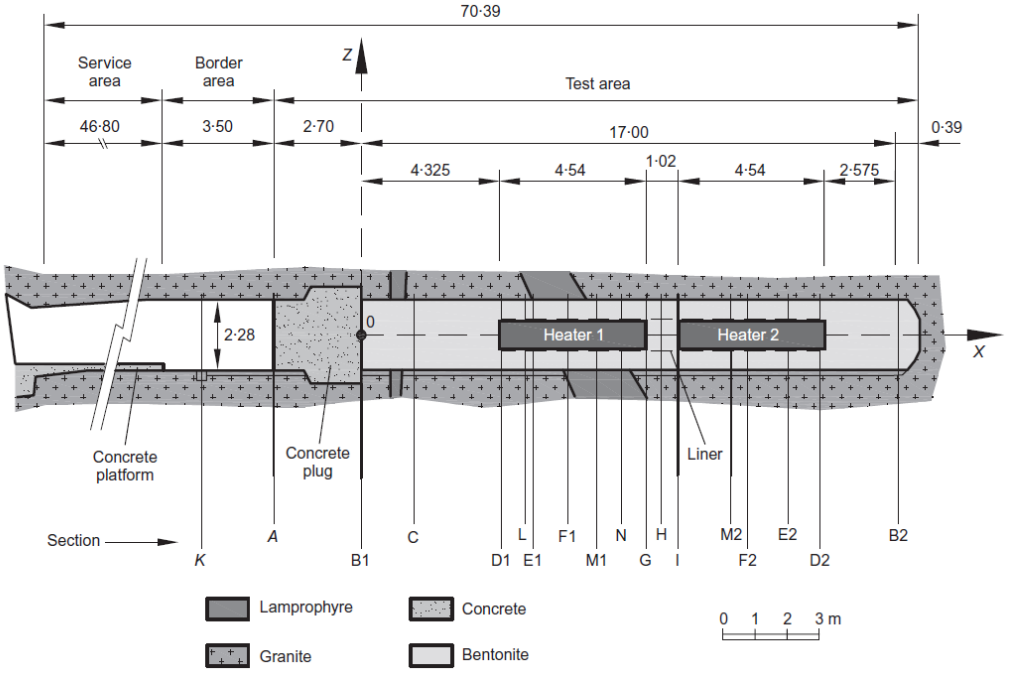

Figure 2.14 Layout of FEBEX in situ test (Gens et al. 2009)

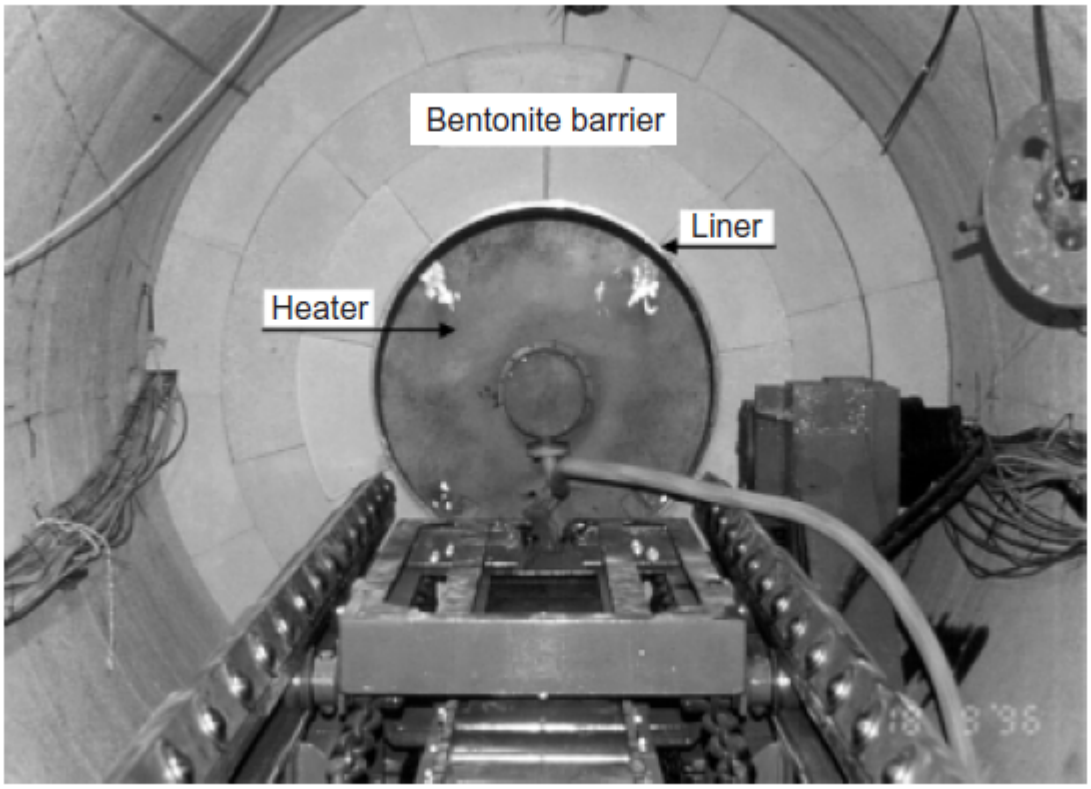

Figure 2.15 Heater placed in the excavated tunnel surrounded by compacted bentonite blocks (Gens et al 2009)

In 2010 Cho et al presented the KENTEX (KAERI Engineering scale THM Experiment for an Engineered Barrier System) which performed at KAERI in Korea to study the THM behaviour of an engineered barrier system. The KENTEX test simulates the repository concept adopted by the Korea.

The KENTEX test consists of a real life sized bentonite specimen tested in laboratory conditions. The deposition hole is simulated by a steel confining cylinder with inner diameter and height being 0.75 m and 1.36 m respectively. A heater with 0.41m diameter and 0.68 m height are placed in the center of the confining cylinder to play the role of the high level waste and its thermal dissipation. The heater encapsulated by compacted Kyungju bentonite rings with 1.5 Mg/m^3 dry density. The temperature at the interface of the cylindrical heater and the buffer material is set to be 90 ℃. At the same

time with the commencement of the heating phase water injected to the system through the nozzles at the side wall of the confining cylinder with a constant pressure of 0.5 MPa. Twelve sensors installed along and around the buffer material to measure the temperature, the humidity and the mechanical pressure generated. The total testing period was 350 days.

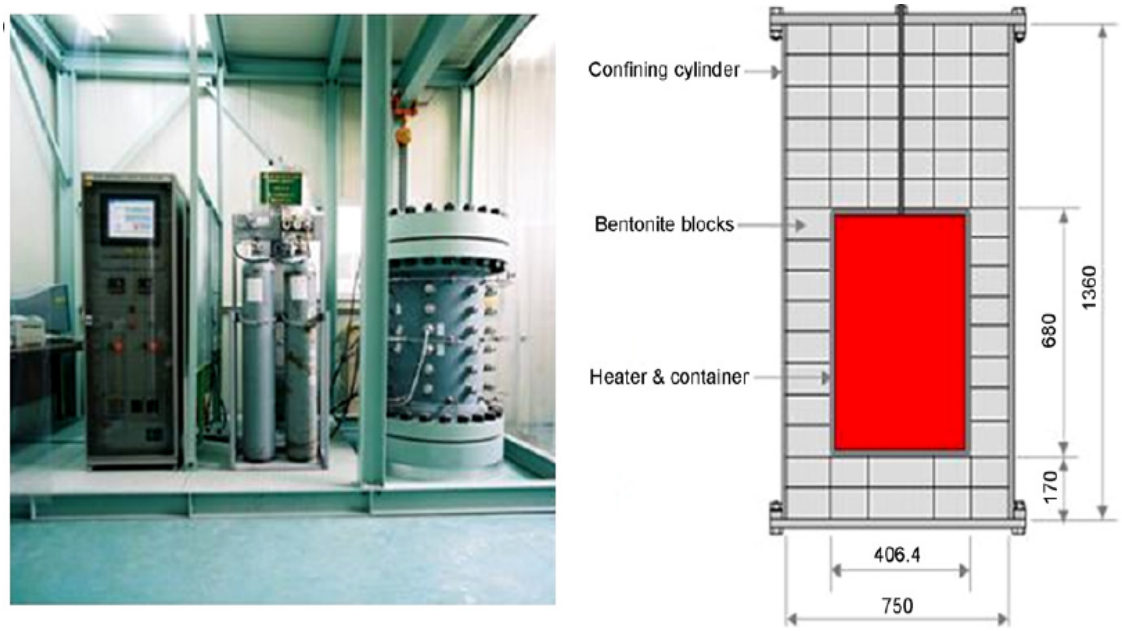

Figure 2.16 View of the KENTEX facility and a cross-section of the confining cylinder (Cho et al. 2010)

Villar et al. (2012) demonstrates a mock up test carried out at the CIEMAT facilities in Madrid. The test is at almost fill scale size and is conducted in a stainless steel confining that simulates the host rock gallery.

The stainless steel confining structure is oriented horizontally and its central part is occupied by two electric heaters with 0.17m diameter and 1.625m length to simulate the heat generation from the high level wastes. The space between the heaters and the steel structure was filled by compacted FEBEX bentonite to act as the buffer material.

The buffer bentonite is 6.0 m long and 1.612 m in diameter with an average dry density 1.65 Mg/m^3 and 17.1% water content. The blocks were manufactured by compacting the bentonite with its hygroscopic water content by applying uniaxial pressures of 40–50 MPa. They were arranged in vertical sections: the sections around the heaters were formed by two concentric rings of blocks, and the other sections were formed by two concentric rings and a core of blocks

The operational stage stared with the simultaneous application of the hydration and heating processes. The power supply of the heaters was automatically adjusted in order to supply a constant temperature of 100 °C at the heater surface and the hydration system supplied granitic water (from the nozzles located on the confining structure) at a constant controlled pressure of 0.5 MPa to hydrate the bentonite mass. More than 500 sensors were installed to measure temperature, total pressure, pore pressure, water injection pressure, relative humidity and strains

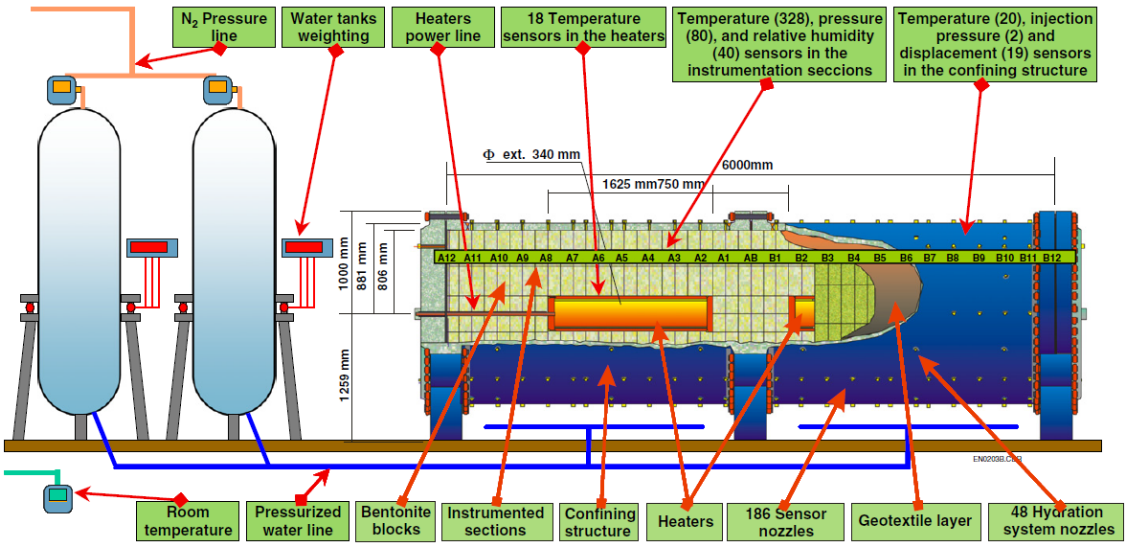

Figure 2.17 General layout of the mock-up test, including instrumented sections.(Villar et al. 2012)

2.8 Mechanisms governing heat, water and solute transfer

In high level waste repository concepts the bentonite buffer is expected to be exposed to thermal and hydraulic loadings at opposite ends. Elevated temperatures are generated in the vicinity of the waste canister whereas hydration occurs at the face in contact with the saturated host rock. Pusch and Yong (2006) described the physical processes occurring in compacted bentonites due to the heating and hydration at opposite ends (Fig. 2.12).

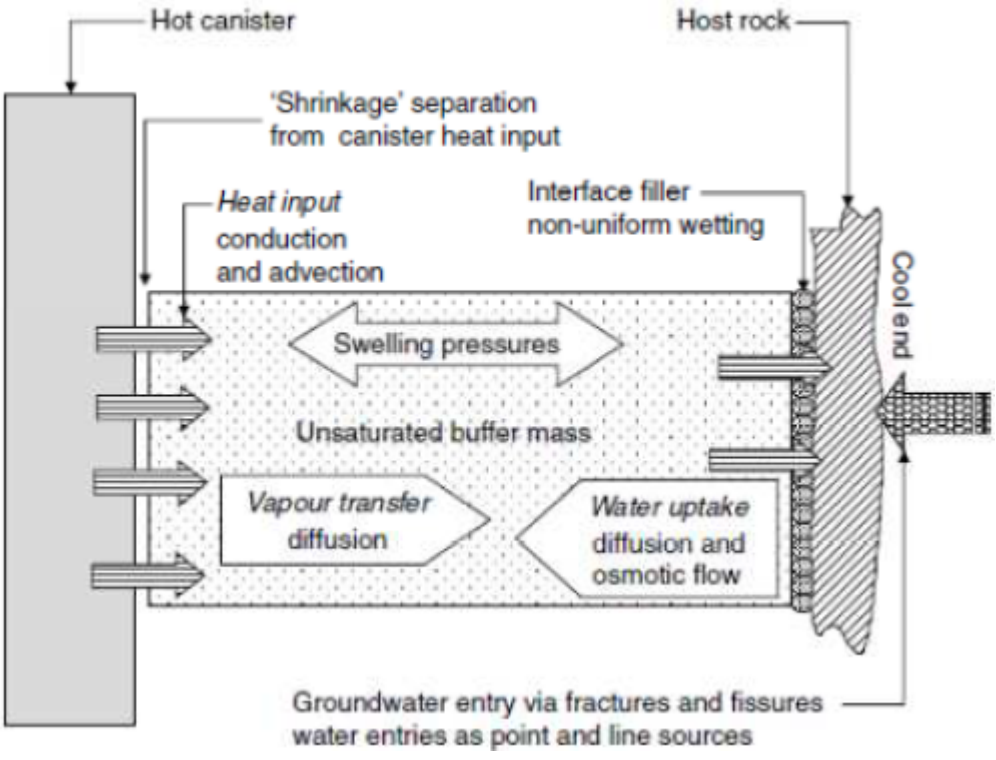

Figure 2.18 A schematic presentation of several processes occurring in an unsaturated porous medium in response to heating (Pusch and Yong, 2006)

Heat conduction transfers the heat from the waste canister to the host rock (Ewen and Thomas, 1987; Ewen and Thomas, 1989; Mitchell, 1993; Mitchell and Soga, 2005; Gens Solé et al., 2007). The applied thermal gradient generates the movement of the water vapour from the hotter towards the colder areas. The saturated host rock supplies ground water to compacted bentonite. An increase in the water content causes swelling of bentonite. Under confined condition, development of swelling pressure occurs.

Ewen and Thomas (1987, 1989), stated that the heat can be transported with the moving vapour in the form of latent heat. According to Villar et al. (1996), the geometry and power of the heater affects greatly the transient temperature distribution in contrast to the water content.

The high temperatures dissipating from the waste canister generates high vapour pressures near the heating zone. The overall pressure in the gas phase increases and an advective flux of vapour away from the heating element is created (Bear and Gilman, 1995). Pusch and Yong (2006) stated that the thermal gradient generated by the two different temperatures at the opposing ends triggers the water movement in the buffer material. The rise of temperature due to the waste canister decreases the capillary pressure and surface tension of water in the buffer material leading to an increase in the liquid phase. The result of this increase is a water flux away from the heat source to distribute the capillary pressure uniformly in the buffer material (Bear and Gilman, 1995). From the above observations it is concluded that the total transfer of water in the buffer material due to the thermal gradient includes both vapour and liquid water.

The thermal and hydraulic gradients encourage the water movement in compacted bentonites. Dissolved salts are carried by the liquid water by advection from the hydration zone. The concentration of the salts increases in the evaporation zone, producing a

diffusive flux of dissolved salts away from the heater (Gurr et al., 1952; Nassar and Horton, 1989; Villar et al., 2008; Cleall et al., 2011; Gómez-Espina and Villar, 2015). Advective and diffusive fluxes of transport may or may not be equal to each other. Once the advective and diffusive fluxes are not equal the concentration of salts near the heater increases until it reaches the solubility threshold and salt begin to precipitate (Bear and Gilman, 1995; Villar et al., 2008; Cleall et al., 2011; Gómez-Espina and Villar, 2015).

The solute transport in bentonites is affected by the chemical and mineralogical interactions, ion exchange reactions and transformation, dissolution and precipitation of minerals (Fernández et al., 2004; Cleall et al., 2007; Fernández and Villar, 2010; Villar et al., 2013; Gómez-Espina and Villar, 2015). Pusch and Yong (2006) stated that the transport rate of ions in clay depends on their concentration gradient and their diffusivity. The main mechanism governing the solute transport in highly compacted bentonites is diffusion due to the low hydraulic conductivity and smaller hydraulic gradients (Martın et al., 2000; Kozaki et al., 2001; Mitchell and Soga, 2005). With an increase in the dry density an increase in the surface diffusion of ions due to the better connectivity of the montmorillonite particles was noted (Kozaki et al., 2001). The temperature is the key variable that mostly influences the process of transport (Martín et al., 2000).

The solute diffusion process seems to have less effect on the sealing potential and the thermo-hydro-mechanical properties of the engineered barriers (Buil et al., 2010). During the solute transport processes the chemical dissolution/precipitation and exchange reaction occurs causing further change in solute concentrations (Fernández et al., 2004; Villar et al., 2008; Fernández and Villar, 2010; Gómez-Espina and Villar, 2010; Fernandez et al., 2012; Villar et al., 2013; Gómez-Espina and Villar, 2015). Further studies are required to investigate the heat, water and solute transfer processes in

compacted bentonites involving thermal and hydraulic gradients to improve the understanding on the subject.

2.9 Summary

The chapter presents a literature review on the behaviour of compacted bentonites as buffer and backfill materials in engineered barrier systems. The structure of montmorillonite and the microstructure of compacted bentonites are presented. The parameters that affect the swelling pressure of the compacted bentonite are reviewed. A detailed review of the various thermo-hydraulic testing apparatuses is presented. The mechanisms governing the mass, heat and solute transport in compacted bentonites are presented.

A review of the literature on the behaviour of compacted bentonites suggested that some aspects of their usage as buffer and backfill materials in the engineered barrier systems require further investigations. These aspects include: (i) the influence thermal gradient and thermal insulation type on the hydro-mechanical response of compacted bentonites, (ii) influence of thermo-hydraulic gradient involving high water injection pressure and high temperature on the thermo-hydraulic response of compacted bentonite, (iii) the influence of thermal gradients and thermo-hydraulic gradients (for temperatures below and above the 100 ℃) on the axial stress development at the opposite end of the heat source in compacted bentonites, (v) the influence of thermal gradients (for temperatures below and above the 100 °C on the solute transport in compacted bentonites, and (vi) influence of high temperature on the mineralogical changes.

CHAPTER 3.
MATERIALS AND METHODS

3.1 Introduction

This chapter presents the properties of the materials used in this investigation, the testing devices used and the test methods adopted for carrying out various laboratory tests. MX80 bentonite was used in the main experiments. Speswhite kaolin was used to perform calibrating the behaviour of the testing devices used. Sections 3.2 and 3.3 present the physical and chemical properties of MX80 bentonite and Speswhite kaolin. The suction - water content relationship of MX80 bentonite is presented in section 3.4. The testing devices used and their components are described in section 3.5. Additionally, Section 3.5 present the procedure adopted for preparing compacted specimens, testing methods, verification of the functionalities of the device accessories, the types of tests performed, and the procedure adopted for extracting specimens from the specimen mould after

completion of the tests. Section 3.6 presents the description of the post-mortem analyses (mineralogical and chemical tests) that were carried out on the extracted specimens. Section 3.7 summarises the work undertaken in this chapter.

3.2 Properties of MX80 bentonite used

MX80 bentonite was procured from TOLSA UK Ltd. (www.tolsa.com) for the research work. The initial water content, liquid limit and plastic limit of the bentonite were determined by following the procedures laid out in the British standards (BS 1377-2 1990). The initial water content, liquid limit and plastic limit of the bentonite were found to be 15.2%, 400% and 58 % respectively.

The specific gravity of soil solids was determined by following the procedure suggested in the British Standards (BS1377-2, 1990). Kerosene was used as the non-polar fluid to determine the specific gravity of the bentonite. The calculations of the specific gravity of the bentonite were performed with the application of the density correction factor for kerosene. The specific gravity of MX80 bentonite used in this study was found 2.8.

The specific surface area for the bentonite was determined by the ethylene glycol mono-ethyl ether (EGME) method (Heilman et al., 1965). The specific surface area for MX80 bentonite was found to be 654 m^2/g.

The ammonium acetate method was used to determine the total and fractional cations present in the bentonite (Klute, 1986; Sparks et al., 1996). The bentonite was found to contain: Na^+ (67.12 meq/100g), K^+ (1.95 meq/100g), Ca^{2+} (44.67 meq/100g) and Mg^{2+} (14.35 meq/100g). The type and amount of soluble ions were determined by

saturation extract method using water that enabled calculating the fractional exchangeable cations as: Na^{+}- 44.83 meq/100g, K^{+} - 1.20 meq/100g, Ca^{2+} - 42.11 meq/100g, and Mg^{2+} - 3.29 meq/100g. The total cations exchange capacity of the bentonite was found to be 91.43 meq/100g.

To determine the mineralogy of the bentonite, the X-ray diffraction analysis was undertaken. The X-ray diffraction utilises the Bragg's law and determines the specific minerals based on the relationship between the intercept angle and the c-axis spacing (Mitchell and Soga, 2005). Two grams of MX80 bentonite was obtained after sieved through a 63 μm sieve at hygroscopic water content and treated with ethylene glycol. The treated material was then placed on a glass plate and inserted in the goniometer where it was bombarded with X-rays. Figure 3.1 shows the Philips automated diffractometer used in this study.

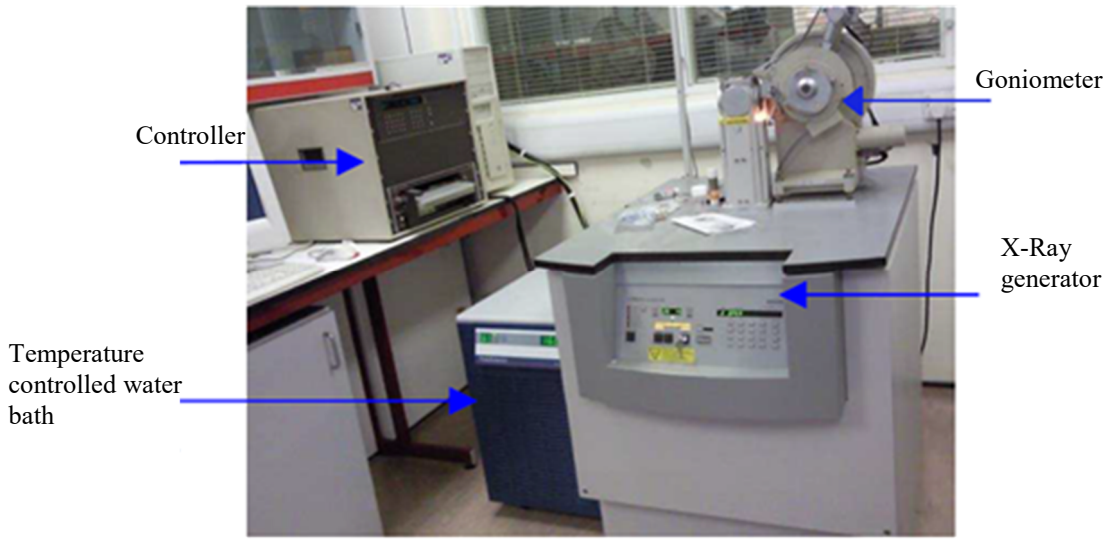

Figure 3.1 Philips automated diffractometer PW1710 used in this study

The minerals were identified from their respective peaks, and the semi-quantitative analysis determined their percentages (Fig. 3.2). The bentonite was found to

contain 82% of montmorillonite, 12% of quartz and 16% of other minerals (e.g. cristoballite, feldspars etc.).

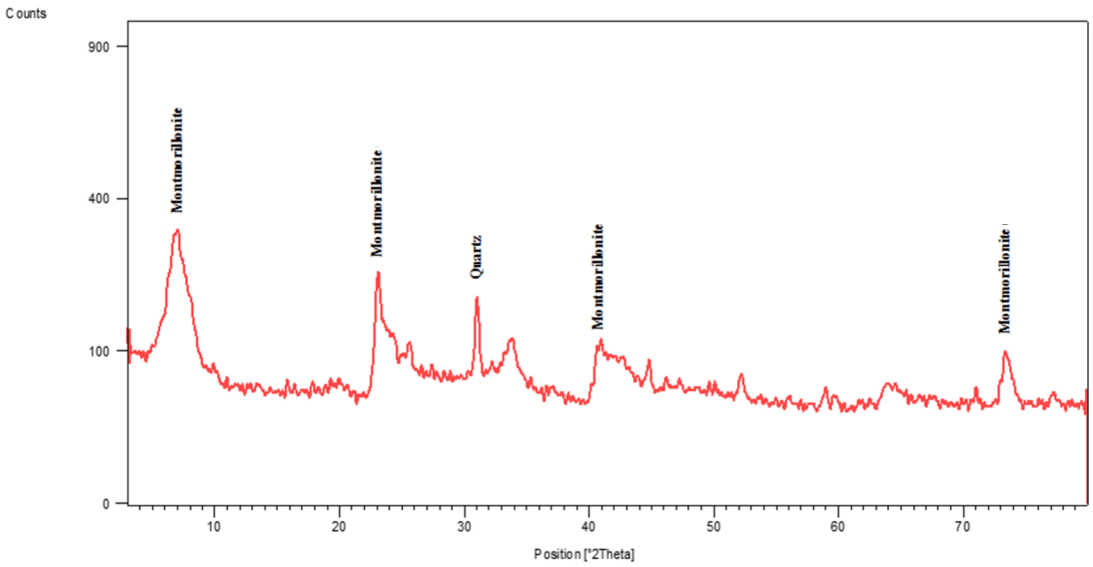

Figure 3.2 X-ray diffraction chart for MX80 bentonite used in this study

3.3 Experimental program for non-isothermal and non-isothermal-hydraulic tests

The main objectives of the investigation was to study in detail the influence of very high temperature gradient on the thermal and hydraulic behaviour of compacted bentonites. Two types of thermo-hydraulic column cells were used for this purpose.

For the tests at 85 °C, the thermo-hydraulic column cell proposed by Tripathy et al. (2015) was used, whereas a new thermo-hydraulic column cell was fabricated and used for the tests at 150 °C. The descriptions of these two devices are presented in the following sections.

3.3.1 Thermo-hydraulic column cell (for tests at 85 °C)

A schematic diagram of the thermo-hydraulic column cell used by Tripathy et al. (2015) is shown in Fig. 3.3. The cell was used for the tests at a temperature of 85 °C. The cell enabled applying both thermal and hydraulic gradients. The cell facilitated measuring the relative humidity and the temperature at predetermined locations along the depth of specimens and the axial pressure at the top of the specimens.

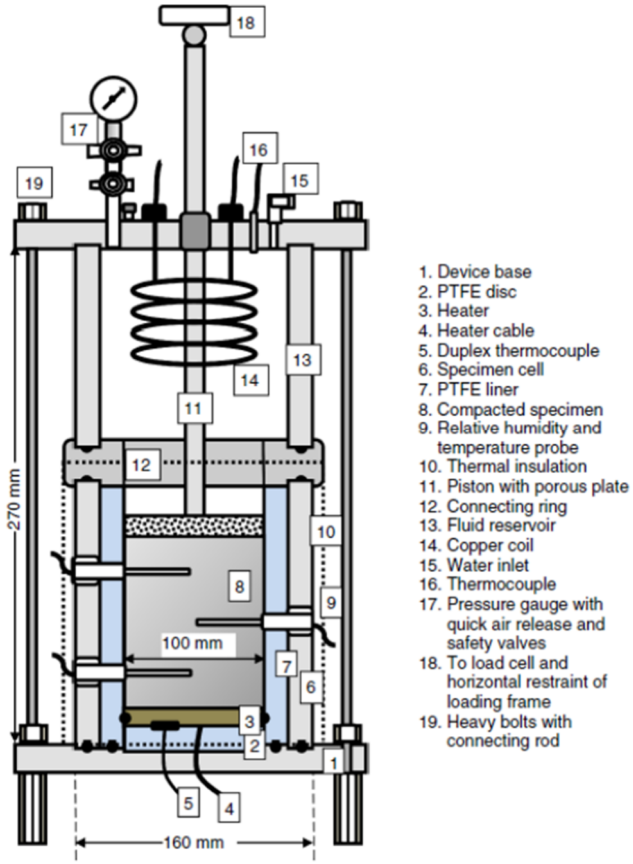

Figure 3.3 A schematic of the thermo-hydraulic column cell used in this at 85 °C. (Tripathy et al., 2015)

The main components of the cell are a stainless steel base, a central section (100 mm diameter and 140 mm high), a connecting ring, and a top part. A polytetrafluoroethylene (PTFE) forms the liner of the central section for reducing the heat

loss through the outer wall of the cell during tests. A metal heater is used to apply thermal loading (85 °C) at the bottom end of the specimen. A dual thermocouple is attached at the centre of the heater. One of the thermocouple is connected to the heater controller and other one is connected to a data logger. The thermocouple connected to the heater controller maintains the temperature of the metal heater at 85 °C. The other thermocouple measures the actual temperature on the surface of the heater. A loading plunger fitted with a metal porous of solid disc rests on top of the specimens.

The central section of the cell contains three holes each separated by a distance of 20 mm but staggered by an angle of 120°. Similarly, three holes were drilled on the specimens, aligned with the holes in the central section of the cell, for accommodating the relative humidity and temperature measurement probes. The relative humidity and temperature measuring probes were manufactured by Vaisala, Helsinki, Finland. The accuracy of the probes used was ±1.0 % for the range of relative humidity between 0 to 100 % and ±1.0 °C for the range of temperature measurement between -40 and 100 °C.

3.3.2 Specimen preparation and testing methods (for tests at 85 ℃)

Four independent tests were carried out on compacted bentonite specimens using the thermo-hydraulic column cell. The dry density of the compacted specimens was kept same for ensuring reproducibility of the test results. Cylindrical specimens were prepared by statically compacting bentonite powder (water content = 15.2 %) to a targeted dry density of 1.65 Mg/m^3 in four layers, each 20 mm thick. Each layer was subjected to a static load of about 90 kN. The height and diameter of the specimens were 80 and 100 mm, respectively. Compaction of bentonite powder was carried out inside the central

section of the cell by static compaction method and using a high-capacity compression testing machine (see Fig. 3.4).

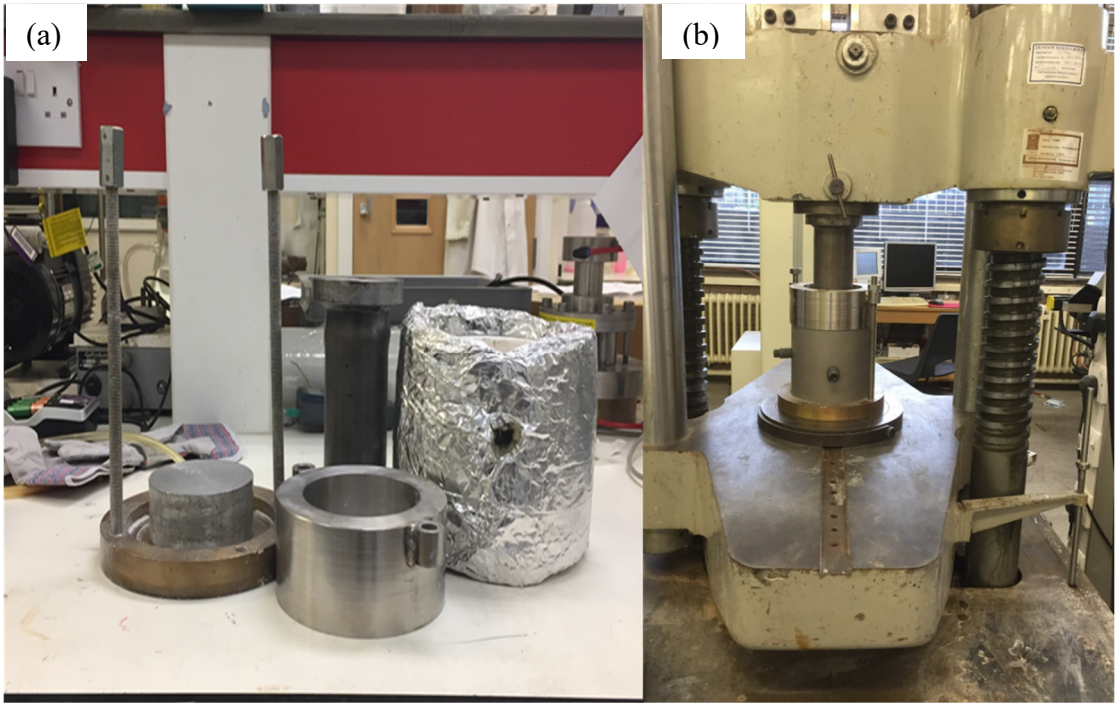

Figure 3.4 (a) Photograph of the compaction mould used and (b) photograph showing the static compaction process

Prior to preparing the specimens, the inner surfaces of the central part of the cell were lubricated with silicon grease. Removal of the applied compaction stress caused an axial expansion of the bentonite specimens. The dry densities of the compacted specimens were calculated based on the mass of compacted specimens and revised heights. The revised initial dry densities of the specimens were found to be similar (1.65 ± 0.1 Mg/m^3).

Prior to the tests, the column cell was transferred to a 50 kN capacity load frame. The relative humidity and temperature measurement probes were inserted through the predrilled holes. High temperature grease was applied at the junctions between different sections of the cell to prevent the vapour leakage. At the end the cell was not 100% as the intrusive method of installing the Relative humidity and Temperature probe creates small

paths from which the vapour can dissipate. The cell was covered with thermal insulator. Two types of external thermal insulations were used, such as 20 mm thick rock wool covered with duct tape and 40 mm thick rock wool with reflective tape. The load cell was placed on top of the plunger and restrained against any movement.

During the thermal gradient tests, the compacted bentonite specimens were heated to a temperature of 85 °C at the bottom end. Temperature control at the top end of the specimens was achieved via circulation of water within an internal copper coil. A heating/refrigerating (heater/cooler) water circulator (not shown) was used to control the temperature of the circulating water within the coil. The heating/refrigerating circulator had a proportional integral-derivative (PID) controller and an adjustable over heating cut out. The empty space on top of the loading plunger was filled with deionized water. During the thermal gradient tests, the temperature of the water suspended at the top section of the THM cell was maintained at 25 °C by circulating water through the coil. The transient temperature, relative humidity and axial pressures were monitored during this test phase. During the thermo-hydraulic tests, in addition to the temperatures applied during the thermal tests, deionized water was supplied from the top end of the specimens at a pressure of 600 kPa. The empty space on top of the loading plunger was filled with deionized water and the specimens were allowed to hydrate. Unfortunately, this experimental setup is not able to measure the amount of water flowing in the system. The relative humidity and the axial pressures were monitored during the thermo-hydraulic tests. The pressure gauge and quick release valve were used to release hydraulic pressure when the thermo-hydraulic tests were terminated.

Table 3.1 presents test conditions and duration of the tests. After termination of the tests, post- mortem analyses were carried out. The descriptions of the post-mortem analyses are presented in section 3.6.

Table 3.1 Experimental program for thermal and thermo-hydraulic tests

Test no.	Type of test	Initial conditions			Insulation type	Test duration (days)	Information gathered					
							During Tests			After the tests		
		w (%)	ρ_d (Mg/m^3)	S_r (%)			T (℃)	RH (%)	p (kPa)	w (%)	Mineralogical composition	Concentration of cations
1.	Thermal	15.2	1.65	45.8	20mm rockwool with duct tape	90	Y	Y	Y	Y	Y	Y
2.		15.2	1.65	45.8	40mm rockwool with reflective tape	160	Y	Y	Y	Y	Y	Y
5.	Thermo-hydraulic	15.2	1.65	45.8	40mm rockwool with reflective tape	285	Y	Y	Y	Y	Y	Y
6.		15.2	1.65	45.8	40mm rockwool with reflective tape	285	Y	Y	Y	Y	Y	Y

w – Water content, ρ_d – Compacted dry density, S_r – Degree of saturation, T – Temperature, RH – Relative humidity, p – axial stress

3.3.3 Thermo-hydraulic column cell (for tests at 150 ℃)

A schematic diagram of the thermo-hydraulic cell is shown in Fig 3.5. The cell was used for the tests at a temperature of 150 °C. The cell enabled applying both thermal and hydraulic gradients. The cell facilitated measuring the relative humidity and the temperature at predetermined locations along the depth of specimens and the axial pressure at the top of the specimens.

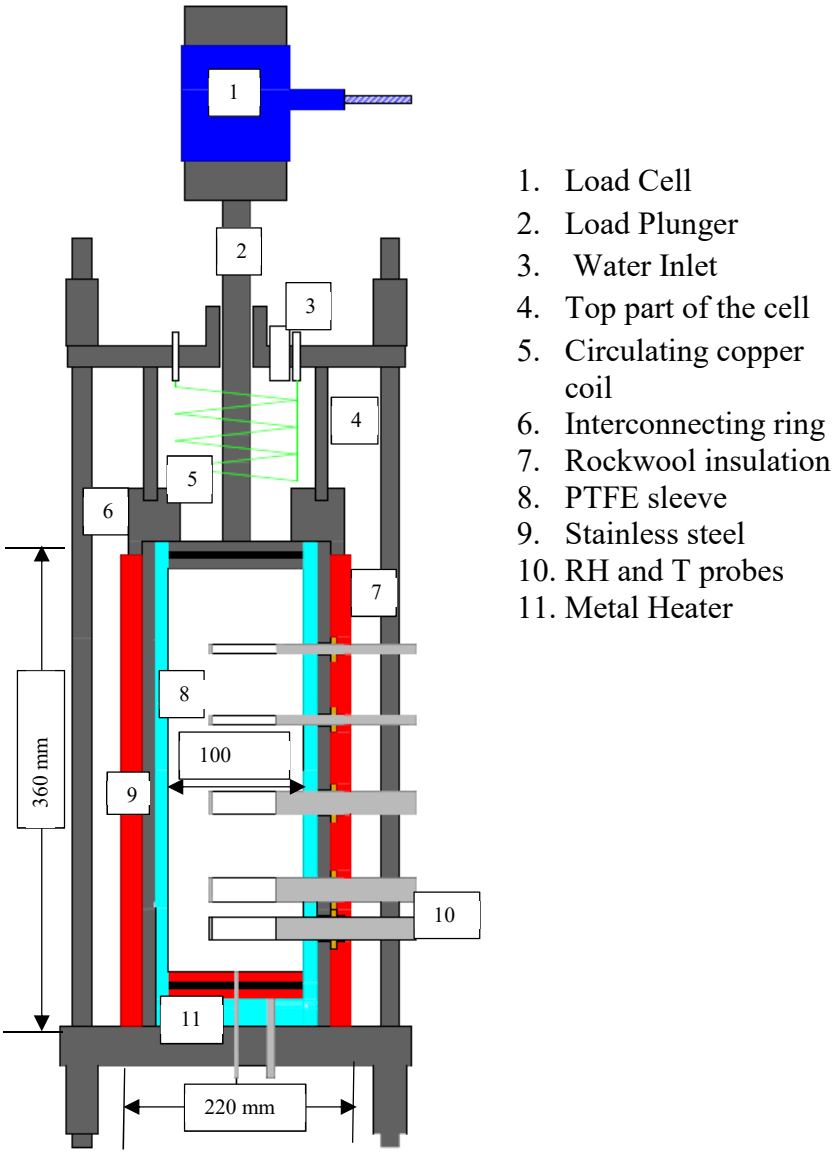

Figure 3.5 A schematic of the high temperature thermo-hydraulic column cell used for the tests at 150 °C.

The design of this cell based on the existing THM cell used for lower temperatures. The main components of the cell are a stainless steel base, a central section (100 mm diameter and 360 mm high), a connecting ring, and a top part. A polytetrafluoroethylene (PTFE) forms the liner of the central section for reducing the heat of the cell during tests. A metal heater is used to apply thermal loading (150 °C) at the bottom end of the specimen. A dual thermocouple is attached at the centre of the heater. One of the thermocouple is connected to the heater controller and other one is connected to a data logger. The thermocouple connected to the heater controller maintains the temperature of the metal heater at 150 °C. The other thermocouple measures the actual temperature on the surface of the heater. A loading plunger with a metal porous or solid disc rest on top of the specimens. Figure 3.6 shows a photograph of the main components of the thermo-hydraulic column.

The central section of the cell contains five holes each separated by a distance of 60 mm the first four. The last hole is placed in a distance of 40 mm from the heater. The holes are staggered by an angle of 90°. Similarly, five holes were drilled on the specimens, aligned with the holes in the central section of the cell, for accommodating the relative humidity and temperature measurement probes. The relative humidity and temperature measuring probes were manufactured by Vaisala, Helsinki, Finland. The accuracy of the probes (HMP110) used in case of the tests at 85 °C was ±2.5% and ±3.5% for the range of relative humidity between 0 to 90% and 90 to 100%, respectively. The accuracy of temperature sensor in this case was ±0.4 °C for the range of temperature measurement between 40 and 80 °C. The accuracy of the probes (HMT315) used in case of the tests at 150 °C was ±(1.5 + 0.015 x reading)% for the range of relative humidity between 0 to 100% and for an operating temperature range of – 40 to 180 °C. The accuracy of the temperature sensor in this case was ±0.2 °C.

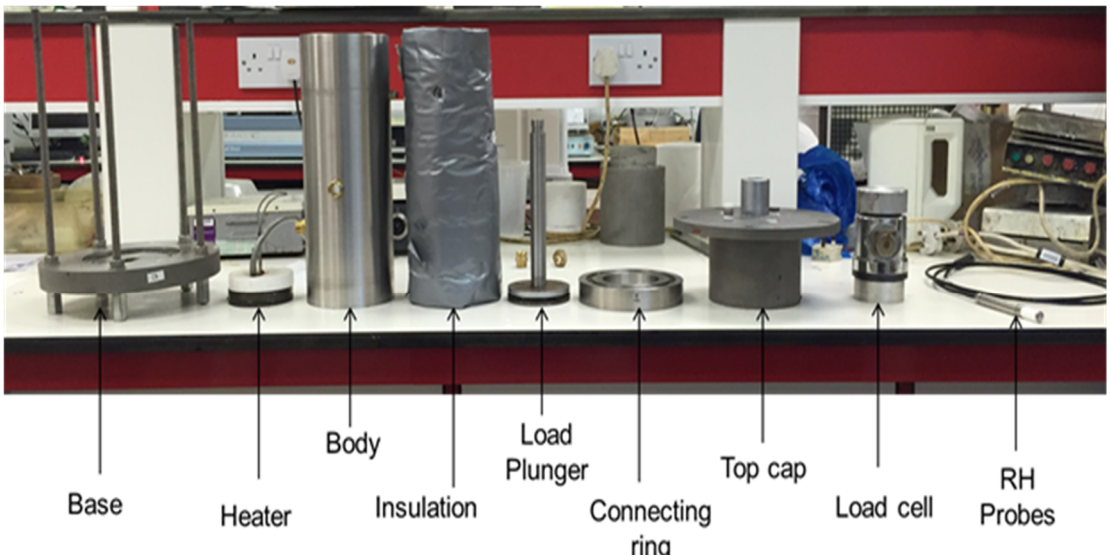

Figure 3.6 Photograph showing the main components of the thermo-hydraulic column cell for tests at 150 °C

3.3.4 Specimen preparation and testing methods (for tests at 150 ℃)

Five independent tests were carried out on compacted bentonite specimens using the thermo-hydraulic column cell shown in Fig. 3.5. The dry density of the compacted specimens was kept same for ensuring reproducibility of the test results. Cylindrical specimens were prepared by statically compacting bentonite powder (water content = 15.2 %) to a targeted dry density of 1.65 Mg/m^3 in 10 layers, each 30 mm thick. Each layer was subjected to a static load of about 120 kN. The height and diameter of the specimens were 300 and 100 mm, respectively. Compaction of bentonite powder was carried out inside the central section of the cell by static compaction method and using a high-capacity compression testing machine (Fig. 3.7).

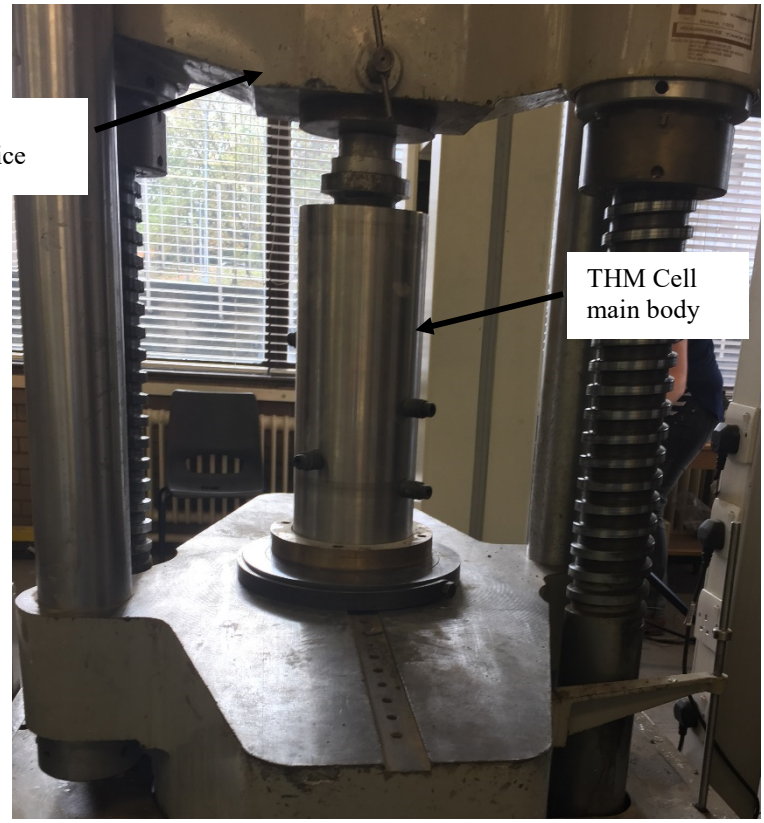

Figure 3.7 Photograph showing the static compaction process

Prior to preparing the specimens, the inner surfaces of the central part of the cell were lubricated with silicon grease. Removal of the applied compaction stress caused an axial expansion of the bentonite specimens. The dry densities of the compacted specimens calculated by using the mass of compacted specimens and their revised heights. The revised initial dry densities of the specimens were found to be similar (1.65.± 0.1 Mg/m^3).

Prior to the tests, the column cell was transferred to a 50 kN capacity load frame. The relative humidity and temperature measurement probes were inserted through the predrilled holes. High temperature grease was applied at the junctions between different sections of the cell to prevent the vapour leakage. The cell was covered with thermal insulator. Two types of external thermal insulations were used, such as 20 mm thick rock wool covered with duct tape and 40 mm thick rock wool with reflective tape. The load cell was placed on top of the plunger and restrained against any movement.

During the thermal gradient tests, thermal loading of 150 °C applied at the bottom end. Temperature control at the top end of the specimens was achieved via circulation of water within an internal copper coil. A heating/refrigerating (heater/cooler) water circulator (Fig 3.8) was used to control the temperature of the circulating water within the coil. The heating/refrigerating circulator had a proportional integral-derivative (PID) controller and an adjustable over heating cut out.

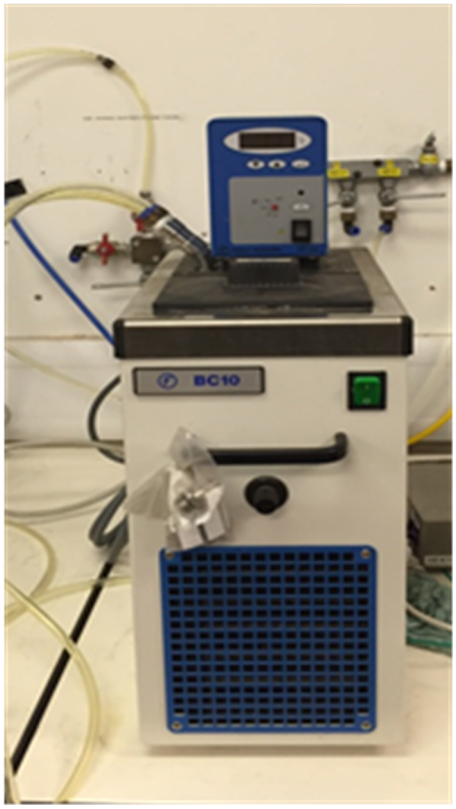

Figure 3.8 Heating/refrigerating water circulator

During the thermal gradient tests, the temperature at the top of the cell was maintained at 25 °C by circulating water through the coil. The transient temperature, relative humidity and axial pressures were monitored during this test. During the thermo-hydraulic tests, in addition to the thermal loading, deionized water was supplied at the top end of the specimens at an injection pressure of 600 kPa and the specimens were allowed to hydrate. The relative humidity and the axial pressures were monitored during the

thermo-hydraulic tests. The pressure gauge and quick release valve were used to release hydraulic pressure when the thermo-hydraulic tests were terminated.

Table 3.2 presents test conditions and duration of the tests. After termination of the tests, post- mortem analyses were carried out. The descriptions of the post-mortem analyses are presented in section 3.6.

3.3.5 Verification of temperature and relative humidity probes

The relative humidity and temperature probes were calibrated prior to using them in the actual tests. Calibration of the temperature was performed at three temperatures, such as 25, 85 and 120 °C. The response of the relative humidity sensors was verified with the aid of saturated potassium chloride solution. Potassium chloride (KCl) solutions were prepared in 1000 ml glass flasks. Figure 3.9 shows a relative humidity and temperature probe inside the flask during the calibration tests. The insertion point of the probe was sealed air-tight during the calibration tests. The relative humidity in the flask corresponding to saturated potassium chloride solution would be 85% at a temperature 25 °C (Ulery and Drees, 2008). The relative humidity and temperature readings of the solution were monitored with elapsed time.

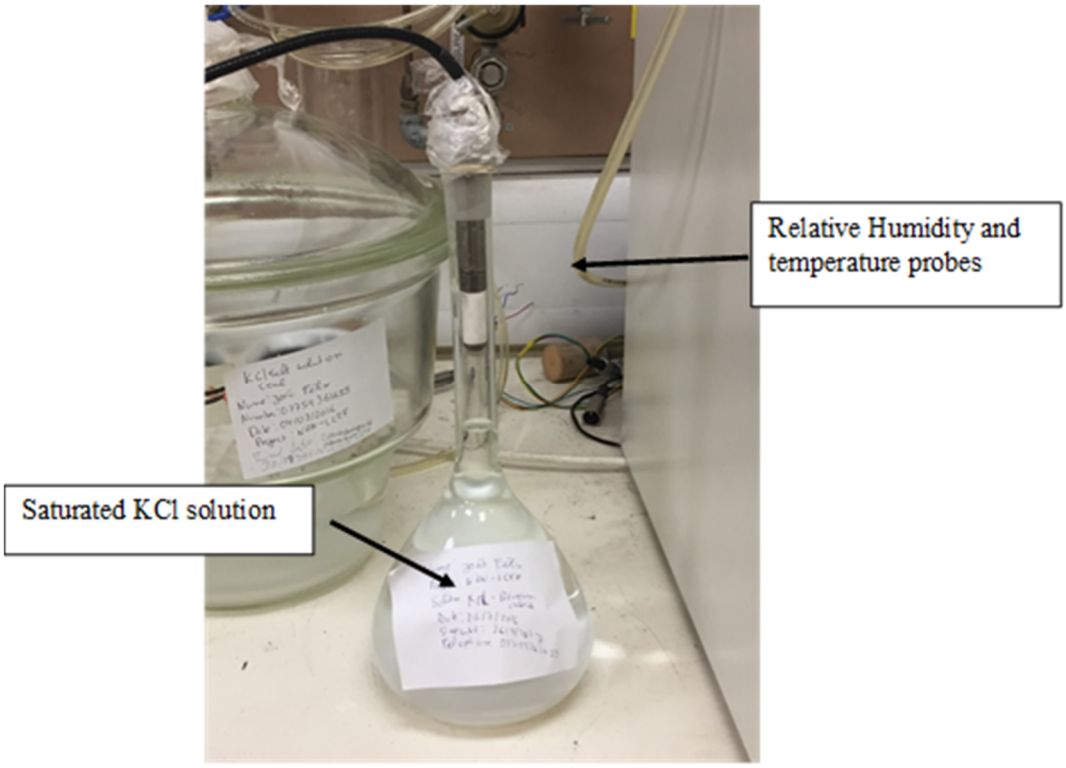

Figure 3.9 Photograph showing the calibration of a relative humidity probe

Figure 3.10 shows the measured relative humidity of the solution with elapsed time. The standard relative humidity of the solution is shown in Fig. 3.10. The values of the relative humidity during the equilibrium of the probes is within the ±1.0% range given by the manufacturer. The calibration process was repeated before each test.

.

Table 3.2 Experimental program for thermal and thermo-hydraulic tests

Test no.	Type of test	Initial conditions			Insulation type	Test duration (days)	Information gathered					
							During Tests			After the tests		
		w (%)	ρ_d (Mg/m^3)	S_r (%)			T (°C)	RH (%)	p (kPa)	w (%)	Mineralogical composition	Concentration of cations
3.	Thermal	15.2	1.65	45.8	20mm rockwool with duct tape	140	Y	Y	Y	Y	Y	Y
4.		15.2	1.65	45.8	40mm rockwool with reflective tape	190	Y	Y	Y	Y	Y	Y
7.	Thermo-hydraulic	15.2	1.65	45.8	40mm rockwool with reflective tape	90	Y	Y	Y	Y	Y	Y
8.		15.2	1.65	45.8	40mm rockwool with reflective tape	300	Y	Y	Y	Y	Y	Y
9.		15.2	1.65	45.8	40mm rockwool with reflective tape	180 (on-going)	Y	Y	Y	Y	Y	Y

w – Water content, ρ_d – Compacted dry density, S_r – Degree of saturation, T – Temperature, RH – Relative humidity, p – axial stress

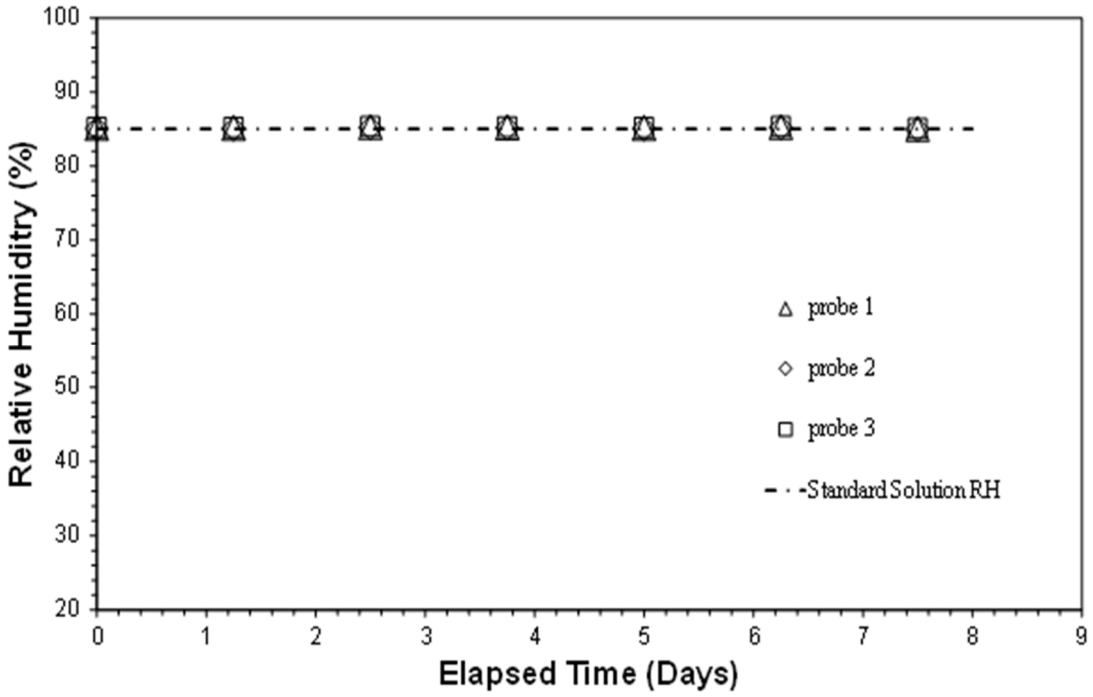

Figure 3.10 Calibration of the relative humidity probes

The accuracy of the temperature sensors in the probes were verified with the aid of a laboratory oven. The probes were inserted in the oven from the top. The entry point of the probe was sealed for air-tight. The oven temperature was set at the 155 °C. Figure 3.11 shows the arrangement of the probe in the oven.

The temperature readings were monitored with elapsed time. The equilibrium temperature of the probe was within the ±1.0 °C range given by the manufacturer. The measured temperature agreed well with the temperature within the oven. The calibration process was repeated before each test.

Figure 3.11 Photograph showing the calibration of the temperature probe

3.3.6 Thermal expansion of the Thermo-hydraulic column cell

Prior to the commencements of the Thermal and thermohydraulic tests the thermal expansion of both existing and new thermohydraulic column cells investigated. The most crucial part in the column design regarding to the thermal expansion is the PTFE liner which is in direct contact with the compacted bentonite specimen.

The expansion of the PTFE liner tested with the following procedure. Dummy thermal tests conducted with two different types of samples. The first sample was made out of the same PTFE as the cell's liner and the second sample made out of Speswhite Kaolin. The Speswhite kaolin chosen as a control sample material for its low expansibility during the thermal loading. Samples with 80 mm height and 100 mm diameter used for thermal tests at 85 °C whereas for the 150 °C the sample are 300mm tall and have 100mm diameter. The samples inserted in the thermohydraulic columns described in sections 3.3.1 and 3.3.3. During the thermal tests the axial pressure exerted from the samples during their thermal loading monitored with the aid of a plunger and a load cell as in the thermal and thermohydraulic tests described above. The duration of each test was 24 hours and it stopped once it ensured that the axial pressure equilibrate. Figures 3.12 and 3.13 show the axial pressures generated from the PTFE and Speswhite kaolin samples during the thermal expansion tests.

From the following graphs demonstrate that the thermal loading has a limited effect on the Speswhite Kaolin whereas the PTFE sample shows a significant increase in its axial pressure for the same testing conditions. From the two tests it is possible to understand that the expansion of the PTFE liner has minimum effect on the recorded axial pressure as it is primarily related to the respective sample's material.

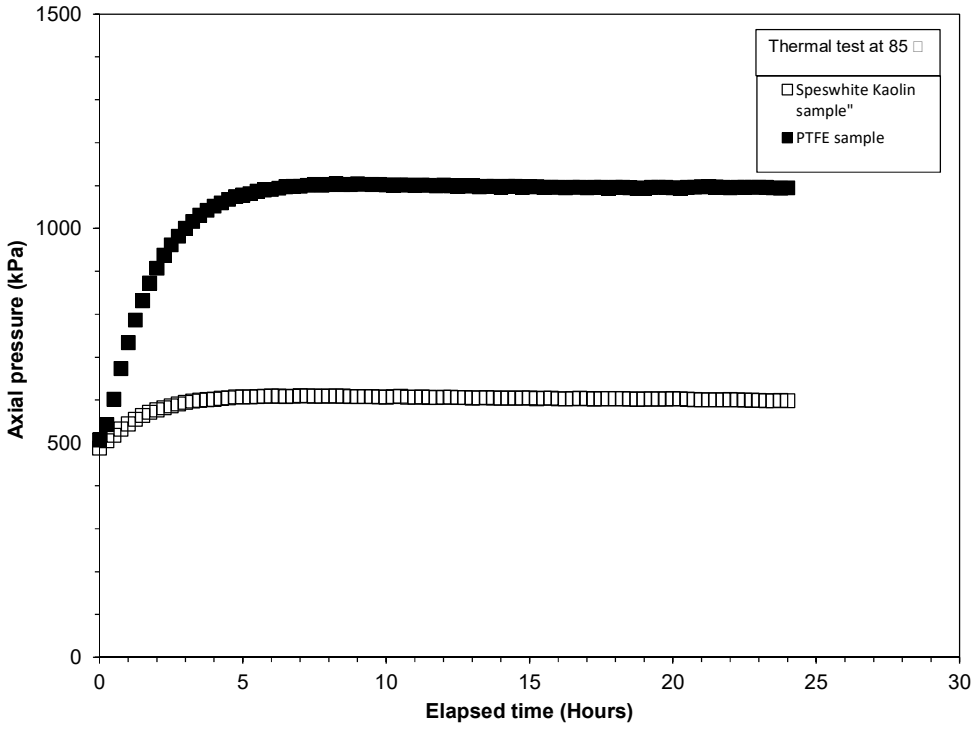

Figure 3.12 Thermal expansion test at 85 °C

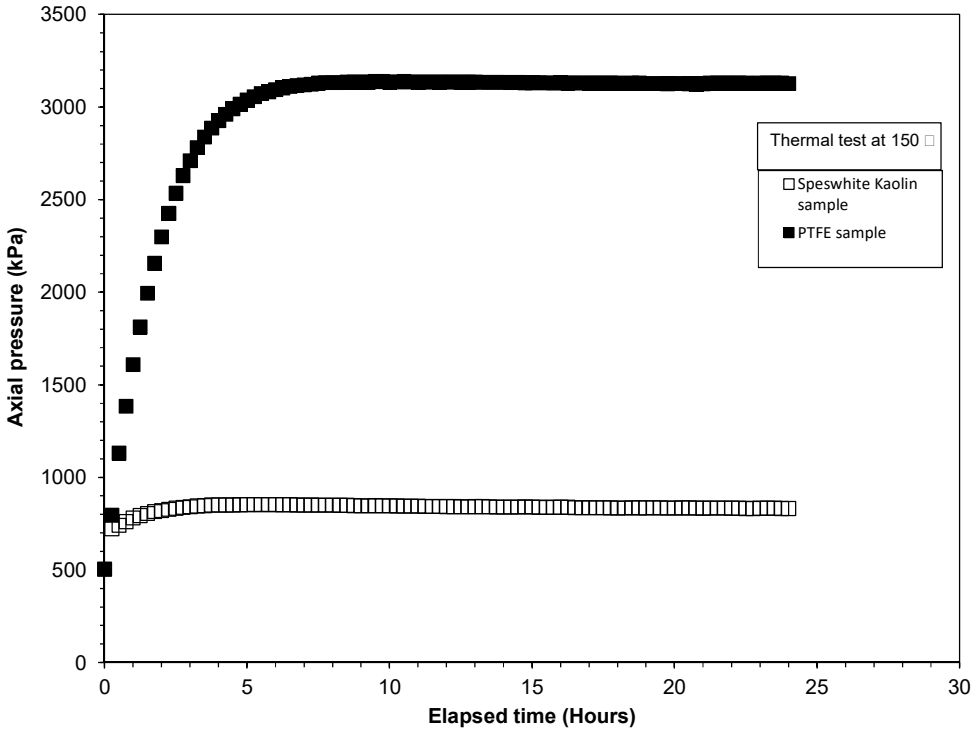

Figure 3.13 Thermal expansion test at 150 °C

3.3.7 Specimen extrusion following non-isothermal and non-isothermal hydraulic tests

Following the completion of the tests shown in Tables 3.1 and 3.2, the compacted bentonite specimens were extruded form the thermo-hydraulic column cells to conduct post-mortem analysis. For the thermo-hydraulic tests, water was drained from the top of the cells. The electric heater and the water circulator bath were switched off. The load cell was disconnected from the load plunger. The cell was transferred from the load frame and placed on a working bench. The top part and the interconnecting ring were detached from the cell. The load plunger was detached from the top of the specimen. The relative humidity and temperature probes were extruded from the specimen with extreme care to avoid any damages as they needed to be reused. During the thermo-hydraulic tests it was extremely difficult to extrude the relative humidity and temperature probes located at the hydrated zones of the specimens. To minimise any damages on the cast heater it was extruded along with the bentonite specimen with the help of a hydraulic extruder (Fig.3.14).

During the extrusion process for the specimens that were tested at 85 °C, the top end of the specimen was placed on the piston of the extruder, whereas the other end was in contact with the reaction plate. The hydraulic jack was used to extrude the heater, PTFE disk and the specimen from the mould.

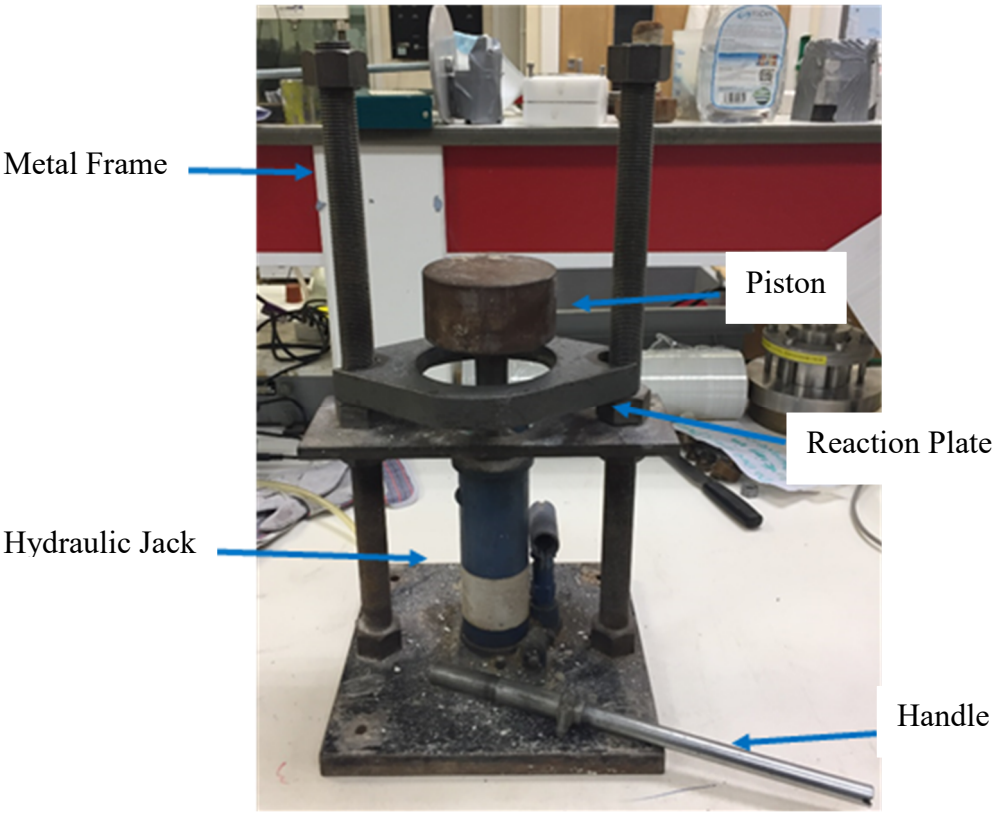

Figure 3.14 Photograph showing the hydraulic extruder used for extruding specimens after tests

For the extrusion process of the specimens that were tested at 150 deg. cent., a high capacity extrusion device was used to extract the bentonite specimens (Fig 3.15). The top side of the specimen rested on a 350 mm thick cylindrical spacer. The central section restrained axially with the aid of the reaction plate and some wooden blocks. An increase in the load on the spacer enabled extruding the heater, PTFE disc and the bentonite specimen from the mould.

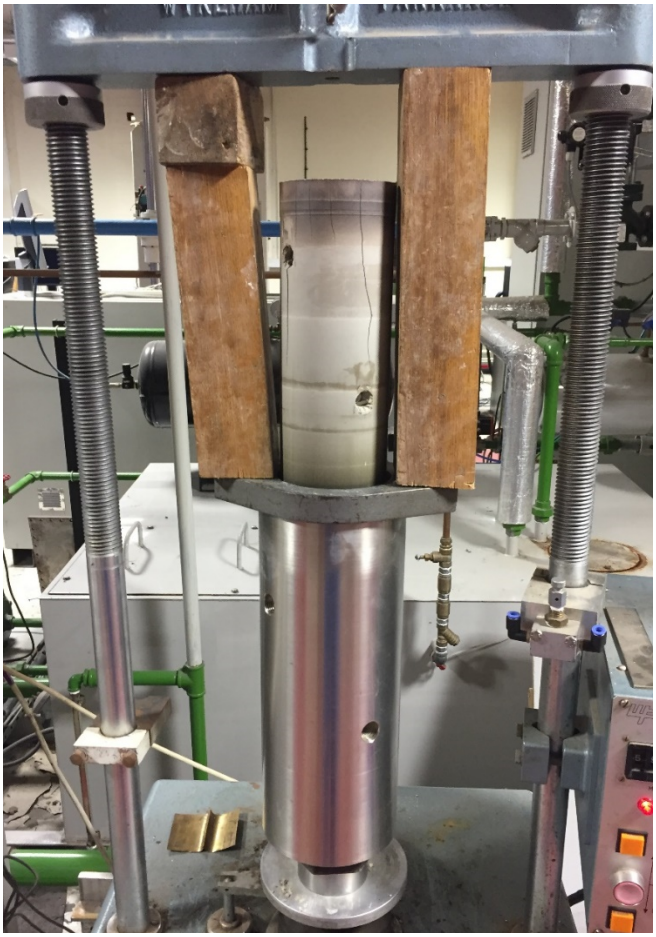

Figure 3.15 Photograph showing the extrusion of the bentonite specimen from the high temperature thermo-hydraulic column cell

3.4 Post-mortem analysis of extruded bentonite specimens

Following the extrusion, the bentonite specimens were analysed to investigate the water content, dry density, mineralogical composition and soluble cations concentration along the depth of the specimens. The specimens were sliced into 20 mm thick pieces. A cutting frame was used to securely cut the material for the desired thickness (Fig. 3.16). A portion of each slice was oven dried and grounded in powder with a mortar and a pestle. The bentonite powder was dry sieved using a 63 μm sieve

and stored in air-sealed plastic bags along with the other portions from the same depth of the specimen for further analyses (see Fig. 3.17).

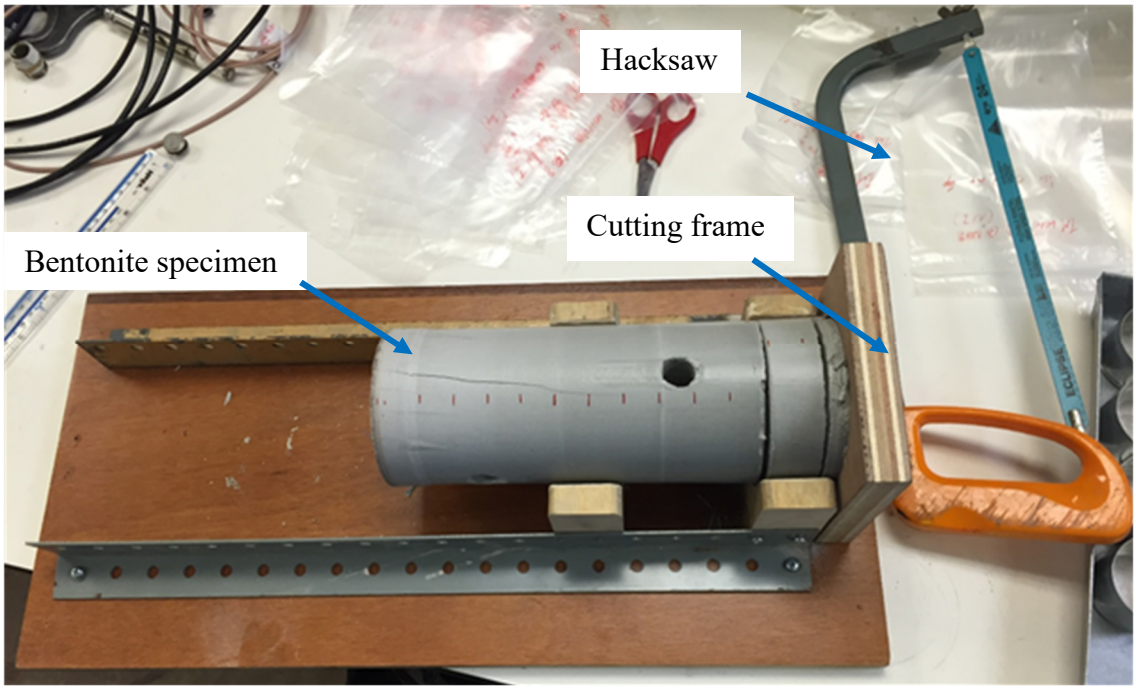

Figure 3.16 Cutting frame and bentonite specimen

Figure 3.17 Bentonite specimens stored in airtight plastic bags

3.4.1 Water content and dry density

The water content of each slice was determined by following the procedure laid out in the British standards (BS 1377-2 1990). The volume of each slice was measured using the molten wax method (ASTM-D, 4943-08-2008). The volume measurements were carried out in duplicate and the average value were considered for the analysis. The dry density and degree of saturation of each slice were calculated using the volume – mass relationships from the measured water content and volume of each slice.

3.4.2 X-ray diffraction analysis

The powder from each slice was subjected to x-ray diffractometer analysis to determine any possible mineralogical changes that have occurred in the non-isothermal and non-isothermal hydraulic tests. The procedure adopted for x-ray diffraction test is described in section 3.1. Each powder specimen was tested under three conditions. The conditions were undried, dried and treated with ethylene glycol.

3.4.3 Soluble cations

The soluble cations concentration was measured with the aqueous extraction technique. 1 gram of oven dried bentonite powder from each slice was mixed with 10 ml of distilled water. The sample mixtures were placed in a reciprocating horizontal mechanical shaker and were shaken for 24 hours (Fig 3.18). Following the shaking process, mixtures were transferred to 50 ml centrifuge tubes and centrifuged to separate the supernatant solutions from the bentonite paste.

Figure 3.18 Reciprocal shaker and sample flasks

The supernatant solution were collected and placed in a one litre capacity water extraction flask. A Buchner funnel was fitted with a Whatman no.42 filter paper and connected to the water extraction flask. The bentonite paste collected from the centrifuge tube was placed on top of the filter paper. The Buchner funnel was fitted with a vacuum supply. The sample paste was filtered with a 0.45 µm filter. The filtered solution with the supernatant solution from the centrifuge was collected and stored for further chemical analysis.

The filtered solutions were tested to find the concentrations of the soluble cations for each slice. The concentrations of Na^{+}, Ca^{2+}, Mg^{2+} and K^{+} were determined with the Inductively Coupled Plasma Optical Emission Spectroscopy (ICP-OS) (Fig. 3.19).

Figure 3.19 Perkin Elmar Optima-2100 DV Inductively Coupled Plasma Optical Emission Spectroscopy (ICP-OES)

3.5 Summary

The physical and chemical properties of the MX80 bentonite used in this study are presented in this chapter. The liquid limit, plastic limit, shrinkage limit, specific gravity, specific surface area, cations exchange capacity and mineralogical components are presented.

The design and fabrication of cells for non-isothermal and non-isotherm hydraulic tests are presented. The procedures followed for specimen preparation, verification tests for the relative humidity and temperature probes, extrusion of the specimens after the completion of the non-isothermal and non-isothermal hydraulic tests, and post-mortem analysis have been presented.

CHAPTER 4.
EFFECT OF TEMPERATURE GRADIENTS ON THERMO-HYDRO-MECHANICAL BEHAVIOUR OF COMPACTED BENTONITE

4.1 Introduction

A number of large scale laboratory and in-situ experimental investigations, under various boundary conditions were carried out in the past to study the coupled thermo-hydro-mechanical behaviour of compacted bentonites. Studies were conducted on compacted bentonites for temperatures above and below the 100 °C by simultaneous application of temperature and hydraulic pressure (Börgesson et al., 2001; Cuevas et al., 2002; Pintado et al., 2002; Villar and Lloret, 2004; Singh, 2007; Villar and Lloret, 2007;

Villar et al., 2008; Villar and Gómez-Espina, 2008; Villar and Lloret, 2008; Villar et al., 2008; Åkesson et al., 2009; Gens et al., 2009; Fernández and Villar, 2010; Gómez-Espina and Villar, 2010; Bag, 2011; Gómez-Espina and Villar, 2015). In many of the cases, variations of the temperature and relative humidity with elapsed time were monitored along the depth of the compacted bentonite specimens. In a few cases, the development of axial pressure due to the application of thermal and thermo-hydraulic gradients for temperatures less than 100 °C was also monitored. After the termination of the tests, changes in the dry density, the water content, the degree of saturation and the concentration of anions and cations were determined. At this stage, studies concerning the influence of temperatures above 100 °C on the variations of the axial pressure, temperature, relative humidity (suction), water content, dry density, degree of saturation and concentrations of ions, are limited. The main objective of this chapter is to bring out the influence of thermal gradients with temperatures above and below 100 °C on the thermo-hydro-mechanical response and variations of volume-mass properties of compacted bentonite specimens. The influence of coupled thermo-hydraulic gradients on the behaviour of compacted bentonites is presented in Chapter 5.

Section 4.2 presents the experimental program that was undertaken for the study. Section 4.3 presents the temperature and relative humidity variations measured at predetermined levels along the length of the bentonite specimens during the non-isothermal tests at high temperatures. The thermal gradients in these tests involved applying either 85 or 150 °C at the bottom end of the specimens while maintaining a temperature of 25 °C at the opposite end. The axial pressures generated during the tests are presented. The profiles of water content, dry density, degree of saturation and suction after termination of the tests are presented. Section 4.4 summarises the key findings derived from this chapter.

4.2 Experimental program

The devices used for carrying out the non-isothermal tests on compacted bentonites at temperatures of 85 and 150 °C are presented in chapter 3 (Figs. 3.3 and 3.5). The procedure adopted for preparing compacted specimens and experimental methods are described in Chapter 3 (Section 3.5). Tables 3.1 and 3.2 present the experimental program followed for the non-isothermal tests.

In total four tests were carried out. The dry density of the compacted bentonite specimens was 1.65 Mg/m^3. The applied temperature at the bottom of specimens for tests 1 and 2 was 85 °C, whereas that for specimens in tests 3 and 4 was 150 °C. The temperature at the top of the specimens was maintained at 25 °C in all cases. The dimensions and the mass of the compacted specimens were measured after compaction process. The volume of the specimens was calculated from the know dimensions. The dry densities of the specimens were calculated from the known mass, volume and water content of each specimen.

Figure 4.1 depicts the tests conditions and the information gathered during the tests with applied temperatures of 85 °C at the bottom and 25 °C at the top of the specimens. The diameter and height of the specimens in these cases were 100 mm and 80 mm respectively. A 20 mm thick rockwool insulation covered with duct tape was used for the specimen in test no. 1, whereas a 40 mm thick rockwool insulation covered with reflective was tape used for the specimen in test no. 2. The duration of the test in case of the specimen in test 1 was 115 days, whereas it was 155 days for the specimen in test 2 (Table 4.1). The temperature and relative humidity along the depth of the specimen were measured with the relative humidity and temperature probes described

in chapter 3 (section 3.5). The relative humidity and temperature probes were bored in the specimens at distances of 20, 40 and 60 mm from the heater. The axial pressure developed at the opposite side of the heater was measured with the aid of a load cell during the full length of the tests. The tests were terminated when the values of temperature and relative humidity along the predetermined depths of the compacted bentonite specimens and the axial pressures at the top of the specimens were equilibrated.

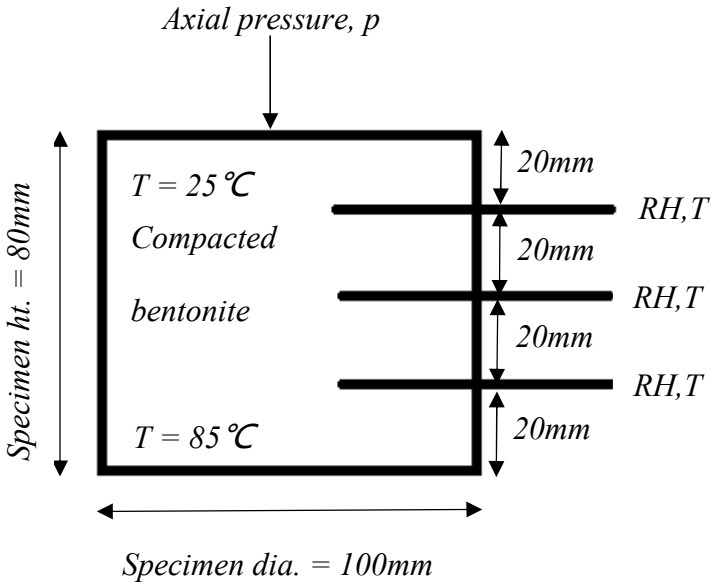

Figure 4.1 Schematic representation of temperature, relative humidity and axial stress measured in compacted bentonite specimens during thermal tests at 85℃.

Figure 4.2 presents the tests conditions and the information gathered during the tests with applied temperatures of 150 °C at the bottom and 25 °C at the top of the specimens. The diameter and height of the specimens in these cases were 100 mm and 300 mm respectively. A 20 mm thick rockwool insulation covered with duct tape was used for the specimen in test no. 3, whereas, a 40 mm thick rockwool insulation covered with reflective tape was used for the specimen in test no. 4. The duration of the test in

case of the specimen in test 3 was 140 days, whereas it was 190 days for the specimen in test 4 (Table 4.1). The temperature and relative humidity along the depth of the specimen were measured with the relative humidity and temperature probes described in chapter 3 (section 3.5). The relative humidity and temperature probes were bored in the specimens at distances of 60, 120, 180 and 240 mm from the heater. The axial pressure developed at the opposite side of the heater was measured with the aid of a load cell during the full length of the tests. Due to a fault in the equipment the axial pressure of the test number 3 couldn't be recorded. The tests were terminated when the values of temperature, relative humidity along the predetermined depths of the compacted bentonite specimens and the axial pressures at the top of the specimens were equilibrated.

After termination of the non-isothermal tests, the specimens were sliced into 20mm using a hacksaw. Each slice was broken down into smaller samples and a part of the sliced sample was powdered for XRD tests. The water content of each slice was determined from oven-drying test. Two parts of each sliced samples were used to measure volume by using the molten wax method (ASTM-D, 4943-08-2008). The dry density and the degree of saturation of the samples were determined from the volume and water content measurements.

The anions and cations concentration in each slice were determined with the aqueous extraction technique by using Ion Chromatography (IC) and Inductively Couple Plasma Optical Emission Spectroscopy (ICP-OES) methods. The effects of the thermal gradient on the distribution of anions and cations in the compacted bentonite specimens are presented in Chapter 6.

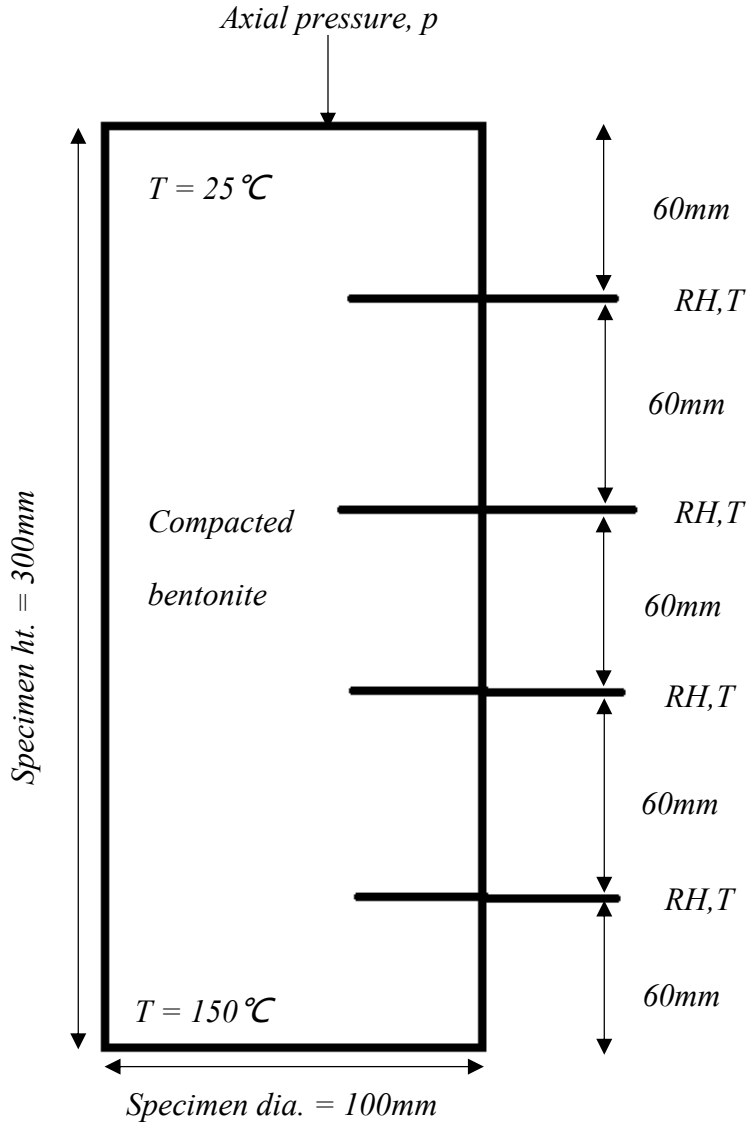

Figure 4.2 Schematic representation of temperature, relative humidity and axial stress measured in compacted bentonite specimens during thermal tests at 150 ℃

4.3 Test results and discussion

The following sections present the influence of insulation type used and the applied temperature gradients adopted during the tests on the thermal, hydraulic and mechanical response of the compacted bentonite specimens.

4.3.1 Temperature variations at an applied temperature of 85 °C

Figures 4.3 and 4.4 present the measured temperatures with elapsed time at predetermined depths of the specimens for the two non-isothermal tests at 85 °C (i.e., Test nos. 1 and 2). The insulation type used was found to influence the thermal equilibrium time. With a 20 mm thick insulation (Test no. 1), the temperature at all predetermined depths equilibrated in about 58 days, whereas the equilibrium was reached within about four hours for the test with a 40 mm thick insulation (Test no. 2). Therefore, thermal conduction through the specimen cell was reduced upon using a 40 mm thick insulation. The test results clearly showed that thermal response of compacted bentonites when subjected to temperature gradients under non-isothermal conditions depends upon the characteristics of the insulation used.

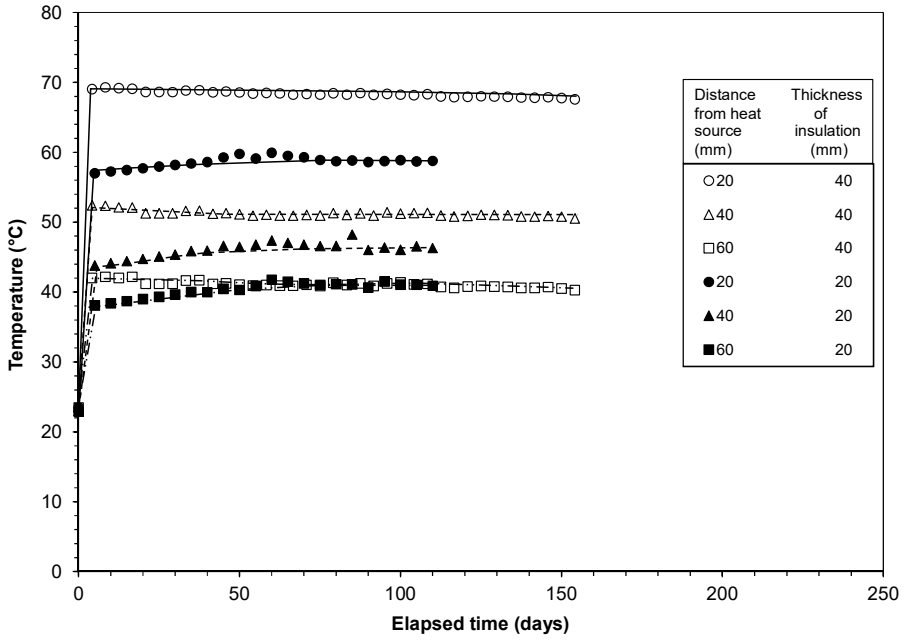

Figure 4.3 Transient temperature variations at specified depths of the specimens due to thermal loading at 85 °C

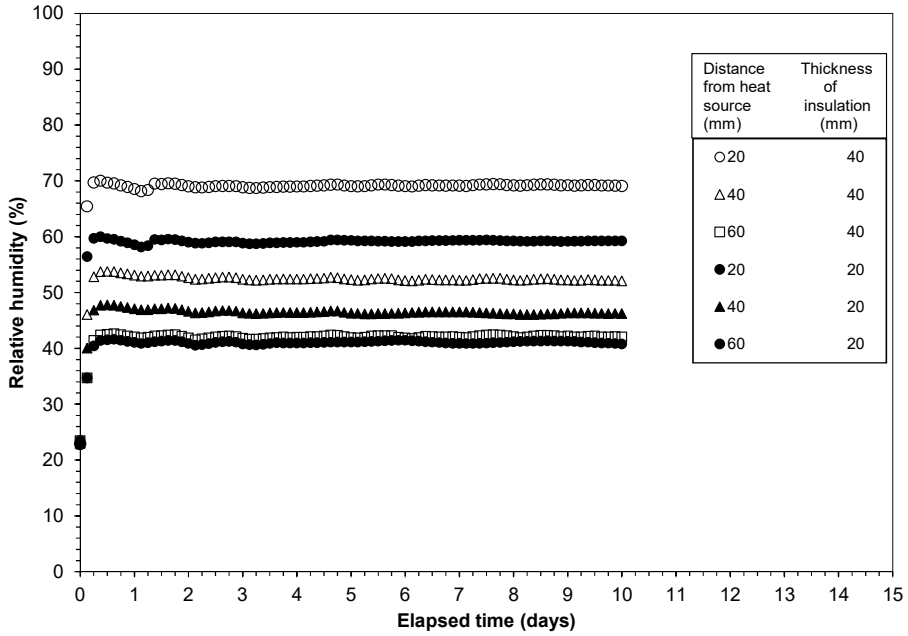

Figure 4.4 Transient temperature variations at specified depths of the specimens due to thermal loading at 85 °C (First 10 days of testing)

Table 4.1 presents the measured equilibrium temperatures at various predetermined depths for the tests. Figure 4.4 shows the equilibrium temperature against distance of the temperature probes from the heat source (i.e., the temperature profiles). For comparison, the test results reported by Tripathy et al. (2015) on MX80 bentonite for similar test conditions are also shown in Fig. 4.5. The maximum temperature generated with compacted bentonite specimen was about 68 °C.

Table 4.1 Influence of outer insulation on equilibrium temperature at various depths for compacted MX80 bentonite (diameter = 100 mm, height = 80 mm)

Distance of temperature probe from heat source (mm)	Equilibrium temperature (°C) with	
	20 mm insulation	40 mm insulation
0*	85	85
20	59	68
40	46	51
60	41	41
80*	25	25

* Temperatures maintained at both ends

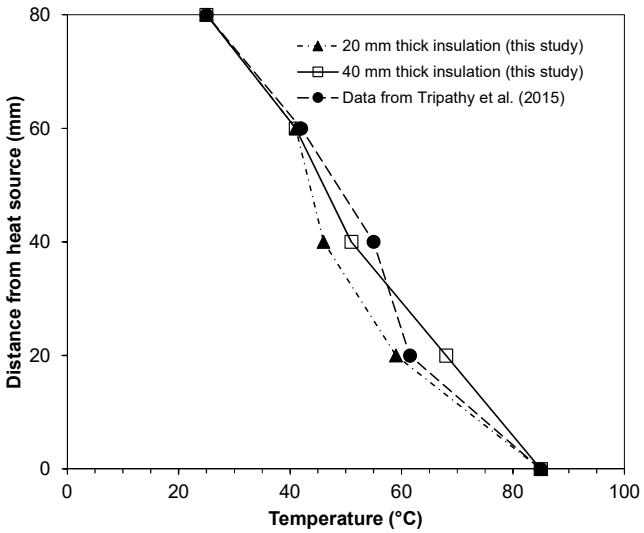

Figure 4.5 Temperature profiles (at the time of termination of the tests) of the specimens due to thermal loading at 85 °C

It can be seen from Table 4.1 and Fig. 4.4 that, the temperatures at distances of 20 to 60 mm from the heat sources were greater for the test with a 40 mm thick insulation as compared to that of a 20 mm thick insulation. The impact of insulation was mainly at distances between 20 and 60 mm from the heat source. The test results in this study generally agree well with the test results reported by Tripathy et al. (2015). A variation in the equilibrium temperature was found to be nearly linear for the case with a 40 mm thick insulation (Fig. 4.5).

The temperature gradient (or thermal gradient) is defined as the ratio of the difference between the temperatures at two points and the corresponding distance between the points. In this study, the distances of various predetermined depths of the specimens from the heat source were considered for calculating the temperature gradients. Figure 4.6 shows the temperature gradient versus distance of predetermined depth of the specimens from the heat source. For the sake of comparison, the calculated results based on the test data reported by Tripathy et al. (2015) are also shown in Fig. 4.6.

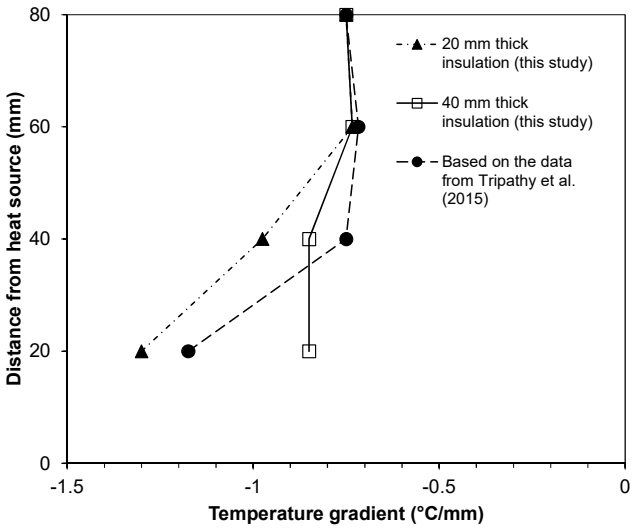

Figure 4.6 Temperature gradient variations at predetermined depths of the specimens due to thermal loading at 85 °C

It can be seen in Fig. 4.6 that, the temperature gradients remained between – 1.3 and - 0.71 °C/mm (i.e., between -13.0 and -7.1 °C/cm) for all cases. The influence of a 40 mm thick insulation reduced the thermal conductance through the specimen cell, particularly at distances between 20 and 60 mm from the heat source. The temperature gradients in the specimen in this case remained within a narrow range (- 0.85 to - 0.73 °C/mm). The results based on (Tripathy et al., 2015)'s data were found to be similar to that for the test results with a 20 mm thick insulation in this study.

4.3.2 Relative humidity variations for an applied temperature of 85 °C

Figures 4.7 and 4.8 present the measured relative humidity with elapsed time at predetermined depths of the specimens subjected to non-isothermal tests at 85 °C (i.e., Test nos. 1 and 2). When a 20 mm thick insulation (Test no. 1) used, the relative humidity at all predetermined depths equilibrated in about 95 days, whereas an equilibrium in terms of the relative humidity was attained within about 142 days for the test with a 40

mm thick insulation (Test no. 2). The test results clearly showed that the thermo-hydraulic response of compacted bentonites when subjected to temperature gradients under non-isothermal conditions depends upon the characteristics of the insulation used. A longer time was required for the equilibration of the relative humidity and with a thicker insulation layer. Additionally, the thermal equilibrium generally occurred sooner (see Fig. 4.3) than the vapour pressure (i.e., the relative humidity) equilibrium.

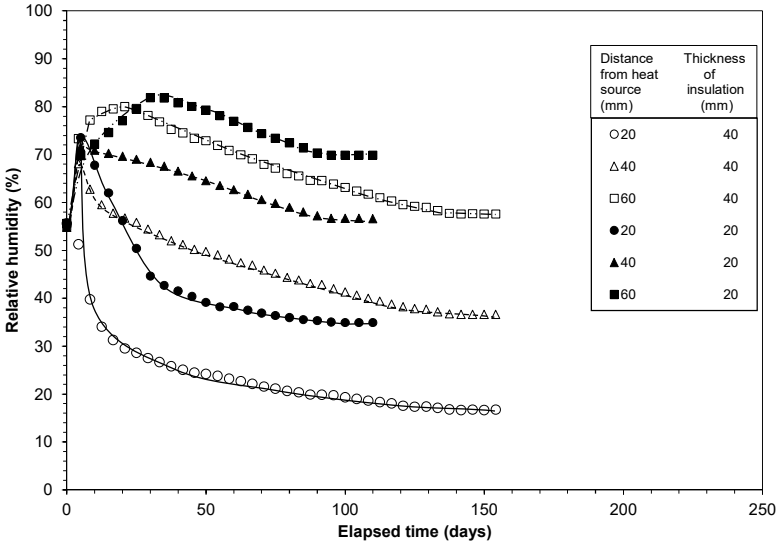

Figure 4.7 Transient relative humidity variations at specified depths of the specimens due to thermal loading at 85 °C

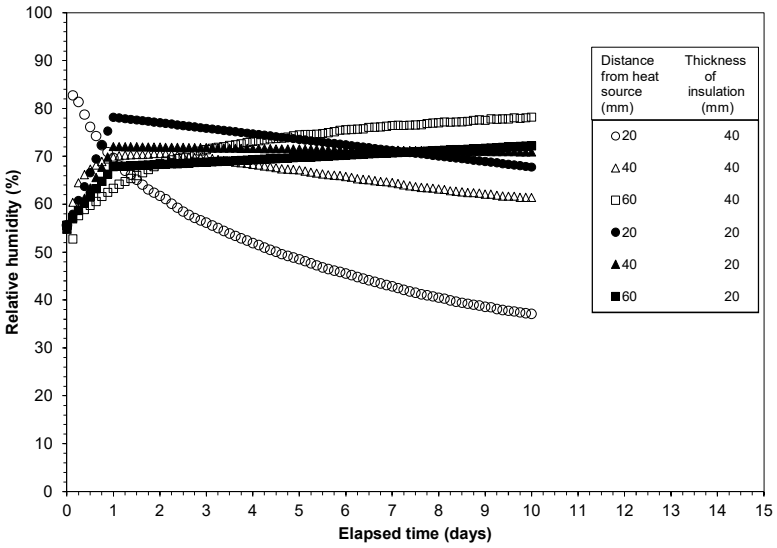

Figure 4.8 Transient relative humidity variations at specified depths of the specimens due to thermal loading at 85 °C (First 10 days of testing)

Table 4.2 presents the measured equilibrium relative humidities at various predetermined depths for test nos. 1 and 2. Figure 4.9 shows the equilibrium relative humidity against distance of the relative humidity probes from the heat source (i.e., the relative humidity profiles). For comparison, the test results reported by Tripathy et al. (2015) on MX80 bentonite for similar test conditions are also shown in Fig. It is important to mention that Tripathy et al (2015) reported lower intial water content in their bentonite specimen (9.6 %). In all cases, the maximum relative humidity measured was less than about 67%.

Table 4.2 Influence of outer insulation on equilibrium relative humidity at various depths for compacted MX80 bentonite (diameter = 100 mm, height = 80 mm)

Distance of relative humidity probe from heat source (mm)	Equilibrium relative humidity (%) with	
	20 mm insulation	40 mm insulation
20	35	17
40	57	37
60	67	58

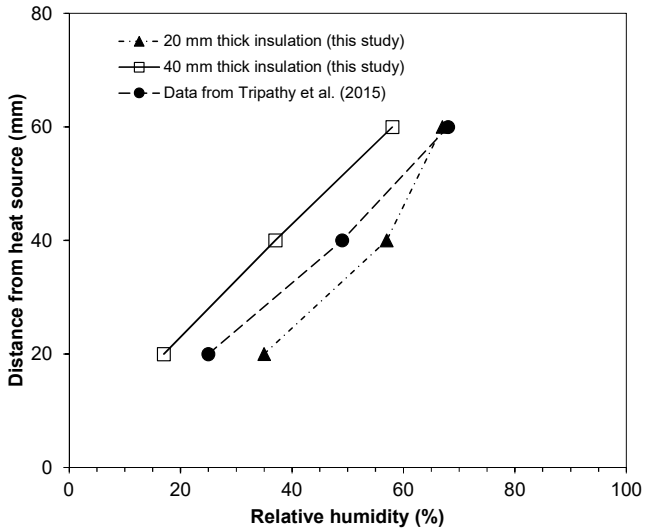

Figure 4.9 Relative humidity profiles (at the time of termination of the tests) of the specimens due to thermal loading at 85 °C

It can be seen from Table 4.2 and Fig. 4.9 that, the relative humidity increased with an increase in the distance from the heat source indicating that a transfer of water vapour took place due to the application of the thermal gradient. The relative humidity at all distances were greater for the test with a 20 mm thick insulation as compared to that of the test with a 40 mm thick insulation. A higher thermal gradient (see Fig. 4.6) should have caused more amount of water vapour transfer towards the top end of the specimen which in turn would tend to produce a higher relative humidity; however, this was not the case as noted from the equilibrium relative humidity data. On the other hand, the vapour pressure is known to be affected by the temperature. At any given amount of water vapour, an increase in the temperature causes a decrease in the relative humidity. Therefore, although the temperatures at distances between 20 and 60 mm for the case of 40 mm insulation were higher; however, the thermodynamic effects of a reduction in the relative humidity due to an increase in the temperature was manifested on the relative humidity data.

Differences between the test results in this study and that reported by Tripathy et al. (2015) can be noted in Fig. 4.9. However, the trend of the results in this study remained similar to that of Tripathy et al. (2015). A variation in the equilibrium relative humidity was found to be nearly linear for the case with a 40 mm thick insulation. The test results are consistent with the equilibrium temperatures at various depths (Fig. 4.5 and Table 4.2) in that, at any depth, the higher the temperature, lesser was the relative humidity.

Figure 4.10 shows the temperature gradient versus relative humidity plot for Test nos. 1 and 2. The calculated results based on the experimental data reported by Tripathy et al. (2015) are also shown in Fig. 4.10 for comparison. Figure 4.10 shows that, the differences in the relative humidity for the test with a 20 mm thick insulation and that

reported by Tripathy et al. (2015) remained throughout the depth of specimens except at a distance of 60 mm from the heat source (see also Fig. 4.9). A significant variation of the relative humidity occurred for a small variation in the temperature gradient for the specimen that was tested with a 40 mm thick insulation. This suggests that, water vapour transfer at a near constant temperature gradient and with higher temperatures in compacted bentonites may yield a lesser relative humidity as the distance from the heat source increased. This is primarily associated with the impact of higher temperature on the relative humidity which decreases at a constant amount of water vapour in the pore spaces of compacted bentonites.

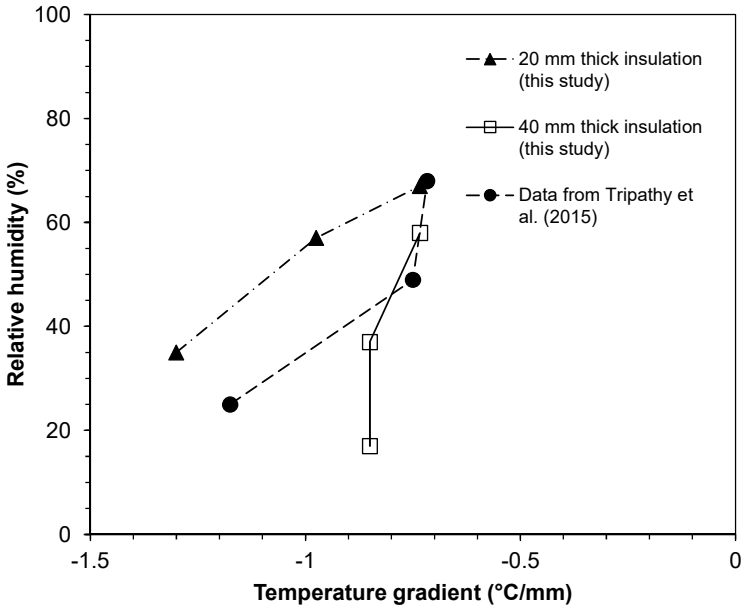

Figure 4.10 Temperature gradient versus relative humidity plot for thermal loading at 85 °C

4.3.3 Temperature variations at an applied temperature of 150 °C

Figures 4.11 and 4.12 present the measured temperatures with elapsed time at predetermined depths of the specimens for the two non-isothermal tests at 150 °C (i.e., Test nos. 3 and 4). The insulation type in these tests did not influence the thermal equilibration time. For both tests (i.e., the tests with 20- and 40-mm thick insulations),

the temperature at all predetermined depths equilibrated within about ten days and thereafter remained nearly unchanged. For the sake of clarity, the initial temperature data are not shown in Fig. 4.11.

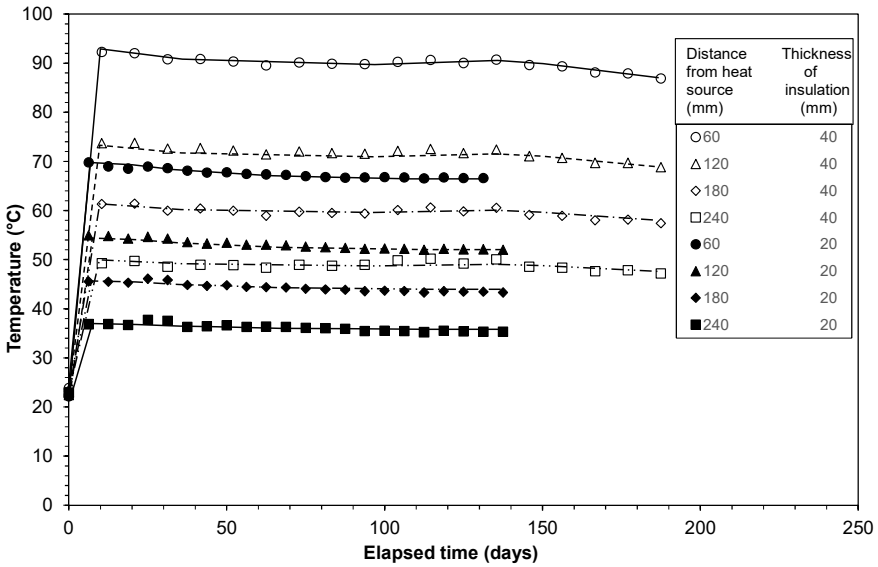

Figure 4.11 Transient temperature variations at specified depths of the specimens due to thermal loading at 150 °C

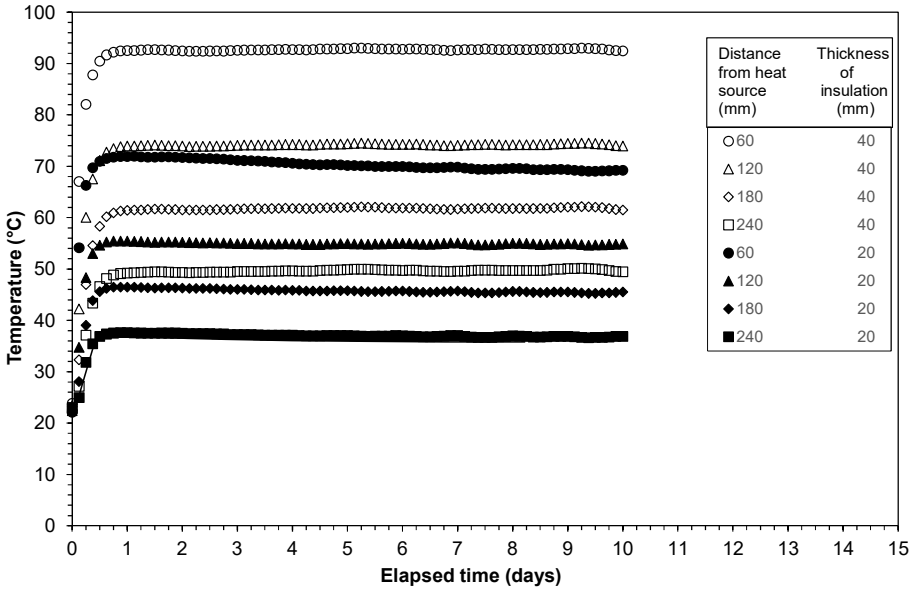

Figure 4.12 Transient temperature variations at specified depths of the specimens due to thermal loading at 150 °C (First 10 days of testing)

Table 4.3 presents the measured equilibrium temperatures at various predetermined depths for the tests. Figure 4.13 shows the equilibrium temperature against distance of the temperature probes from the heat source. For comparison, the results obtained from the tests with 80 mm high specimens (i.e., Test nos. 1 and 2) are also shown in Fig. 4.13.

Table 4.3 Influence of outer insulation on equilibrium temperature at various depths for compacted MX80 bentonite (diameter = 100 mm, height = 300 mm)

Distance of temperature probe from heat source (mm)	Equilibrium temperature (°C) with	
	20 mm insulation	40 mm insulation
0*	150	150
60	67	88
120	52	70
180	43	58
240	35	47
300*	25	25

* Temperatures maintained at both ends

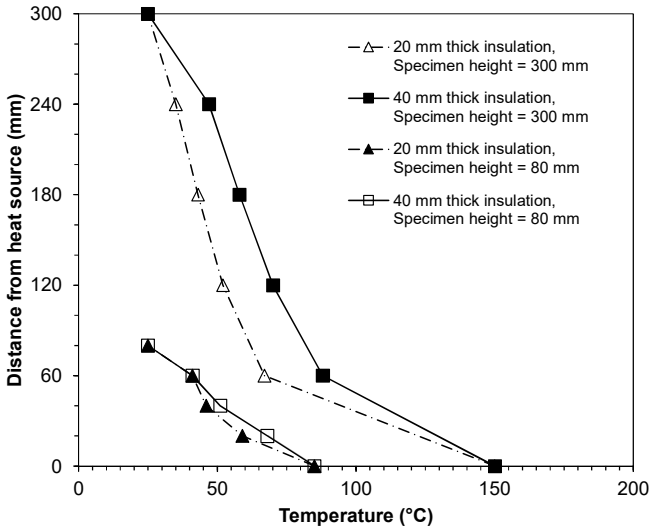

Figure 4.13 Temperature profiles (at the time of termination of the tests) of the specimens due to thermal loading at 150 °C

It can be seen from Table 4.3 and Fig. 4.13 that, the temperatures at all salient distances from the heat source were greater for the test with a 40 mm thick insulation (Test no. 4) as compared to that of a 20 mm thick insulation (Test no. 3). Similar results

were also noted for specimens in tests 1 and 2 (Fig. 4.5 and Table 4.2). Up to a distance of 60 mm from the heat source, the temperatures of the specimens in tests 3 and 4 were greater than that of specimens in tests 1 and 2. A variation in the equilibrium temperature was found to be non-linear for the specimens in tests 3 and 4 (Fig. 4.13).

The distances of various salient depths of the specimens from the heat source were considered for calculating the temperature gradients. Figure 4.11 shows the temperature gradients in the specimens at various distances from the heat source. For the sake of comparison, the results obtained for the specimens in test nos. 1 and 2 are also shown in Fig. 4.14.

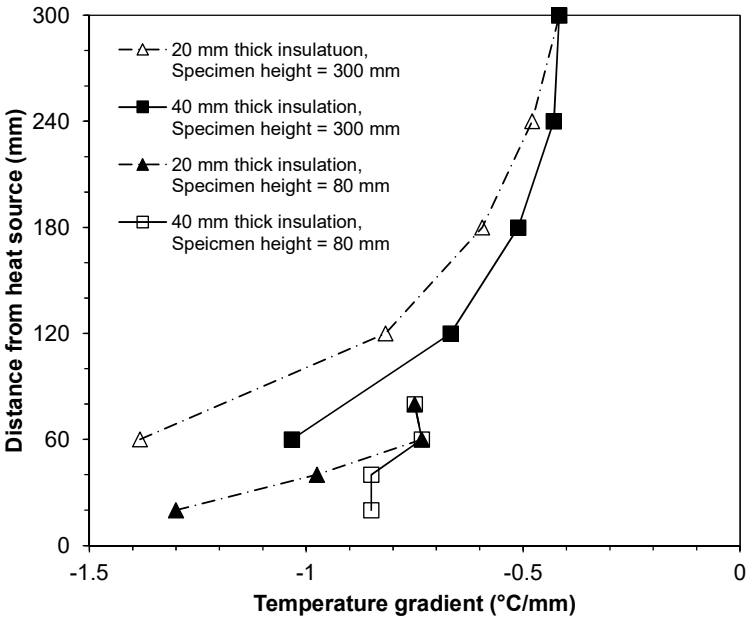

Figure 4.14 Temperature gradient at predetermined depths of the specimens due to thermal loading at 150 °C

It can be seen Fig. 4.14 that, the temperature gradients for the specimens in test nos. 3 and 4 remained between – 1.4 and - 0.4 °C/mm (i.e., between -14.0 and – 4.0 °C/cm) for all cases. The influence of a 40 mm thick insulation reduced the thermal conductance at all predetermined distances. Comparing the thermal gradients in test

nos 1 and 2 with test nos. 3 and 4, it can be seen that an application of a temperature of 150 °C introduced higher (near the heat source) and lesser (at large distances) thermal gradients in the specimens.

4.3.4 Relative humidity variations at applied temperature of 150 °C

Figures 4.15 and 4.16 present the measured relative humidities with elapsed time at predetermined depths of the specimens for the two non-isothermal tests at 150 °C (i.e., Test nos. 3 and 4). The relative humidity at all predetermined distances from the heat source and for both insulation type did not tend to show any equilibrium. The relative humidity increased and further decreased at distances of 60, 120 and 180 mm from the heat source, whereas it increased at a distance of 240 mm from the heat source.

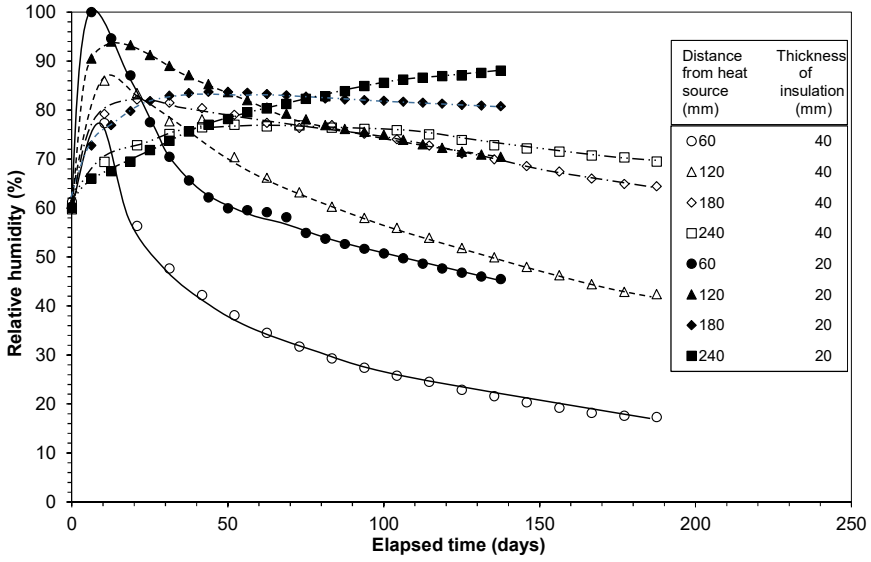

Figure 4.15 Transient relative humidity variations at specified depths of the specimens due to thermal loading at 150 °C

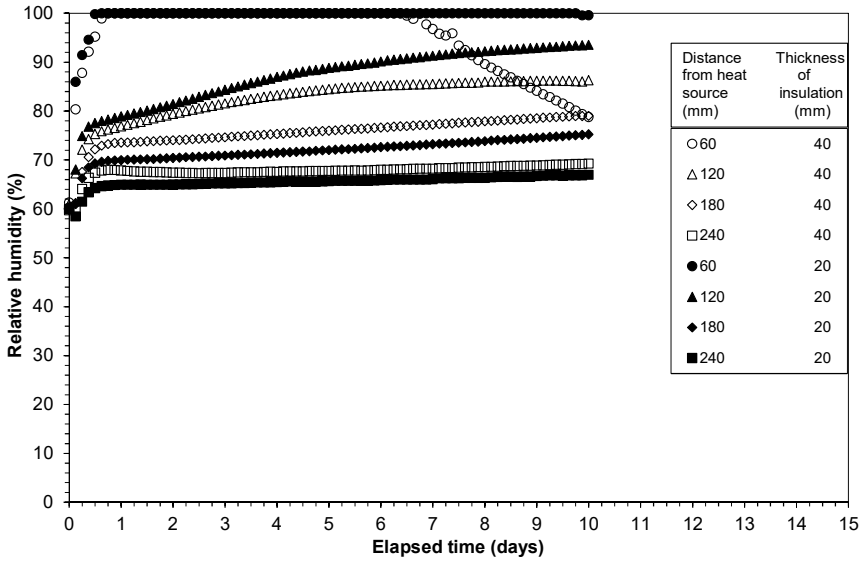

Figure 4.16 Transient relative humidity variations at specified depths of the specimens due to thermal loading at 150 °C (First 10 days of testing)

Table 4.4 presents the measured relative humidities at various predetermined depths at the time of termination of the tests. Figure 4.17 shows the relative humidity against distance of the relative humidity probes from the heat source. For comparison, the test results for specimens in test nos. 1 and 2 are also shown in Fig. 4.17. In all cases, the maximum relative humidity measured in the specimens was less than about 87%.

Table 4.4 Influence of outer insulation on the relative humidity at various depths for compacted MX80 bentonite (diameter = 100 mm, height = 300 mm)

Distance of relative humidity probe from heat source (mm)	Relative humidity (%) with	
	20 mm insulation	40 mm insulation
60	45	17
120	71	42
180	81	66
240	87	71

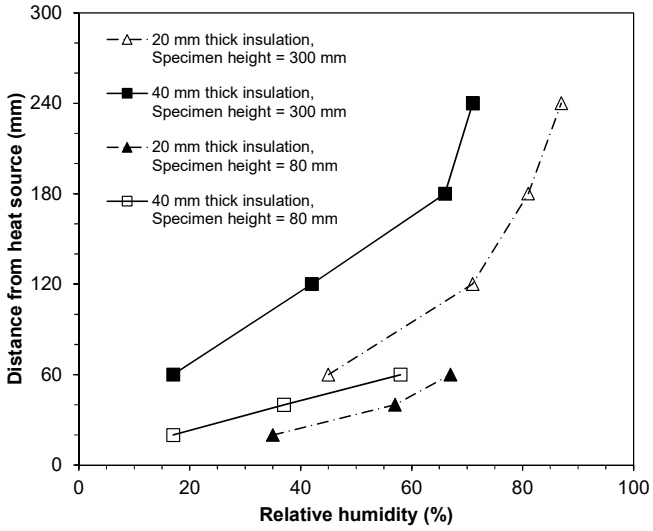

Figure 4.17 Relative humidity profiles (at the time of termination of the tests) of the specimens due to thermal loading at 150 °C

It can be seen from Table 4.4 and Fig. 4.17 that, the relative humidity increased with an increase in the distance from the heat source indicating that a transfer of water vapour took place due to the application of the thermal gradient. The relative humidity at all distances were greater for the test with a 20 mm thick insulation as compared to that of the test with a 40 mm thick insulation. A higher thermal gradient (see Fig. 4.14) should have caused a greater amount of water vapour transfer towards the top end of the specimen which in turn would tend to produce a higher relative humidity; however, this was not the case as noted from the equilibrium relative humidity data. A reduction in the relative humidity for the specimens tested with a 40 mm thick insulation is attributed due to the thermodynamic effects of a reduction in the relative humidity due to an increase in the temperature. The relative humidity profiles were found to be non-linear for the non-isothermal tests at applied temperature of 150 °C.

Figure 4.18 shows the temperature gradient versus relative humidity plot for Test nos. 3 and 4. The results obtained for Test nos. 1 and 2 are also shown in Fig. 4.8 for comparison. Figure 4.18 shows that higher thermal gradients caused a decrease in the

relative humidity at distances near the heat source and an increase in the relative humidity at distances away from the heat source. A reduction in the relative humidity at constant thermal gradient for specimens tested with 40 mm thick insulations is attributed due to the impact of higher temperature on the relative humidity which decreases at a constant amount of water vapour in the pore spaces of compacted bentonites.

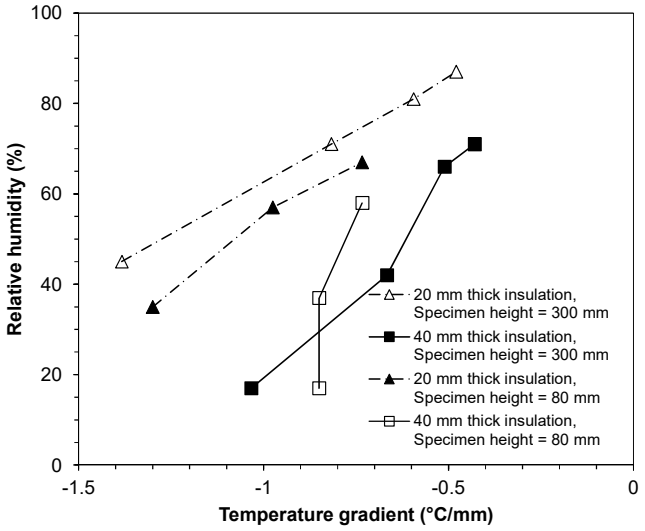

Figure 4.18 Temperature gradient versus relative humidity plot due to thermal loading at 150 °C

4.3.5 Axial pressure development in non-isothermal conditions

Figure 4.19 shows the elapsed time versus the measured axial pressures at the opposite end of the heat source for the compacted bentonite specimens in non-isothermal Test nos. 1 (with 20 mm thick insulation) and 2 (with 40 mm thick insulation). The applied temperature in this case was 85 °C. Due to a technical fault with the load cell, the axial pressure development during Test no. 3 at 150 °C and with 20 mm thick insulation couldn't be recorded. Figure 4.20 depicts the axial pressure generated during the non-isothermal test at 150 °C (Test no. 4 with 40 mm thick insulation).

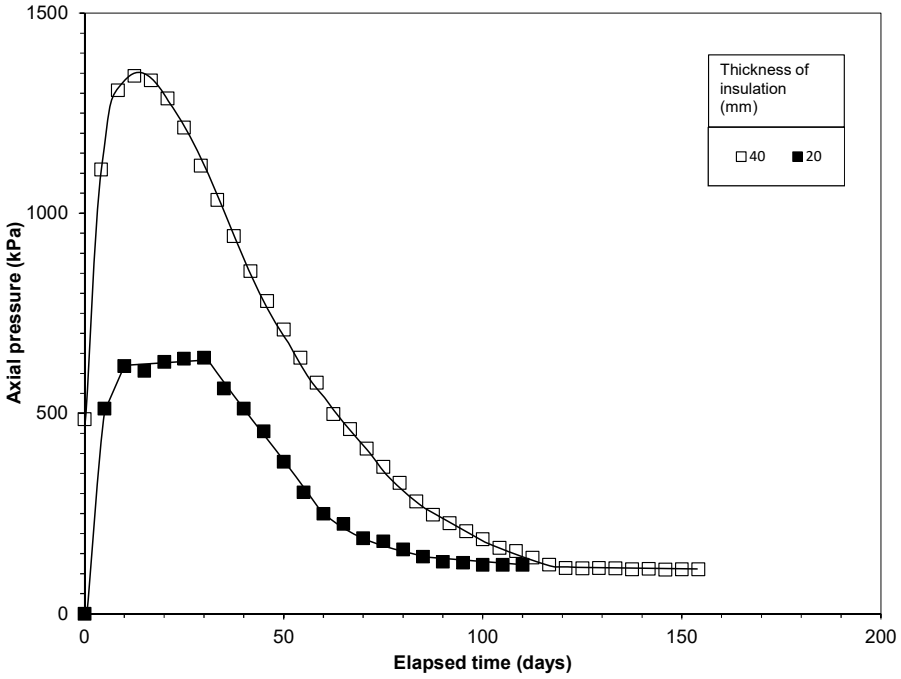

Figure 4.19 Elapsed time versus axial stress plot for thermal tests on compacted bentonite specimens at 85°C

It can be seen Figs. 4.19 and 4.20 that, the axial pressures for the compacted bentonite specimens firstly increased and then decreased with elapsed time before attaining an equilibrium at which, no further significant changes in the axial pressures was noted. The maximum measured axial pressures for the specimens in Test nos. 1, 2 and 4 were 640, 1345 and 2400 kPa, respectively. The differences in the maximum axial pressures for the specimens are attributed due to the applied temperature during the tests and the insulation type used.

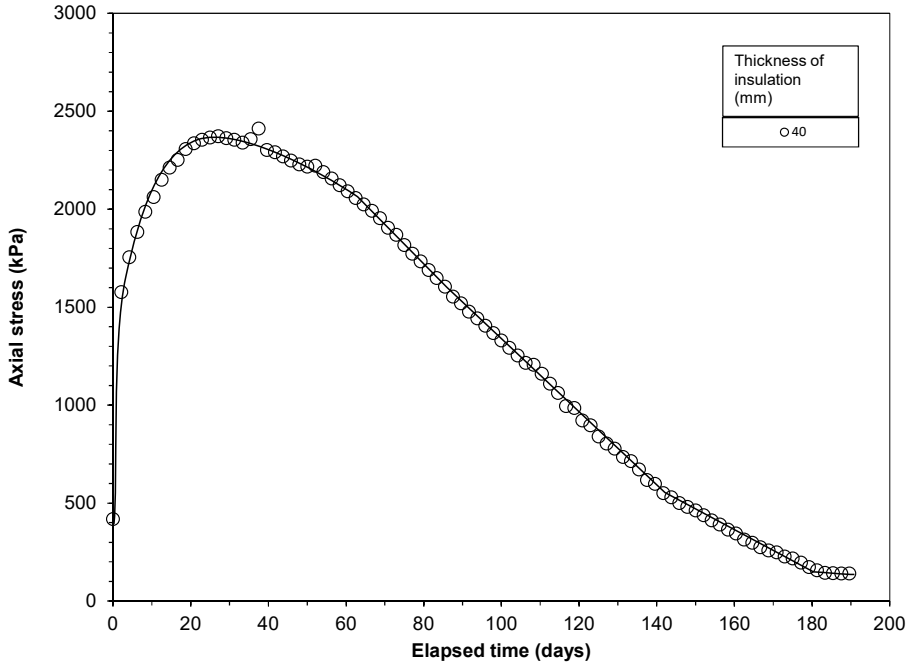

Figure 4.20 Elapsed time versus axial stress plot for thermal tests on compacted bentonite specimens at 150°C

Between the results of Test nos. 1 and 2 (Fig. 4.19), the specimen tested with a 40 mm thick insulation exhibited a greater maximum axial pressure. Similarly, between the results of Test nos. 2 and 4 (Figs. 4.19 and 4.20), the higher the applied temperature, greater was the maximum axial pressure exhibited by the specimen.

The test results presented in Figs. 4.19 and 4.20 show that, the maximum axial pressures were recorded at different elapsed times for the specimens, such as 30 days for Test no. 1 (20 mm thick insulation and with an applied temperature 85 °C), 13 days for Test no. 2 (40 mm thick insulation and with an applied temperature of 85 °C) and 27 days for Test no. 4 (40 mm thick insulation and with an applied temperature of 150 °C). Similarly, the equilibrium axial pressures were recorded at different elapsed times for the specimens, such as after about 100 days for Test no. 1, about 120 days for Test no. 2 and about 185 days for Test no. 4. The relative equilibrium was attained in similar elapsed times for the specimens in Tests 1 and 2 (section 4.3.2). However, as shown in

section 4.3.4, the relative humidity did not equilibrate when the Test no. 4 was terminated.

At equilibrium, the axial pressures recorded were found to be significantly smaller than the maximum axial pressures (Figs. 4.19 and 4.20). The equilibrium axial pressures were 120, 115 and 145 kPa for the specimens in Test nos. 1, 2 and 4 respectively.

Tripathy et al. (2015) stated that, an increase and further decrease in the axial pressure exhibited by compacted bentonite specimens due to an application of a thermal gradient is attributed due to the combined influence of several factors, such as (1) water vapour movement from the hotter to the cooler end of the specimen, (2) volumetric shrinkage of the specimen towards the heater end due to an increase in the temperature and movement of moisture from the hotter to the cooler end, (3) compression of the specimen towards the heater end due to the development of the axial pressure, (4) expansion of the specimens due to an increase in the temperature for the layers having high suctions, (5) contraction of layers due to an increase in the temperature for the layers with low suctions, (6) expansion of the testing device upon an increase in the temperature, and (7) migration and redistribution of moisture to farther distances in order to equalize the suction (usually from top to bottom).

From the test results of profiles of the temperature and the relative humidity (Figs. 4.13 and 4.17), it becomes clear that an increase in the temperature, either due to the use of a thicker insulation or due to an application of a higher temperature, causes a decrease in the relative humidity within the compacted bentonite specimens. From the consideration of the relative humidity increase in compacted bentonites during the hydration process and its impact on swelling thrust development, it was anticipated that specimens with a higher relative humidity would tend exhibit a greater axial pressure.

However, a reverse trend was noted in the test results; the specimens with a lower relative humidity exhibited greater maximum axial pressure (Test no. 1 versus Test no. 2 or Test no. 2 versus Test no. 4 in Figs. 4.19 and 4.20). Therefore, the hydration mechanism cannot be held solely responsible for axial pressure development in compacted bentonites under non-isothermal conditions. Other issues, such as thermal expansion of bentonite, gas pressure generation and thermal expansion of the specimen cell may contribute to the axial pressure development for such boundary condition. The test results also indicate that, the equilibrium axial pressure in compacted bentonites when subjected to thermal loading was not influenced by the applied thermal gradient. All three specimens exhibited near similar axial pressures at equilibrium.

4.3.6 Profile of water content, dry density, degree of saturation and suction

Figures 4.21 (a), (b), (c) and (d) show the water content, dry density, degree of saturation, and suction profiles of the specimens tested, respectively. The data presented in Figs. 4.21 (a), (b) and (c) are based on analyses of the samples of bentonite slices (20 mm thick) after termination of each tests. Therefore, the results are plotted corresponding to the mid-level of each slice. The suction data presented in Fig. 4.21 (d) are based on the relative humidity and temperature data at the end of each test. The suctions were calculated based on the thermodynamic relationship between the relative humidity and suction (Fredlund et al., 2012).

The results presented in Fig. 4.21 indicate two distinct aspects, such as (i) towards the opposite end of the heat source, the bentonite specimens underwent a wetting process as indicated by an increase in the water content, a decrease in the dry density, an increase

in degree of saturation and a decrease in suction and (ii) towards the heat source, the specimens underwent a shrinkage process as indicated by a decrease in the water content, an increase in the dry density, a decrease in the degree of saturation and an increase in suction.

The distance at which the transition (i.e., less or more than initial values) occurred was found to increase from the heat source due to either the use of a thicker insulation or due to an application of higher temperature during the test. For the same size of specimens, a larger part of the specimen underwent the shrinkage process and only a small part of the specimen underwent the wetting process when a 40 mm thick insulation was used. Similarly, due to an application of a higher temperature, a larger part of the specimen underwent a shrinkage process and a smaller part underwent a wetting process.

Recalling that the use a thicker insulation and an application of higher temperature produced higher temperature and lower relative humidity within the specimens (Figs. 4.13 and 4.17). The test results presented in Fig. 4.21 in terms of the water content, dry density and degree of saturation, complement well the results presented in Figs. 4.13 and 4.17 in terms of the temperature and relative humidity.

Table 4.5 Mass of water contained in the samples subjected to thermal tests.

		20 mm insulation	40 mm insulation
Initial mass of water for 80 mm sample	181.5 g		
Initial mass of water for 300 mm sample	680 g		
Mass of water for 80 mm sample (Post-test)		108 g	65 g
Mass of water for 300 mm sample (Post-test)		634 g	346 g

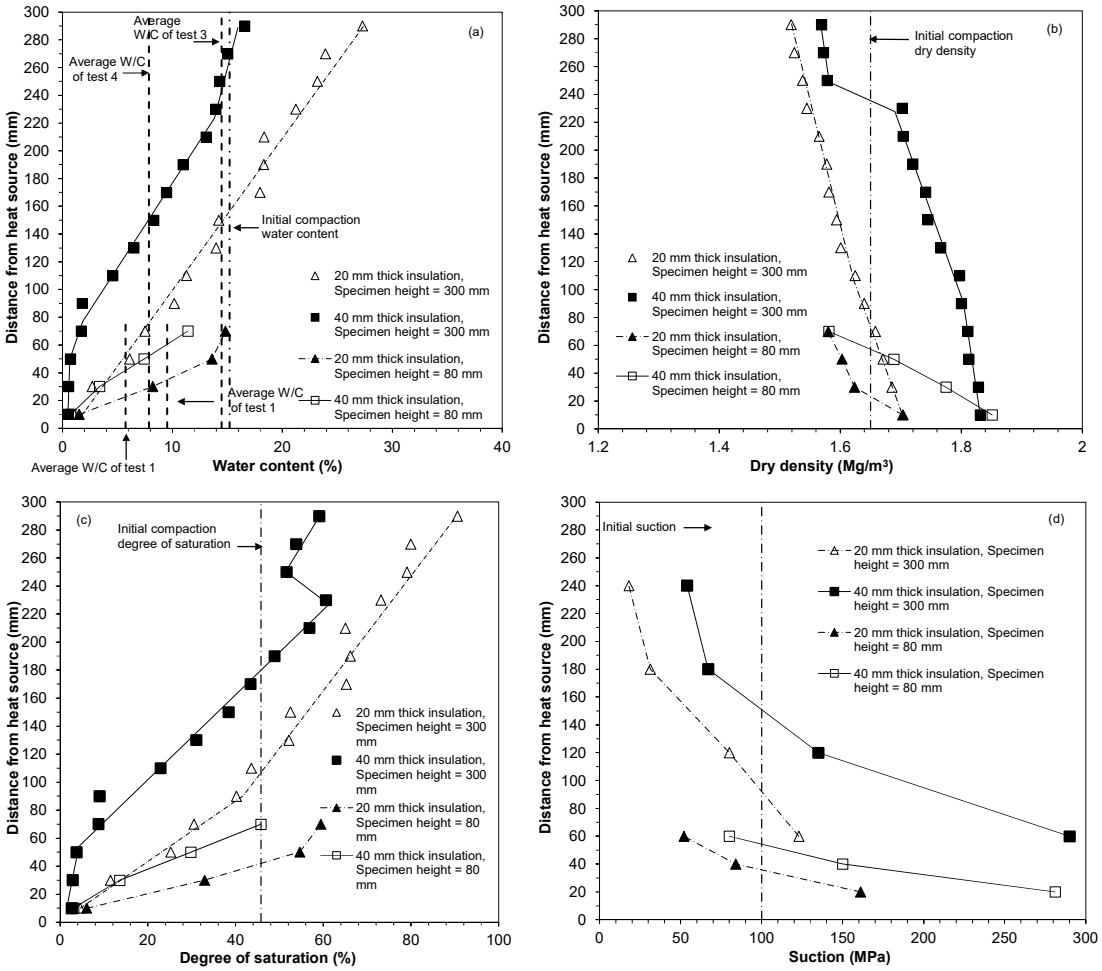

Figure 4.21 Profiles of (a) Water content, (b) Dry density, (c) Degree of saturation and (d) suction at the end of thermal tests at 85 and 150°C

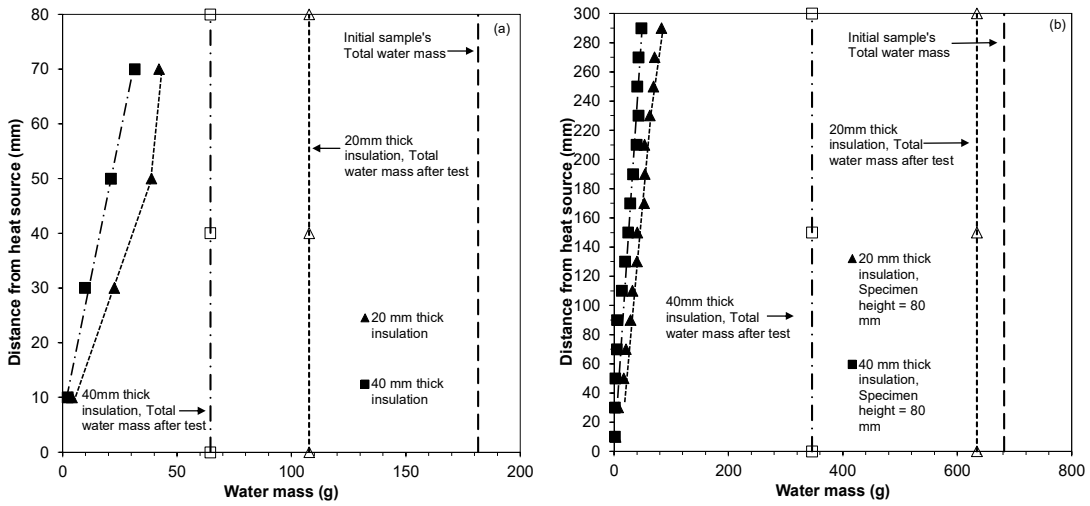

Figure 4.22 Water mass profiles, (a) Thermal tests at 85°C (b) Thermal tests at 150 °C

Table 4.5 and figure 4.22 demonstrate the mass of water in the bentonite samples prior and subsequent the testing processes. As it is observed the water mass of the samples after the testing is significantly lower that the initial weight of the water. Also, there are significant differences between the samples tested with 20mm and 40 mm insulations. For the tests at 85 °C the sample with 20mm insulation showed a 40% loss of its water mass whereas the sample tested with 40mm insulation showed a 64% loss. On the other hand, the tests at 150 °C showed a 7% and 49% loss for the 20mm and 40mm insulation respectively. The increased insulation leads to higher temperatures along the sample thus more water vapour is generated. Potential leakages in the cell lead to the loss on water mass from the sample. Also, the complexity of the process to derive the water mass and water content post mortem measurements allows the dissected specimens to partially dry during the testing procedure. From figure 4.22 (b) and table 4.5 it is also possible to observe that the size of the specimen affects its loss of water mass. For both insulations thicknesses the 300mm tall samples lost less water than the 80mm tall specimens. Finally, it must be noted that the water mass measurements took place after the completion of the tests. Observing that the tests with 40mm insulation took longer than the tests with 20mm insulation it is safe to assume that the water mass loses are also depended with time as the samples are exposed to potential leakages for a longer period

If the axial thrust is considered to be on account of the wetting of the specimens at the opposite end of the heat source, the results presented in Figs. 4.13, 4.17 and 4.21 do not support the axial pressure results presented in Figs. 4.19 and 4.20. On the other hand, the table 4.5 and figure 4.22 present that the total mass of water in the bentonite samples decreases during the testing period thus even though the redistribution is achieved towards the colder areas the total loss of mass could affect the overall response

of the sample's axial pressure development There are several aspects which need further considerations to explore such anomalies between the axial pressure, temperature, and relative humidity: (i) a leakage of water vapour from the specimen during a test, (ii) gas pressure generation and dissipation due to thermal loading, and (iii) rigidity of the restraint under the conditions of axial pressure development at very high temperature. A study of all these aspects are beyond the scope of the current investigation.

4.4 Summary

In this chapter, the influence of the thermal gradient on the thermo-hydro-mechanical response of compacted bentonite specimens is presented. At the opposite end of the bentonite specimens two different temperature boundary conditions were considered, such as (i) 85 °C and 25 °C for specimens with dia. = 100 mm and

height = 80 mm and (ii) 150 °C and 25 °C for the specimens with dia. = 100 mm and height = 300 mm.

The test results obtained are the transient temperature and relative humidity at predetermined depths of the specimens, axial pressure at the opposite side of the heat source. The test results of water content, dry density, and degree of saturation along the depth of the bentonite specimens were determined after the termination of the tests.

Under similar conditions, the water content, relative humidity and degree of saturation decreased, whereas the dry density increased at distances closer to heat source indicating that the specimens underwent a shrinkage process. These findings are in agreement with the results reported in literature (Singh, 2007; Villar et al., 2008; Gens

et al., 2009; Gómez-Espina and Villar, 2010; Bag, 2011; Gómez-Espina and Villar, 2015; Tripathy et al., 2015).

The axial pressure increased and further decreased during the tests before attaining an equilibrium. The equilibrium axial pressures were found to be far smaller than the maximum axial pressures exhibited by the specimens. The development of maximum axial pressures in the specimens, and similar axial pressures at the equilibrium, were found to be not directly linked with the water content redistribution within the compacted bentonite specimens. The water mass balance graphs showed a loss in the water mass of each specimen after testing.

CHAPTER 5.
EFFECT OF TEMPERATURE AND HYDRAULIC GRADIENTS ON THERMO-HYDRO-MECHANICAL BEHAVIOUR OF COMPACTED BENTONITE

5.1 Introduction

Several laboratory tests have been carried out in the past that focused in investigating the behaviour of compacted bentonites and bentonite-sand mixtures when subjected to thermal, hydraulic, and thermo-hydraulic gradients (Martın et al., 2000; Börgesson et al., 2001; Cuevas et al., 2002; Pintado et al., 2002; Singh, 2007; Villar and Lloret, 2007; Samper et al., 2008; Villar et al., 2008; Villar and Gómez-Espina, 2008; Åkesson et al., 2009; Pusch et al., 2010; Bag, 2011; Tripathy et al., 2015). A detailed review of these studies suggested that a majority of the laboratory tests were conducted by

considering an applied temperature of less than 100 °C. The reported laboratory tests have been conducted at various water injection pressures. The water injection pressure was varied between 0 to 1.5 MPa. In some of the investigations, variations of the temperature and relative humidity were monitored with elapsed time along the depths of the compacted bentonite specimens. A variation of the axial stress during the tests was monitored in some cases (Tripathy et al., 2015). In some of the investigations, changes in the dry density, the water content, the degree of saturation and the concentration of anions and cations were measured after the termination of the tests. These information are crucial in order to understand the thermo-hydraulic-mechanical-chemical response of the engineered barriers both under short and long-term in situ conditions involving anticipated temperature, water pressure and fluid type.

Studies concerning the thermo-hydraulic response of compacted bentonites at temperatures exceeding 100 °C is of significant interest, particularly for understanding the early-life phase of deep geological disposal facilities. Very high temperatures of spent fuel, radioactive decay of wastes, and formation of high thermal zones at and near the interface of waste canisters and compacted bentonite buffer are some of the in-situ conditions which demand detailed investigations concerning the thermo-hydraulic behaviour of compacted bentonites at very high temperatures. Birgersson and Karnland (2014) stated that bentonite barriers may be subjected to both water and gas pressures gradients that are not fully separable.

The main objective of this chapter is to bring out the influence of thermo-hydraulic gradients involving applied temperatures of 85 and 150 °C and at a predetermined water injection pressure of 600 kPa on the behaviour of compacted bentonites. Section 5.2 presents the experimental program undertaken for the study. Section 5.3 presents the temperature and relative humidity variations measured at

predetermined levels along the depth of bentonite specimens and axial pressure generated at the opposite end of the heat source during the thermo-hydraulic tests. The profiles of water content, dry density, degree of saturation and suction after termination of the thermal tests are also presented in section 5.3. Section 5.4 summarises the important findings that emerged from the investigation.

5.2 Experimental program

The devices used for carrying out the non-isothermal hydraulic tests at temperatures of 85 and 150 °C are presented in chapter 3 (Figs. 3.3 and are 3.5). The compaction mould used for preparing the statically compacted bentonite specimens and experimental methods are described in chapter 3 (section 3.5). Tables 3.1 and 3.2 present the experimental program followed for the thermo-hydraulic tests.

The dry density of the compacted bentonite specimens used in the study was 1.65 Mg/m^3. In total, five numbers of thermo-hydraulic tests (Test nos. 5, 6, 7, 8, and 9) were conducted. Test nos. 5 and 6 were carried out by applying temperatures of 25 (at top) and 85 °C (at bottom) at the opposite ends of the bentonite specimens. In this case, distilled and de-aired water was supplied from the top end of the specimen at a pressure of 600 kPa. Test no. 7 was carried out by applying temperatures of 25 °C at top and 150 °C at bottom end of the bentonite specimen. In this case, distilled and de-aired water was supplied from the top end of the specimens at a pressure of 5 kPa. Test nos. 8 and 9 were similar to that of Test no. 7, but the water injection pressure from the top of the specimens was 600 kPa. The 600 kPa pressure was chosen as is representative to the water pressure that can be found in in the depths that the nuclear waste disposal galleries are meant to be constructed. The 5 kPa of water injection used for test 7 was the result of a mechanical fault during the first days of

testing. The mass and the dimensions of the compacted specimens were measured after compaction which allowed calculating the dry density of the specimens.

Figure 5.1 shows the tests conditions considered and the information gathered Test nos. 5 and 6. For both tests, the thermal insulation used comprised of a 40 mm thick rockwool layer covered with a layer of reflective tape. The height and the diameter of the specimens were 80 and 100 mm, respectively. The duration of tests was 285 days (Table 3.1). The temperature and relative humidity along the depth of the specimen were measured with the relative humidity and temperature probes described in chapter 3 (section 3.5). The relative humidity and temperature probes were located at distances of 20, 40 and 60 mm from the heat source. The axial pressure developed at the opposite end of the heat source was measured with the aid of a load cell during the tests. The tests were terminated when the values of temperature and relative humidity at salient depths of the specimens and the axial pressure at the opposite end of the heat source equilibrated.

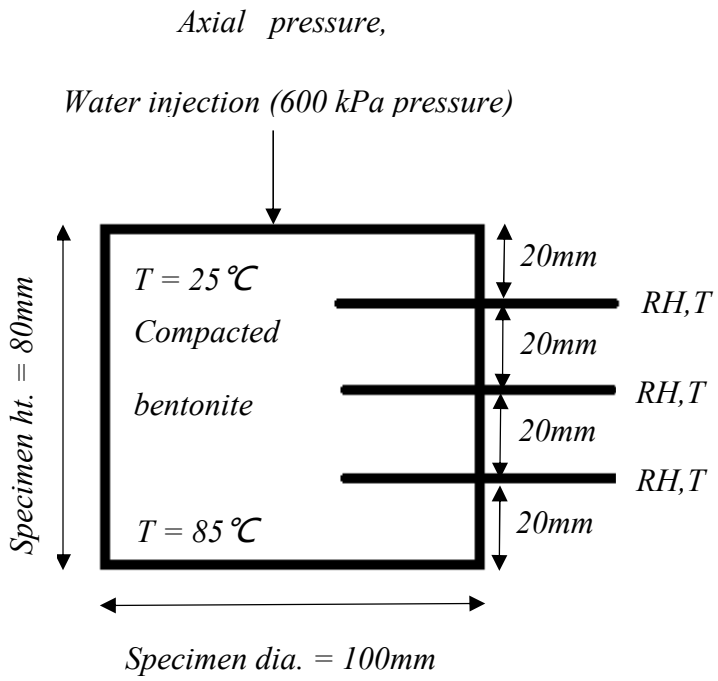

Figure 5.1 Schematic representation of temperature, relative humidity and axial stress measured in compacted bentonite specimens during thermo-hydraulic tests at 85℃.

Figure 5.2 presents the test conditions considered and the information gathered during Test nos. 8 and 9. The test conditions for Test no. 7 was similar to that shown in Fig. 5.2, except that the water injection pressure was 5 kPa. The height and the diameter of the specimens were 300 and 100 mm, respectively. The durations of Test nos. 7, 8 and 9 were 90, 300 and 180 days, respectively (Table 3.2). The temperature and relative humidity along the depth of the specimen were measured with the relative humidity and temperature probes described in chapter 3 (section 3.5). The relative humidity and temperature probes were located at distances of 40, 60, 120, 180 and 240 mm from the heat source. The axial pressures developed at the opposite end of the heat source during the tests were measured with the aid of a load cell. The tests terminated when the values of temperature and relative humidity at salient depths of the specimens and the axial pressure at the opposite end of the heat source equilibrated.

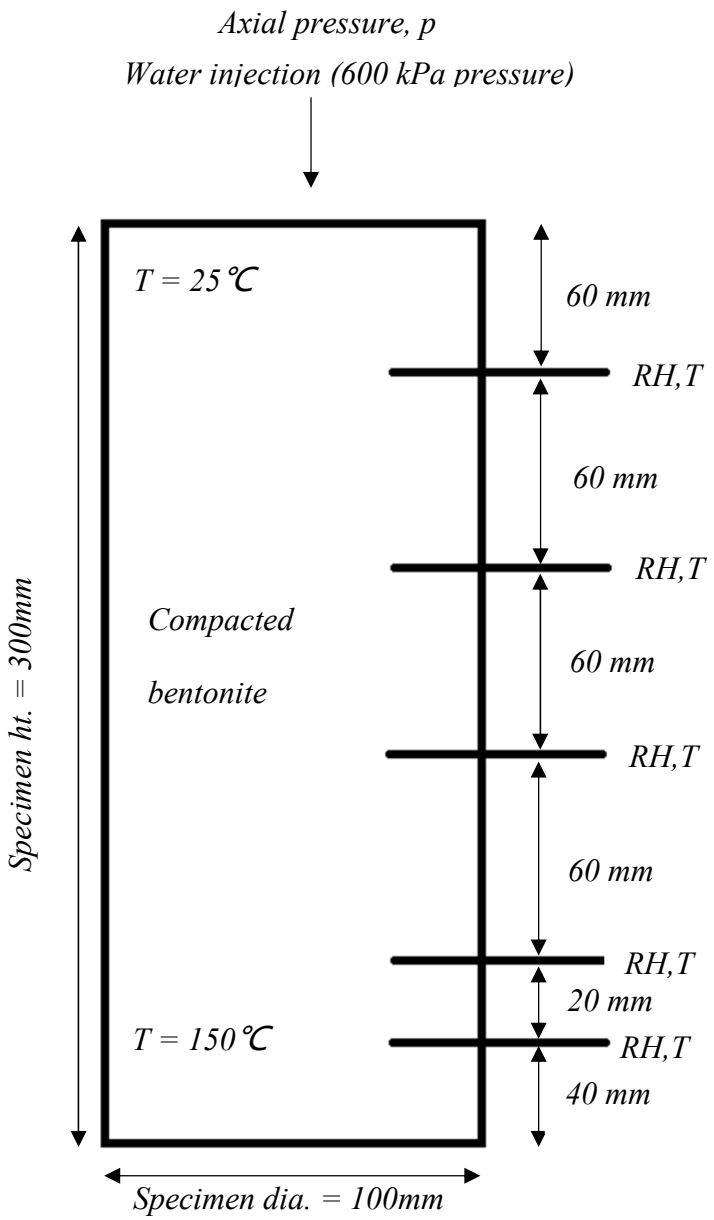

Figure 5.2 Schematic representation of temperature, relative humidity and axial stress measured in compacted bentonite specimens during thermo-hydraulic tests at 150 °C

The water content, dry density and degree of saturation of the bentonite specimens at the predetermined depths were determined after termination of the tests. The procedures adopted for determining these properties are presented in Chapter 3. The test results concerning the anion and cations concentrations at predetermined depths of the specimens are presented in Chapter 6.

5.3 Test results and discussion

The following sections present the influence of the applied temperature and hydraulic gradients adopted during the tests on the thermal, hydraulic and mechanical response of the compacted bentonite specimens

5.3.1 Temperature variations at an applied temperature of 85 °C

Figure 5.3 presents the measured temperatures with elapsed time at predetermined depths of the specimens for the two non-isothermal tests at 85 °C (i.e., Test nos. 5 and 6). The temperature at all predetermined depths equilibrated in about 150 days for both tests.

Table 5.1 presents the measured equilibrium temperatures at various predetermined depths of the specimens in Tests 5 and 6. Figure 5.4 shows the equilibrium temperature against distance of the temperature probes from the heat source (i.e., the temperature profiles).

It can be seen from Figs. 5.3 and 5.5 and Table 5.1 that, the maximum temperature generated within the compacted bentonite specimens was similar (about 75 °C) at a distance of 20 mm from heat source. The maximum temperature generated was found to be greater than that was noted for the thermal tests under similar condition of applied temperature (see Table 4.2 for 40 mm thick insulation).

The equilibrium temperatures at distances of 40 and 60 mm from the heat source for both specimens are found to be slightly greater than the equilibrium temperature noted for the specimen that was tested with by applying only the thermal gradient (data in Table 4.2 with 40 mm thick insulation).

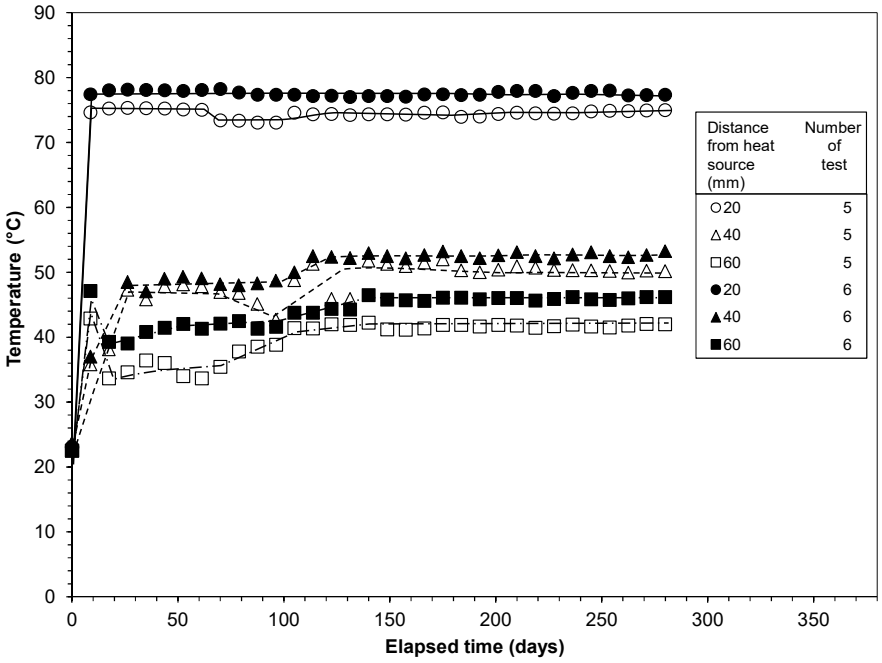

Figure 5.3 Transient temperature variations at specified depths of the specimens due to thermo-hydraulic loading at 85 °C

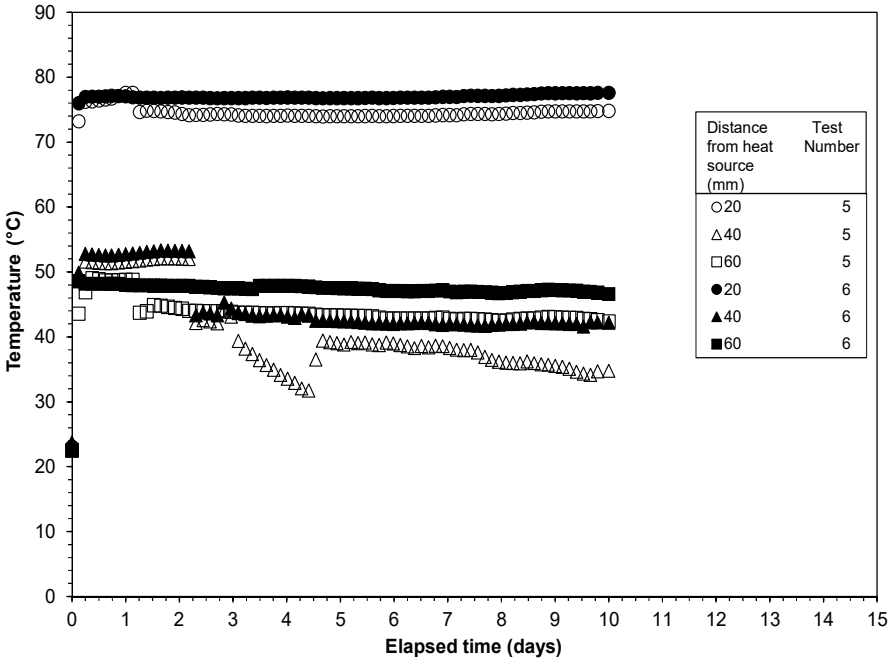

Figure 5.4 Transient temperature variations at specified depths of the specimens due to thermo-hydraulic loading at 85 °C (First 10 days of testing)

The test results indicated that, the temperature at various salient depths of the compacted bentonite specimens when subjected to thermo-hydraulic gradient were generally greater than that for the specimen with an applied thermal gradient.

Table 5.1 Influence of thermal and hydraulic gradient on equilibrium temperature at various depths for compacted MX80 bentonite (diameter = 100 mm, height = 80 mm)

Distance of temperature probe from heat source (mm)	Equilibrium temperature (°C)	
	Test no. 5	Test no. 6
0*	85	85
20	75	77
40	49	52
60	42	46
80*	25	25

* Temperatures maintained at both ends

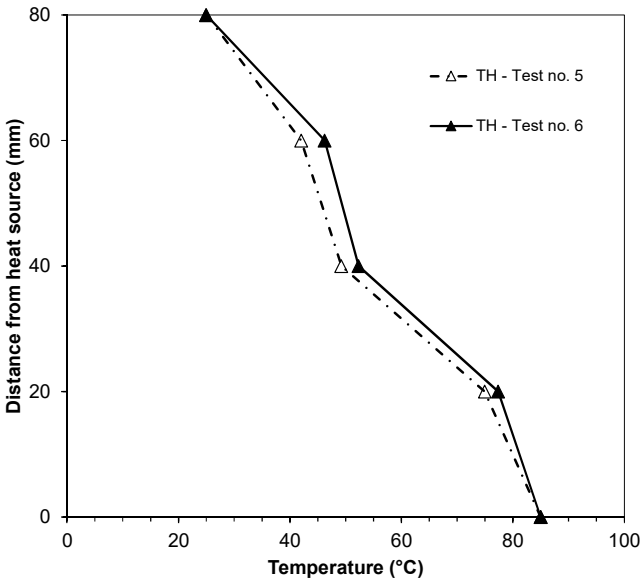

Figure 5.5 Temperature profiles (at the time of termination of the tests) of the specimens due to thermo-hydraulic loading at 85 °C

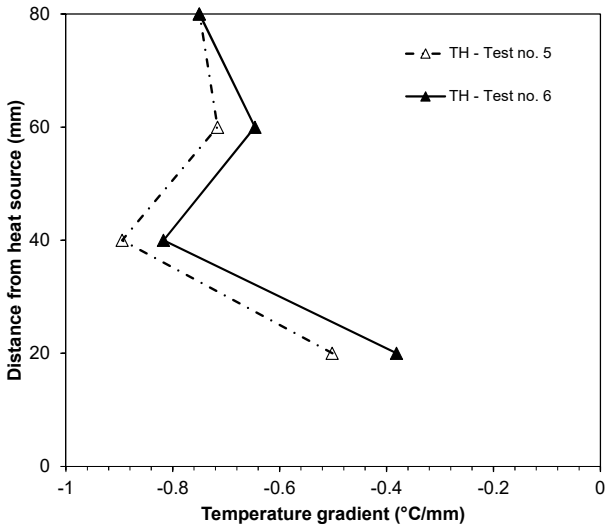

Figure 5.6 Temperature gradient variations at predetermined depths of the specimens due to thermo-hydraulic loading at 85 °C

Figure 5.6 presents the temperature gradient at various salient depths of the specimens. The temperature gradient for both specimens remained similar. It can be seen in Fig. 5.6 that, the temperature gradients remained between – 0.89 and - 0.38 °C/mm (i.e., between -8.9 and -3.8 °C/cm). Comparing the temperature gradients in the thermo-hydraulic tests and thermal test (Fig. 4.6), it can be noticed that the range of thermal

gradient is similar in case of thermo-hydraulic tests as compared to the thermal test (-13.0 to -7.1 °C/cm). Additionally, the temperature gradient at a distance of 20 mm from the heat source is smaller for thermo-hydraulic tests as compared to the thermal tests. This is attributed due to a higher temperature generated at a distance of 20 mm from the heat source for the thermo-hydraulic tests.

The thermal conductivity of soils increases with an increase in the water content. Tang et al. (2008) stated that, the thermal conductivity of compacted bentonite increases with an increase in the water content. The test results in this study indicate that the difference in the equilibrium temperature at various depths due to an applied thermal and thermo-hydraulic gradient are not significantly different. However, the changes are distinct due to an applied thermo-hydraulic gradient which is primarily attributed due to a change in the water content of compacted bentonites.

5.3.2 Relative humidity variations for an applied temperature of 85 °C

Figures 5.7 and 5.8 present the measured relative humidity with elapsed time at predetermined depths of the specimens for the two thermo-hydraulic test at 85 °C (i.e., Test nos. 5 and 6). The injection of water with a constant pressure of 600 kPa lead to the increase in the relative humidity along the full length of the specimens.

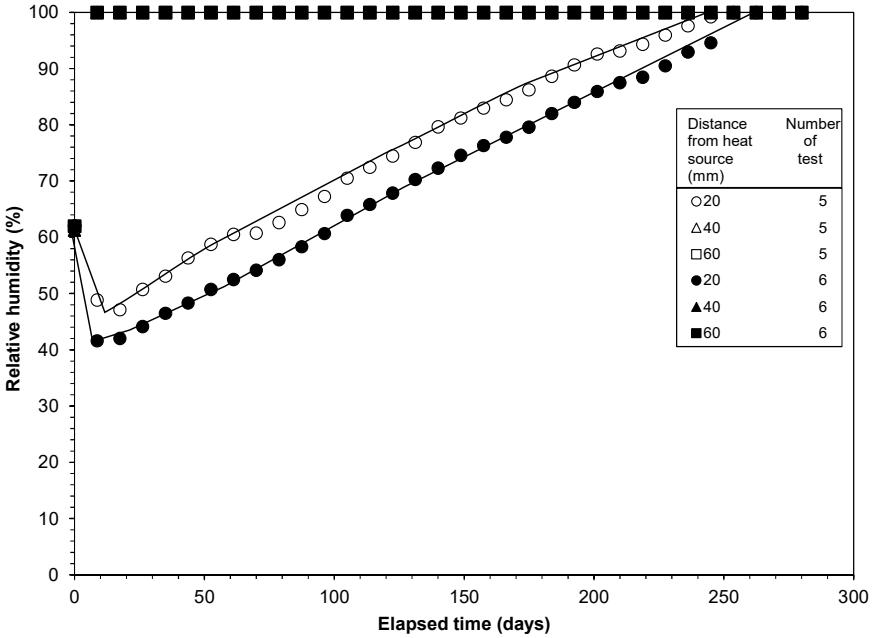

Figure 5.7 Transient relative humidity variations at specified depths of the specimens due to thermo-hydraulic loading at 85 °C

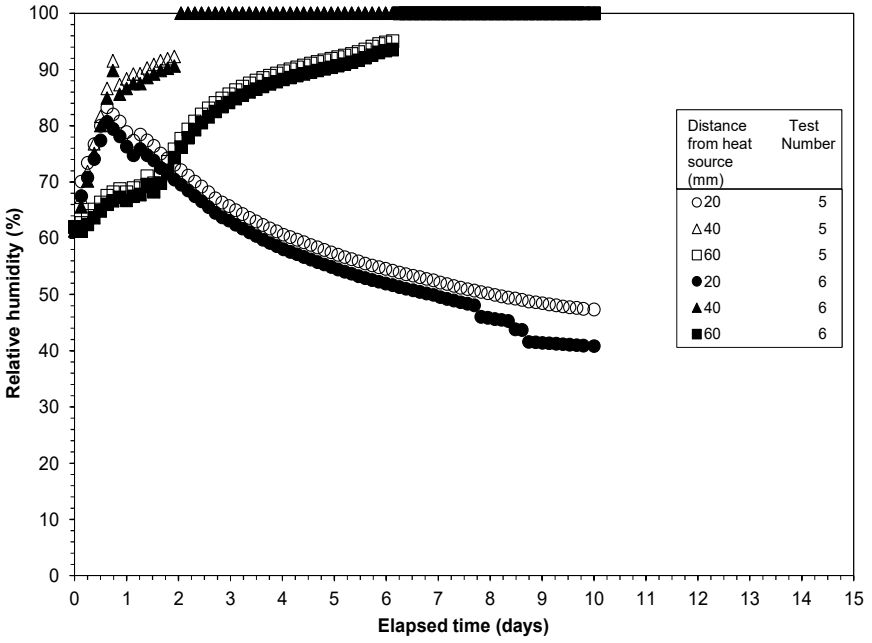

Figure 5.8 Transient relative humidity variations at specified depths of the specimens due to thermo-hydraulic loading at 85 °C (First ten days of testing)

The relative humidity increased with an elapsed time for both specimens. The relative humidity equilibrated in about 250 days at all depths. The measured relative humidity at distances of 40 and 60 mm from the heat source was 100 % within about

seven days. This is attributed due to the supply of water from the top of the specimens. The relative humidity at a distance of 20 mm from heat source increased and attained 100 %. A difference in the transient relative humidity at a distance of 20 mm from the heat source between the specimens in Tests 5 and 6 is attributed due to a difference in the temperature response (see Fig. 5.3).

The results in terms of the relative humidity from non-isothermal tests (Table 4.2 and Fig. 4.9) clearly showed that, an increase in the relative humidity at the opposite end of the heat source is solely due to water vapour movement from hot to cold end. In case of an applied thermo-hydraulic gradient, a combined action of the water vapour movement due to thermal gradient and an increase in the water content due to supplied water can significantly increase the relative humidity at the cold end. An increase in the relative humidity in compacted bentonite causes a decrease in suction resulting in swelling of compacted bentonites. Under restrained condition (i.e., constant volume condition), redistribution of water content accompanied by the development of axial stress may be expected to occur. The results of the axial stress development from thermos-hydraulic tests are presented in section 5.3.5, whereas the water content data are presented in section 5.3.6.

5.3.3 Temperature variations at an applied temperature of 150 °C

Figures 5.9 and 5.10 present the measured temperatures with elapsed time at predetermined depths of the specimens for the three thermo-hydraulic tests at 150 °C (i.e., Test nos. 7, 8 and 9). The insulation used for all three tests was 40 mm thick rockwool covered with reflective tape. The temperature at all predetermined depths

equilibrated within about 25 days and thereafter remained nearly unchanged. For the sake of clarity, the initial temperature data are not shown in Fig. 5.9.

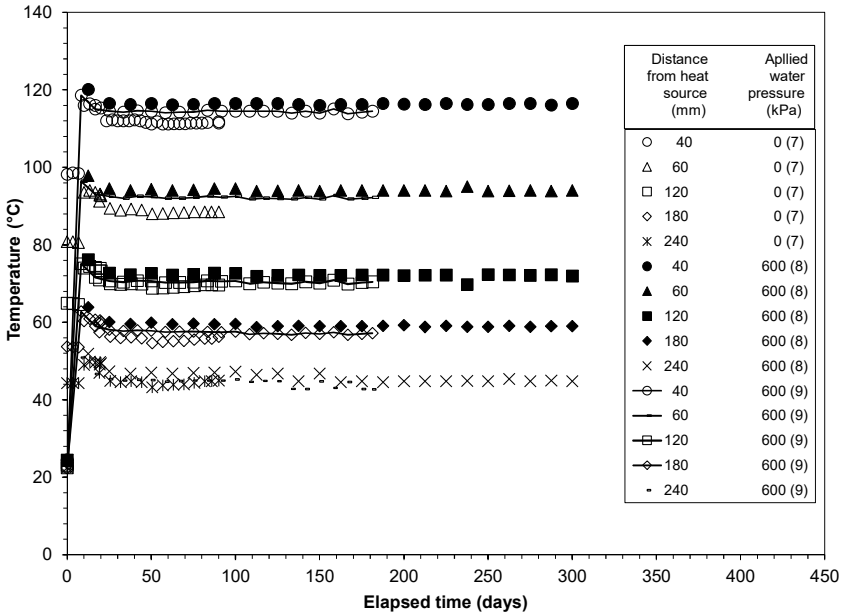

Figure 5.9 Transient temperature variations at specified depths of the specimens due to thermo-hydraulic loading at 150 °C

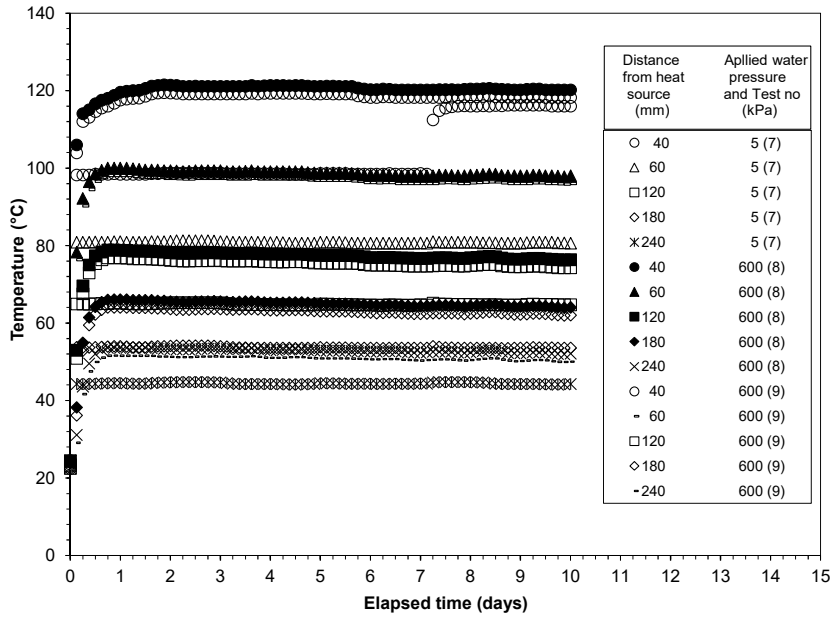

Figure 5.10 Transient temperature variations at specified depths of the specimens due to thermo-hydraulic loading at 150 °C (First 10 days of testing)

Table 5.2 presents the measured equilibrium temperatures at various predetermined depths for the tests. Figure 5.8 shows the equilibrium temperature against distance of the temperature probes from the heat source. For comparison, the results obtained from the tests with 80 mm high specimens (i.e., Test nos. 5 and 6) are also shown in Fig. 5.11.

Table 5.2 Influence of thermal and hydraulic gradient on equilibrium temperature at various depths for compacted MX80 bentonite (diameter = 100 mm, height = 300 mm)

Distance of temperature probe from heat source (mm)	Equilibrium temperature (°C)		
	Test 7	Test 8	Test 9
0*	150	150	150
40	112	116	114
60	89	94	92
120	70	72	70
180	56	59	57
240	45	45	43
300*	25	25	25

* Temperatures maintained at both ends

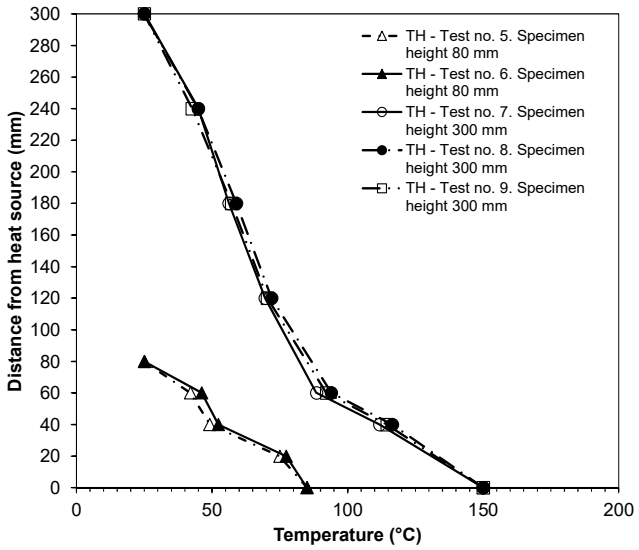

Figure 5.11 Temperature profiles (at the time of termination of the tests) of the specimens due to thermo-hydraulic loading at 150 °C

The distances of various salient depths of the specimens from the heat source were considered for calculating the temperature gradients. Figure 5.12 shows the

temperature gradients in the specimens at various distances from the heat source. For the sake of comparison, the results obtained for the specimens in test nos. 5 and 6 are also shown in Fig. 5.12.

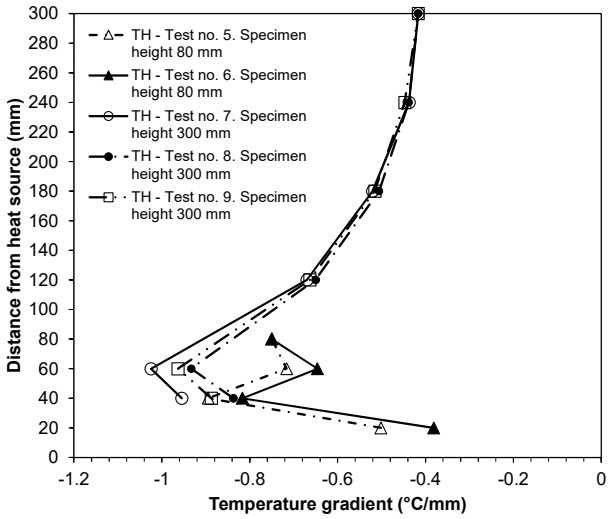

Figure 5.12 Temperature gradient variations at predetermined depths of the specimen due to thermo-hydraulic loading at 150 °C

It can be seen in Fig. 5.9 that, the temperature gradients for the specimens in test nos. 7, 8 and 9 remained between – 1.05 and - 0.4 °C/mm (i.e., between -10.5 and – 4.0 °C/cm) for all cases. Also, it can be seen that the different water pressures didn't affect the temperatures and thermal gradients along the salient levels of the specimens. Comparing the thermal gradients in test nos. 5 and 6 with test nos. 7, 8 and 9, it can be seen that an application of a temperature of 150 °C introduced higher thermal gradients in the specimens.

5.3.4 Relative humidity variations at applied temperature of 150 °C

Figure 5.10 presents the measured relative humidities with elapsed time at predetermined depths of the specimens for the three thermo-hydraulic tests at 150 °C

(i.e., Test nos. 7, 8 and 9). The duration of Test no. 7 was 100 days. Therefore, the relative humidity had not equilibrated, whereas for, the other two tests it equilibrated along the full length of the specimens after 130 days. During the first 35 days the relative humidity at distances of 60 and 120 mm increased sharply and then decreased. This is attributed due to the vapour movement from the heat end towards the colder side of the specimens.

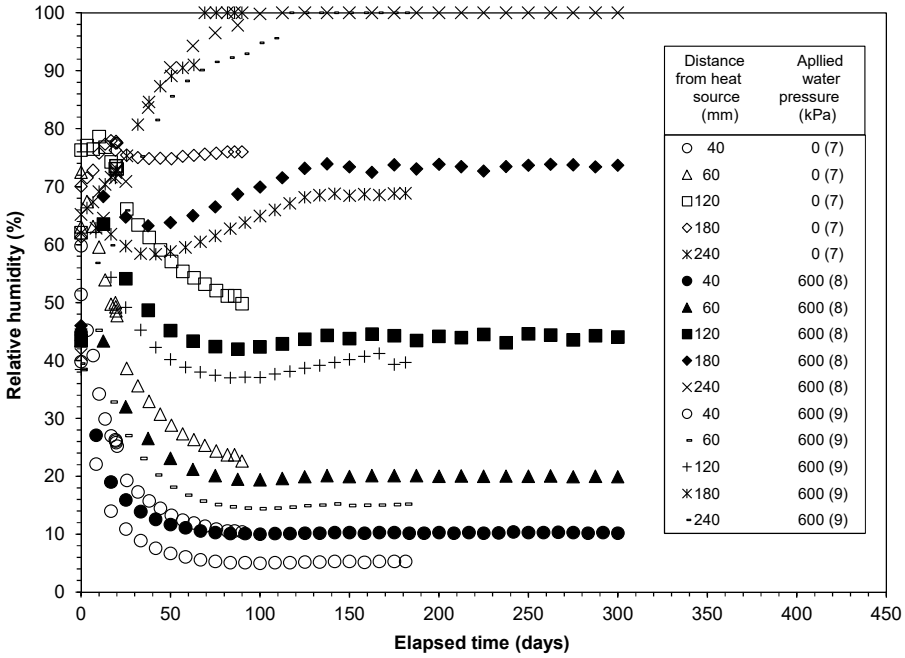

Figure 5.13 Transient relative humidity variations at specified depths of the specimens due to thermo-hydraulic loading at 150 °C

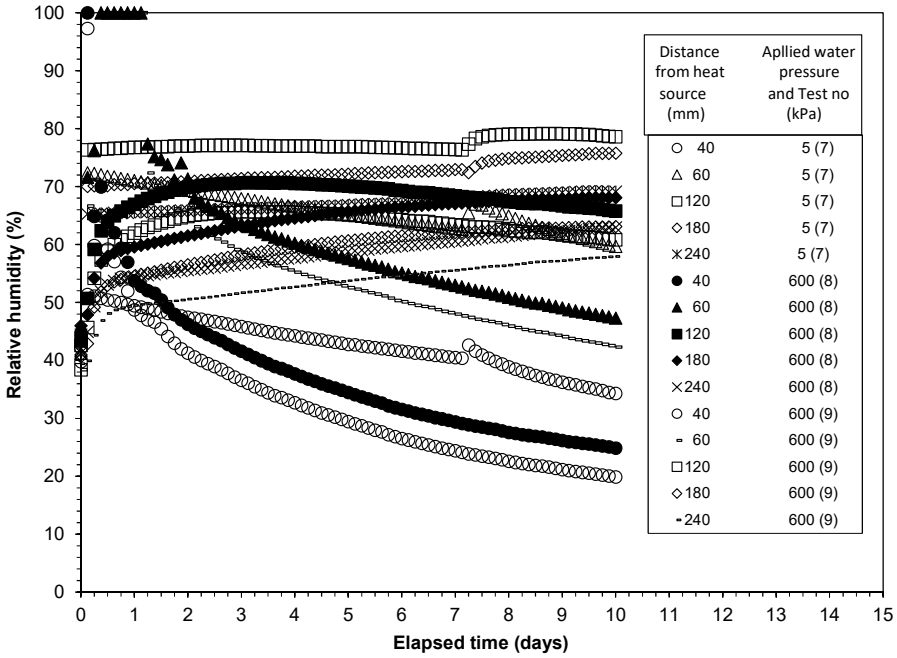

Figure 5.14 Transient relative humidity variations at specified depths of the specimens due to thermo-hydraulic loading at 150 °C (First 10 days of testing)

Table 5.3 presents the measured relative humidities at various predetermined depths at the time of termination of the tests. Figure 5.15 shows the relative humidity against distance of the relative humidity probes from the heat source.

Table 5.3 Influence of thermal and hydraulic gradient on equilibrium relative humidity at various depths for compacted MX80 bentonite (diameter = 100 mm, height = 300 mm)

Distance of temperature probe from heat source (mm)	Relative humidity (%)		
	Test 7	Test 8	Test 9
40	10	10	5
60	23	20	15
120	50	44	40
180	76	74	69
240	100	100	100

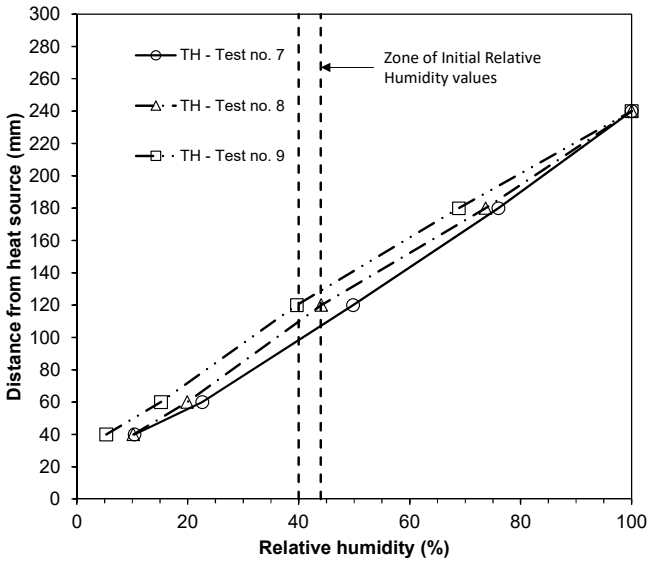

Figure 5.15 Relative humidity profiles (at the time of termination of the tests) of the specimens due to thermo-hydraulic loading at 150 °C

It can be seen from Table 5.3 and Fig. 5.15 that, the relative humidity decreased towards the heat source, whereas it increased as the distance from the heat source increased. Unlike in Test nos. 5 and 6 where the relative humidity attained at all predetermined depths was 100%, for Test nos. 7, 8 and 9 (height of specimens = 300 mm), except at a distance of 240 mm where the measured relative humidity was 100%, at all other depths the relative humidity remained less than 100%. The test results indicate that water migration due to the supply of water at the cold end may not cause a significant increase in the relative humidity for thicker compacted bentonites when the applied temperature is very high.

5.3.5 Axial pressure development in non-isothermal conditions

Figure 5.16 shows the elapsed time versus the measured axial pressures at the opposite end of the heat source for the compacted bentonite specimens in non-isothermal tests (Test nos. 5 and 6). The applied temperature and water pressure in this case were 85 °C and 600 kPa. Figure 5.17 depicts the axial pressure generated during the non-isothermal hydraulic tests (Test nos. 7, 8, and 9) at 150 °C. The applied water pressure for test no 7 was 5 kPa whereas for Test nos. 8 and 9 water was injected at a pressure of 600 kPa.

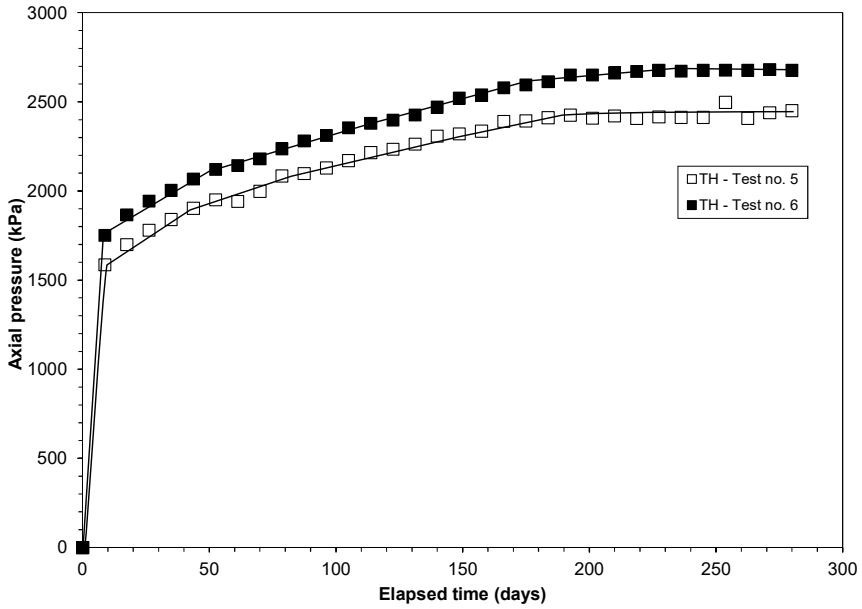

Figure 5.16 Elapsed time versus axial stress plot for thermo-hydraulic tests on compacted bentonite specimens at 85°C

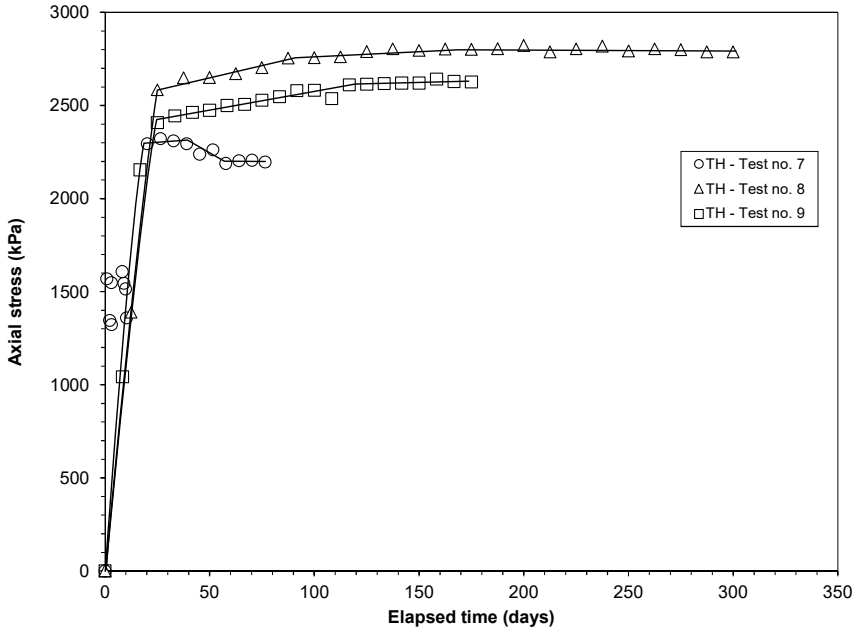

Figure 5.17 Elapsed time versus axial stress for thermo-hydraulic tests on compacted bentonite specimens at 150°C

It can be seen Figs. 5.16 and 5.17 that, the axial pressures for the compacted bentonite specimens increased with elapsed time before attaining an equilibrium at which, no further significant changes in the axial pressures was noted. The measured equilibrium axial pressures for the specimens in Test nos. 5, 6, 7, 8 and 9 were 2677, 2451, 2196, 2627 and 2803 kPa, respectively. The test results indicated that the differences in the applied temperature (85 and 150 °C) and hydraulic boundary condition (with or without water injection), the axial pressure in compacted bentonites in this study remained between 2 to 3 MPa. This suggests that, thermal gradient effects are more pronounced in the axial pressure development in compacted bentonites under restrained condition. Additionally, applications of temperatures of 85 and 150 °C caused changes in terms of thermal gradient and relative humidity; however, their impact on the development of axial stress remained within about 1.0 MPa.

5.3.6 Profiles of water content, dry density, degree of saturation and suction

Figures 5.18 (a), (b), (c) and (d) show the water content, dry density, degree of saturation, and suction profiles of the specimens tested, respectively. The data presented in Figs. 5.18 (a), (b) and (c) are based on analyses of the samples of bentonite slices (20 mm thick) after termination of each tests. Therefore, the results are plotted corresponding to the mid-level of each slice. The results of Test no. 9 is not presented since the test is in progress for exploring long-term effects. The suction data presented in Fig. 5.18 (d) are based on the relative humidity and temperature data at the end of each test. The suctions were calculated based on the thermodynamic relationship between the relative humidity and suction (Fredlund et al., 2012).

The results presented in Fig. 5.18 indicate that the results of tests conducted at a temperature of 85 °C are different than the tests at 150 °C. The specimens in Tests nos. 5 and 6 underwent a wetting process as indicated by an increase in the water content, a decrease in the dry density, an increase in degree of saturation and a decrease in suction. On the other hand the specimens subjected to 150 °C showed a combined behaviour. The top half of the specimen towards the cold end underwent a wetting process as shown from the increased water content, degree of saturation and the decreased dry density and suction, whereas the reverse was the trend for the bottom half the specimens. The water content and degree of saturation decreased whereas the dry density and the suction increased. The test results clearly indicated that, at an applied temperature of 150 °C, the specimens underwent a drying process towards the heat source.

Table 5.4 Mass of water contained in the samples subjected to thermal tests.

	Test 5	Test 6	Test 7	Test 8
Initial mass of water for 80 mm sample	181.5g	181.5g		
Initial mass of water for 300 mm sample			680g	680g
Mass of water in the sample (Post-test)	185g	187g	571g	480g

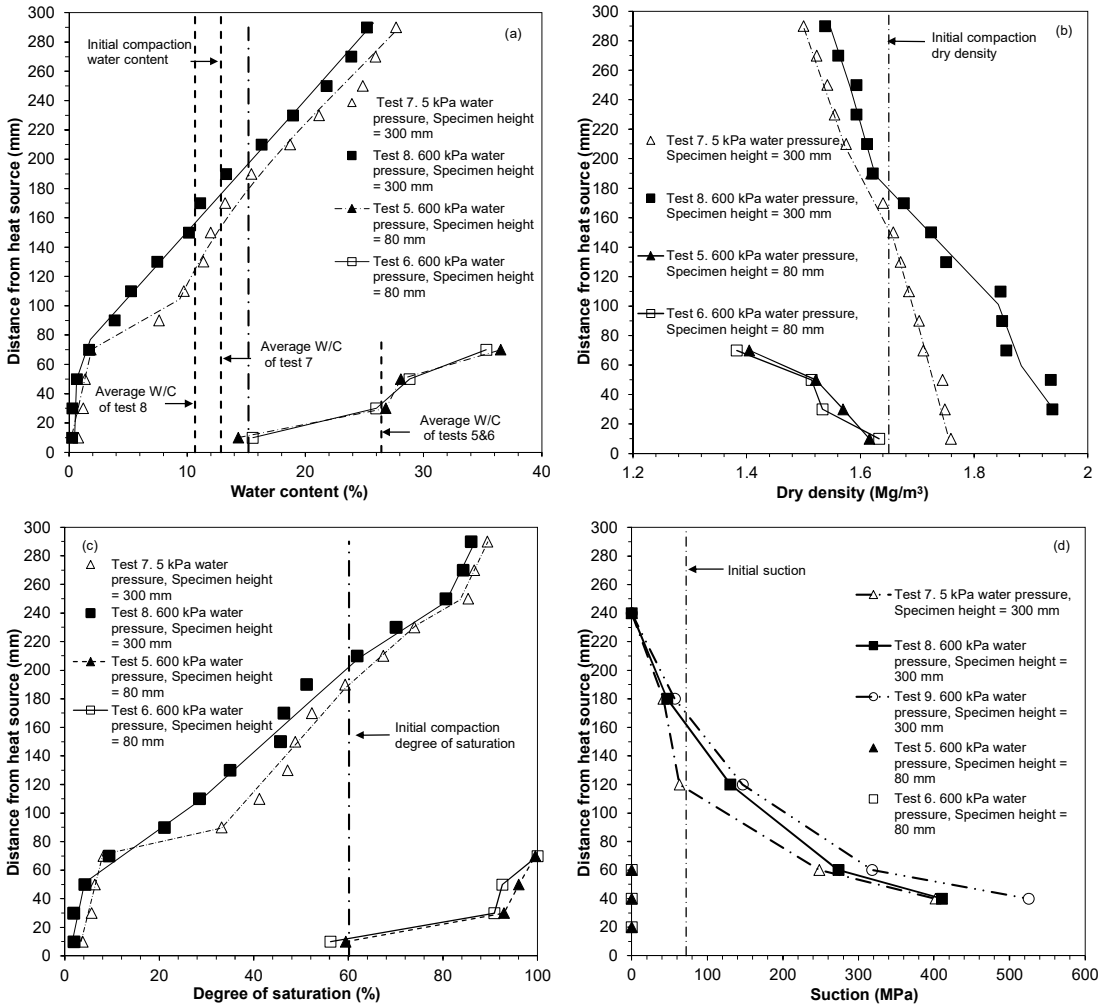

Figure 5.18 Profiles of (a) Water content, (b) Dry density, (c) Degree of saturation and (d) suction of the specimens after thermo-hydraulic tests at 85 and 150°C

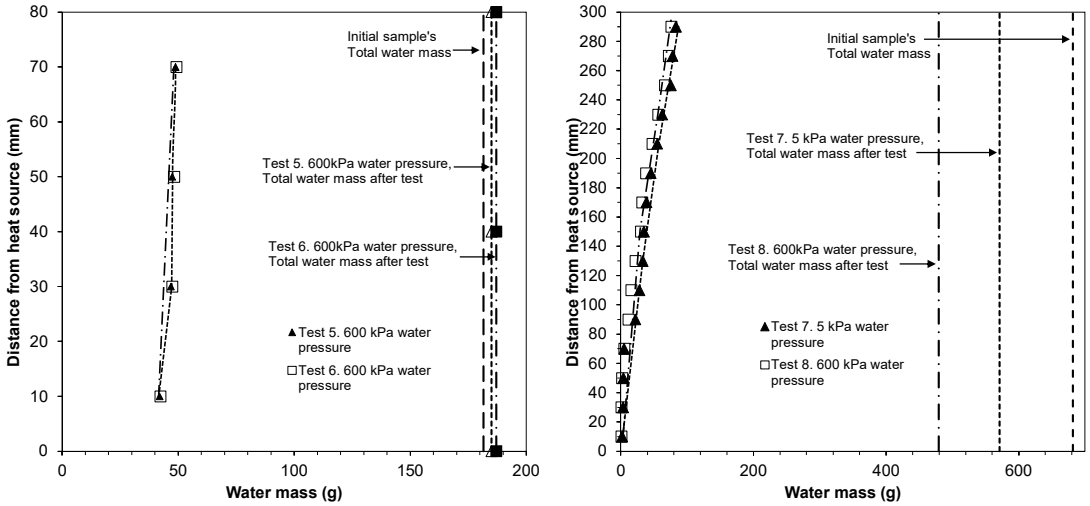

Figure 5.19 Water mass profiles, (a) Thermohydraulic tests at 85°C (b) Thermohydraulic tests at 150 °C

Table 5.4 and figure 5.19 demonstrate the mass of water in the bentonite samples prior and subsequent to the testing processes. The water mass in the samples subjected to 85 °C increased in comparison with their initial value. The average increase of the water mass is minimal but in addition with the results from section 4.3.6 it is suggested that the water infiltration overcomes the evaporation of the water due to the thermal loading. The sample in test 6 showed the highest increase with 3% from its initial value. Generally, both tests show a similar response as the output is given for the same time period and both terminated when all the RH sensors reached the equilibrium which in this case is when they reached the 100%. It has to be noted that the flooding of the sensors does not mean that the bentonite sample is fully saturated as the last sensor is placed at 20mm from the heater. Thus, at the sample's actual equilibrium the mass of the absorbed water is possible to be higher than the one reported above.

On the other hand, both tests nos 7 and 8 show a decrease in their water mass. Tests nos 7 and 8 show a 17% and 30% decrease in their initial water mass respectively. The areas where the temperature was above the 100 °C formed a zone where the water

evaporated towards the colder areas not allowing the infiltration of the injected water. The decrease of the overall water mass can be explained from the potential leakages of the cell's column (RH probe shafts). The water content profile in figure 5.18 shows that the samples underwent a drying process between the heater and the 140 mm away from it. Along this area are three RH probe shafts thus the leakage potentials are increased regardless the water tightness of the connections. The combination of the probable leakages and the non-infiltrated zones lead to the overall decrease of the sample's water mass. Also, evidently the loss of water is time depended as the tests nos7 and 8 have the same constraints and their only difference was the testing period. Tests 7 and 8 run for 90 and 300 days respectively.

Finally, the complexity of the process to derive the water mass and water content post mortem measurements allows the dissected specimens to partially dry during the testing procedure.

5.3.7 Shapes of Temperature and Relative Humidity Profiles

According to Tripathy et al (2017) the shapes of temperature profiles presented in Figures 4.13 and 5.11 are found to be similar to an inverted S-shaped curve. The experimental data presented in Figures 4.13 and 5.11 were best-fitted with a two-parameter model (Equation (1)) as shown in Figures 5.20 and 5.21. The fitting parameters are shown in Table 5.5

$$D = \frac{D_{\max}}{\left[1 + \left\{(aT)^b\right\}\right]^{\left(1-\frac{1}{b}\right)}}, \tag{1}$$

where D is the distance from the heat source, D_{max} is thickness of bentonite, a and b are the fitting parameters, and T is the temperature at a distance of D from the heat source.

Table 5.5 Model fitting parameters for temperature profiles.

Test No.	Type of Test	Height of Specimen (mm) [1]	Temperature at Bottom/Top (°C/°C)	Model Parameters	
				a	*b*
T1	Non-isothermal	80	85/25	0.023	5
T2		80	85/25	0.020	5
T3		300	150/25	0.022	5
T4		300	150/25	0.017	5
TH5	Non-isothermal hydraulic	80	85/25	0.021	5
TH6		80	85/25		
TH7		300	150/25		
TH8		300	150/25	0.017	5
TH9		300	150/25		

Diameter of specimen = 100 mm. a and b: fitting parameters.

The value of the parameter *a* decreased for an increase in the thickness of insulation, an increase in the temperature, an increase in the thickness of bentonite, and for the hydraulic tests. The value of the parameter *b* remained unchanged. Equation (1) can be used to calculate the distance at which an anticipated temperature will prevail.

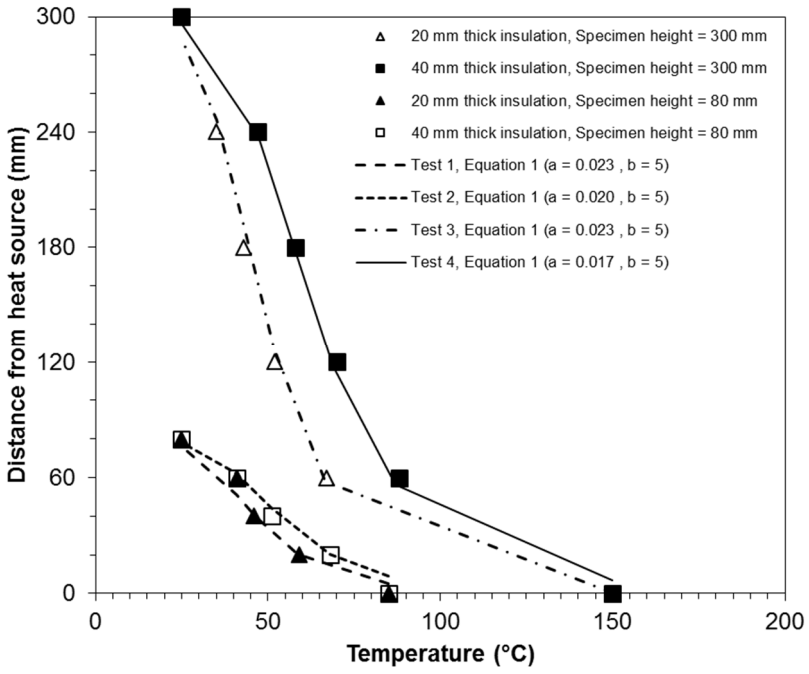

Figure 5.20 Temperature Profile shapes for Non-isothermal tests

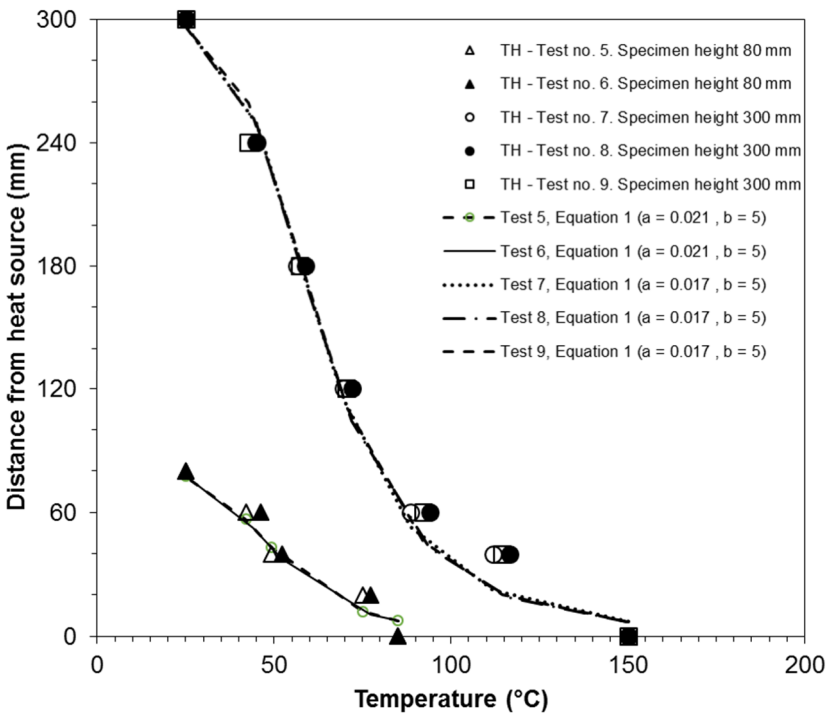

Figure 5.21 Temperature Profile shapes for Non-isothermal/Hydraulic tests

The shapes of relative humidity profiles for non-isothermal and non-isothermal hydraulic tests (Figures 4.17 and 5.15) are found to be dissimilar. A generalized two parameter model (Equations (2), (3)) was used to best-fit the relative humidity profiles, as shown in Figures 5.22 and 5.23. The model parameters are shown in Table 3. In all cases, very high values of the coefficients of regression were found. Equation (2) can be used to estimate the distance at which a specific value of the relative humidity will prevail or the relative humidity at any distance from the heat source. The parameters shown in Table 5.6 are for the duration of the tests considered in this study and hence may not be reliable for calculating the relative humidity at equilibrium conditions for the non-isothermal applied boundary condition. The relative humidity profiles for Tests TH7, TH8, and TH9 (Figure 5.23) were best fitted with a linear relationship (Equation (3).

$$RH_D = \frac{1}{n}\log_e\left(\frac{D}{m}\right) \quad (2)$$

$$RH_D = \left[\frac{D-17.71}{2.23}\right], \quad (3)$$

where m and n are the best-fit parameters and RH_D is the relative humidity at a distance of D from the heat source.

Table 5.6 Model parameters for the relative humidity profiles in non-isothermal tests.

Test No.	Model Parameters	
	m	*n*
T1	6.0375	0.0339
T2	13.296	0.0267
T3	13.559	0.0321
T4	40.950	0.0240

m and n: best-fit parameters.

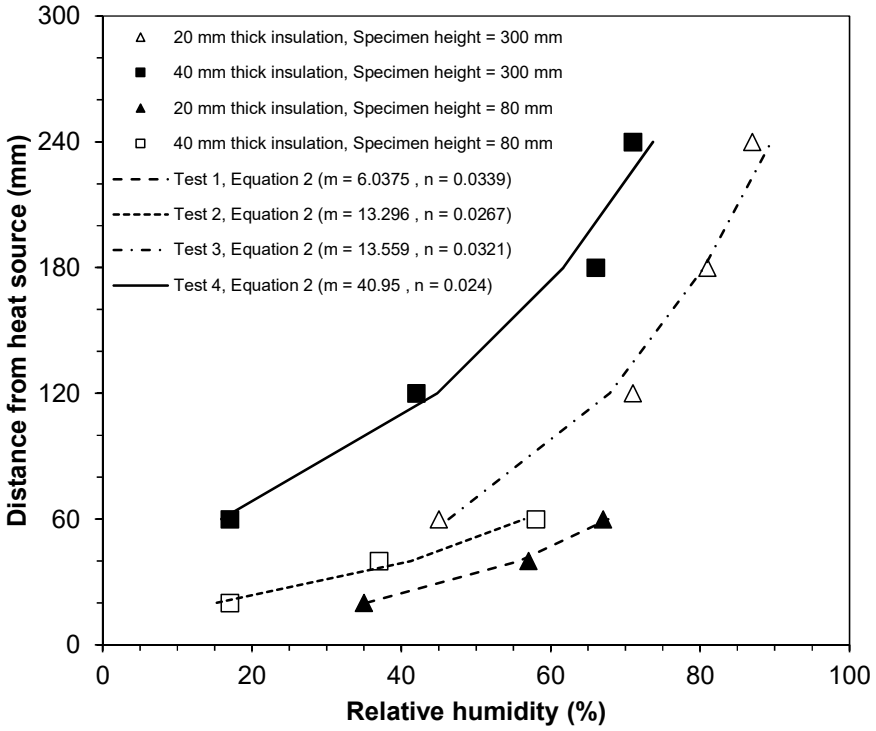

Figure 5.22 Relative humidity Profile shapes for Non-isothermal tests

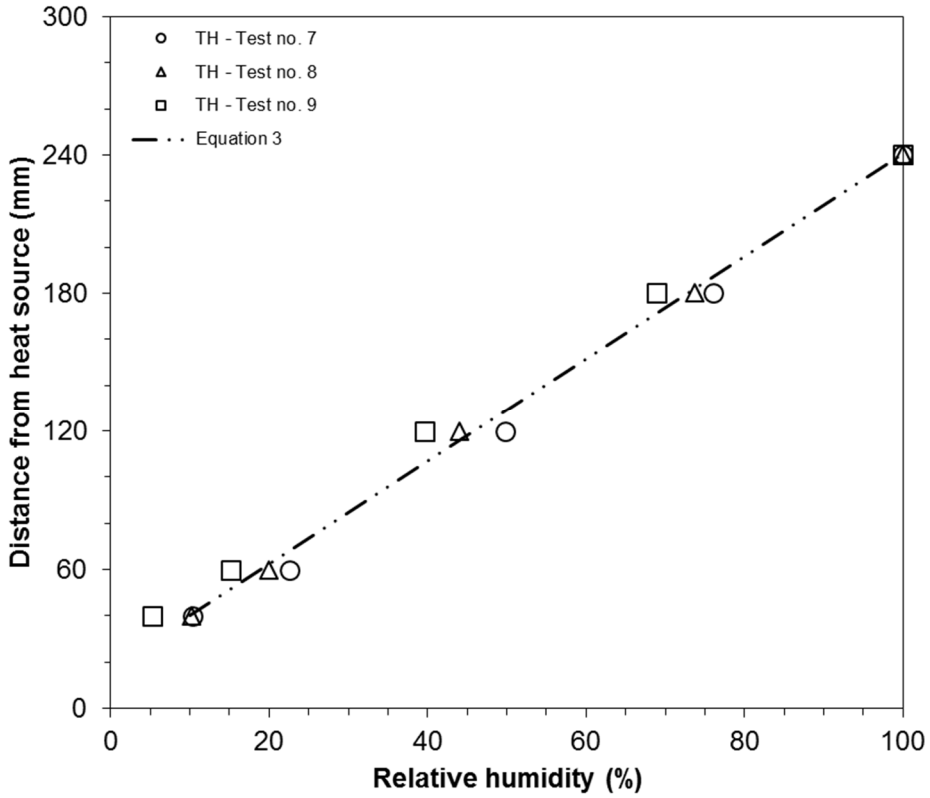

Figure 5.23 Temperature Profile shapes for Non-isothermal Hydraulic tests

The experimental data of MX80 bentonite reported by Villar et al. [2014] were considered for comparing with the model results in this study. Villar et al. [2014] carried out laboratory tests on MX80 bentonite (70 mm diameter and 500 mm high) with initial dry density and water content of 1.53 Mg/m^3 and 6.4%, respectively. The applied temperature at the base of the specimen was 140 °C. Following the heating phase for about 239 days, the specimen was hydrated with water from the opposite end of the heat source with an injection pressure of 6.0 kPa. Figure 5.24 (a,b) show the temperature and relative humidity profiles for the non-isothermal and non-isothermal hydraulic phases of the test, respectively. The experimental data for the simultaneous heating and hydration phase correspond to a test duration of 620 days. The calculated results for the temperature and relative humidity are shown in Figure 5.24. It can be seen that the model results in this study generally predicted higher values of the temperature and the relative

humidity; however, the shapes of the profiles are captured well. The difference in the experimental and calculated results originate from the differences in the initial compaction conditions, the applied temperature, the size of specimen, the insulation type used, and the duration of the tests.

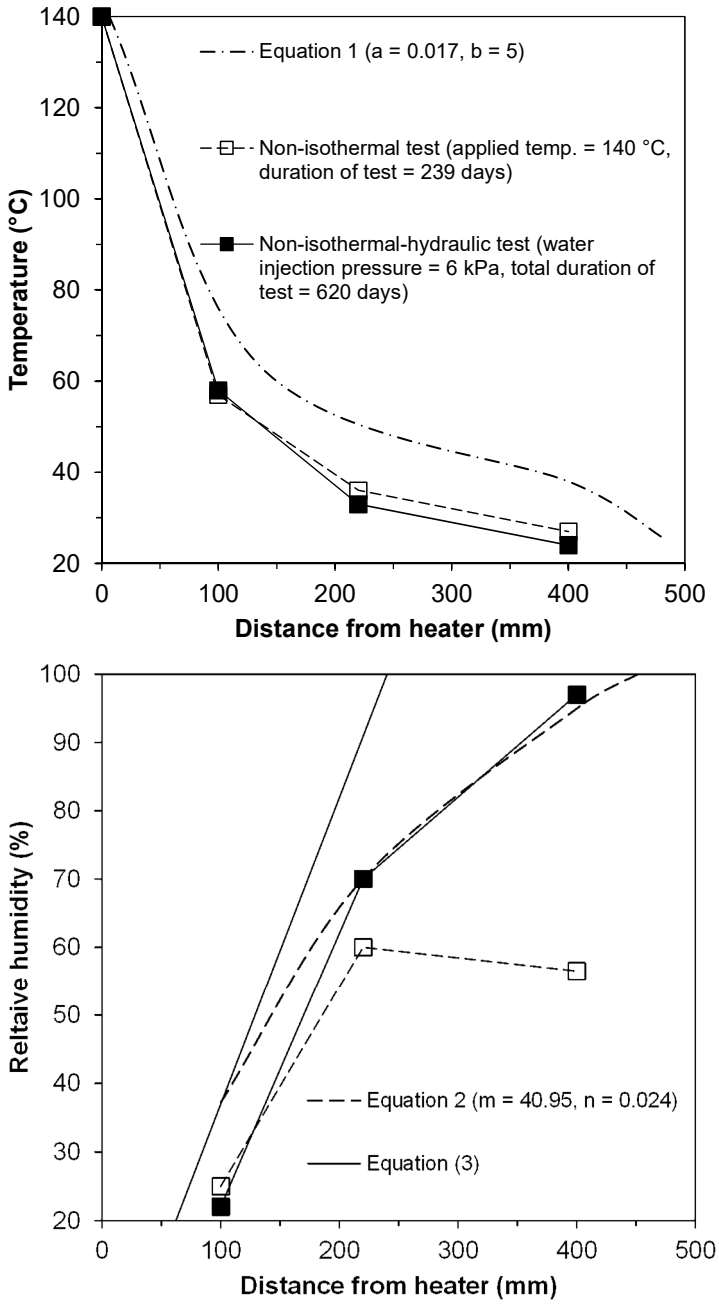

Figure 5.24 Comparison of test results from the literature [Villar et al, 2017] and model results in this study for: (a) temperature profiles; (b) relative humidity profiles.

5.4 Summary

In this chapter, the influence of the thermal and hydraulic gradients on the thermo-hydro-mechanical response of compacted bentonite specimens is presented. At the opposite end of the bentonite specimens two different temperature boundary conditions were considered, such as (i) 85 °C and 25 °C for specimens with dia. = 100 mm and height = 80 mm and (ii) 150 °C and 25 °C for the specimens with dia. = 100 mm and height = 300 mm. A water injection pressure of 600 kPa was considered.

The test results obtained are the transient temperature and relative humidity at predetermined depths of the specimens, axial pressure at the opposite side of the heat source. The test results of water content, dry density, and degree of saturation along the depth of the bentonite specimens were determined after the termination of the tests.

The temperature of the samples subjected to 85 °C increased along their full length and equilibrate when the relative humidity reached equilibrium. The temperature values are similar with the values obtained from the non-isothermal test described in chapter 4. The relative humidity increased along the full length of the specimen until it reached the 100%. The middle part of the specimen reached first the 100% relative humidity as the combined action of the water injection from the cold end and the vapour movement from the hot end took place. The water injection caused the increase of the water content and degree of saturation whereas the dry density and suction decreased.

The samples subjected to 150 °C equilibrate thermally within 25 days along their full length and weren't affected by the changes in the relative humidity. The relative humidity varied along the length of the samples. The parts closer to the cold end showed an increased relative humidity compared to their initial with a maximum value of 100% whereas the relative humidity of sections closer to the heating elements decreased indicating a vapour

movements from the hot end towards the colder area. The variation of the relative humidity is demonstrated also at the profiles of the water content, dry density, degree of saturation and suction. At the cold end of the specimen with the increased relative humidity the water content and degree of saturation increased whereas the dry density and suction decreased demonstrating a wetting process of the material. On the other hand at the hot end of the sample we observed the opposite phenomena where the water content and degree of saturation decreased while the dry density and suction increased, indicating the drying process that this part underwent.

For both type of tests the axial pressure remained between 2 and 3 MPa. That is a clear indication that even though the application of different thermal gradients showed a different behaviour of the temperature and relative humidity the impact on the axial pressure when the specimen is hydrated remained within 1.0 MPa.

Three formulas used to model the temperature and relative humidity behaviour of the bentonite samples used in this study. The temperature results are fitted with a two parameter equation and the given profiles are similar to an inverted S-shaped curve. The fitting parameters are related to the height of the specimen and the type of the insulation used for each test. Two equation used to model the results for the relative humidity values at any given distance from the heat source in the compacted bentonite sample. The non –isothermal tests modelled with the two parameter equation 2 with the parameters being related to the duration and the insulation of each test. On the other hand the non-isothermal hydraulic tests at 85 °C weren't modelled as their equilibrium value was 100% RH whereas the tests at 150°C where fitted with a simple linear equation.

The equations derived from this study were used to model and compare the values from the work of Villar et al (2014). The modelled results are higher than what reported from Villar but that is expected due to the differences in their initial conditions. Despite the

difference in the measured and calculated values, the shape given from the model is similar to the shape taken from the experimental values for both the temperature and relative humidity values.

CHAPTER 6.
EFFECTS OF TEMPERATURE AND HYDRAULIC GRADIENTS ON MINERALOGY AND SOLUTE TRANSPORT IN COMPACTED BENTONITE

6.1 Introduction

The concept for the safe disposal of high-level radioactive waste in many countries considered bentonite and bentonite-based materials as the key components of the engineered barrier systems. Pre-compacted bentonite blocks can be used to form the buffer around the waste canister, while bentonite can also be used to backfill and seal the disposal tunnels and the underground facilities. The high retention capacity, low permeability and high swelling ability makes bentonites as the ideal hosting materials

once the waste canister failed to confine the waste (Gómez-Espina and Villar, 2015). A good understanding of the migration of radionuclide and the mineralogical changes in the buffer material are of great importance as they are important factors that define the integrity of the repository. An understanding of the radionuclide migration requires a good knowledge of the pore water composition of the bentonite, as it influences greatly the release and transport behaviour of the radionuclide (Kozaki et al., 2001; Fernández et al., 2004; Kaufhold et al., 2009; Fernández et al., 2017).

The primary function of the buffer surrounding the canisters with high-level radioactive waste is to be less permeable than the surrounding rock and to be able to adsorb any released radionuclides. It must also be sufficiently ductile to prevent the build-up of critically high stresses in the canisters due to seismically, tectonically or thermally induced shearing along fractures that intersect the deposition holes. The ductility property of the material used is prerequisite for self-sealing of voids and gaps that may be formed at the clay/canister contacts. If the gaps remain open or are filled with clay with low density they produce permeable paths that can cause fast transport of water carrying radionuclides. For closing or compressing the technological voids the swelling and creep potentials of the materials are the key requirements. If cementation takes place these properties can deteriorate so much that the waste isolation capacity of the buffer decimates (Wang et al., 1990; Pusch et al., 2003; Pusch et al., 2010; Grim and Guven, 2011; Andrini et al., 2017).

This chapter presents the investigation on the possible mineralogical changes and the salt migration in compacted bentonite due to the application of thermal and thermo-hydraulic gradients. Compacted bentonite specimens were subjected in thermal and thermo-hydraulic gradients as described in Chapters 4 and 5. After the completion the tests, the specimens were sliced into disks of 20 mm thick and 100 mm diameter. The

concentration of the cations and the mineralogy of each disk (sample) were determined. Section 6.2 presents a brief literature review concerning the influence of thermal loading and chemical changes in compacted bentonites. Section 6.3 presents the experimental program for the mineralogical and chemical analyses undertaken in this study. Section 6.4 presents the test results and discussion. The main findings emerging from this work are summarised in section 6.5.

6.2 Background

Bentonite mainly consists of 2:1 montmorillonite clay mineral. Montmorillonites are formed from high temperature silicates in low temperature environments and in hydrothermal systems at temperatures of 100 to 150 °C. When the mineral montmorillonite is exposed to higher temperatures and pressures, it tends to be transformed in to more stable silicate phases, such as illite/montmorillonite mixed layers, illite, chlorite etc. (Inoue, 1995). The transformation of the montmorillonite might occur due to changes in its kinetic and hydrologic constraints. Time, concentration of exchangeable cations, saturation and pressure are variables that could affect the montmorillonite composition in compacted bentonites (Pusch et al., 1991; Madsen, 1998).

Couture (1985) reported that significant cementation effects took place in heat-treated bentonite at 150 °C and above which resulted in loss of expandability, in particular under unsaturated conditions. A later study showed that no significant changes occur when a compacted bentonite is heated under unsaturated conditions in the temperature range of 90 to 150 °C (Oscarson and Dixon, 1990). Recent studies showed no significant

changes in swelling pressure when powder bentonite samples are subjected to temperatures of 90 to 110 °C. On the contrary, dense bentonite pellets showed some reduction of swelling at 125 °C and significant reduction at 150 °C (Pusch, 2000; Pusch et al., 2003).

Mitchell and Soga (2005) stated that the basal spacing ($d_{(100)}$) of montmorillonite may vary from 10 to 18 Å depending upon the treatments offered to the samples prior to x-ray diffraction tests, whereas the mineral illite is characterized by a basal spacing of about 10 Å, which remains fixed both in the presence of polar liquids and after drying. Thermal and thermo-hydraulic gradients can cause movement vapour and redistribution of water content within compacted bentonites. Therefore, analysis of XRD spectra of samples from compacted bentonites after subjecting them to both thermal and thermo-hydraulic gradients is expected to indicate the aspects associated with mineralogical changes.

According to Samper et al. (2008) the transportation of chemicals in a compacted bentonite specimen is achieved due to advection, molecular diffusion and dispersion. Bentonite consists of 80-85% montmorillonite and 15-20% of other accessory minerals (calcite, pyrite, quartz, gypsum, mica, feldspar, biotite, siderite, and albite) (Bradbury and Baeyens, 2003) which participate in the ion exchange when dissolve in water. The chemical concentration measurements in a bentonite specimen are affected by aqueous complexation, acid base, precipitations/dissolutions and cations exchange (Cleall et al., 2007; Samper et al., 2008; Fernández and Villar, 2010).

The ion transport in compacted bentonites due to the applications of thermal and thermo-hydraulic gradients occurs due to several processes, such as evaporation, condensation, advection, and molecular diffusion (Samper et al., 2008; Fernández and

Villar, 2010). Evaporation of water from the heat source establishes a chemical concentration gradient within compacted bentonites. Additionally, in the presence of hydraulic gradient (suction gradient), advection and dissolution/precipitation of solutes influence the transport and redistribution of ions within the compacted bentonite systems.

The applied thermal gradient across a compacted bentonite specimen affects the solute transport phenomenon by increasing the solute concentration at the hot end of the specimen due to evaporation and molecular diffusion. During the thermo-hydraulic loading apart from the concentration gradient and diffusion processes discussed above, advection and dissolution/precipitation of solutes at the cold end governs the solute transport.

There are two different approaches that can be adopted to perform the chemical analysis of compacted bentonites, such as saturation extraction technique and ammonium acetate technique. The former provides the information concerning the soluble ions, whereas the latter provides information concerning the total exchangeable cations present in bentonites. Both methods have been adopted in the past by several researchers. In general, both methods provide evidence concerning any changes of the quantity ions, both near the heat source and the hydration source. It is a usual practice to determine both cations and anion concentrations at various salient levels along the depth of bentonite specimens to explore the chemical changes on account of applied thermal and thermo-hydraulic gradients. However, studies in the past have shown that, anion and cations concentration show specific trends at near and away from the heat source. Mitchell and Soga (2005) stated that the diffusive flow in clays is driven by chemical concentration gradients and that in most cases cations–anion pairs diffuse together. Determination of cations exchange capacity has been carried out by some researchers in the past (Villar et al., 2008; Gómez-Espina and Villar, 2010; Dohrmann and Kaufhold, 2014). In the present

investigation the fractional cations exchange capacity of bentonite samples at various predetermined depths were determined by using the ammonium acetate extraction method and the ICP-OS analysis. The determination of fractional cations exchange capacity were carried out following termination of the tests.

6.3 Experimental program

Compacted bentonite specimens were subjected in thermal and hydraulic gradients with different boundary temperatures and test durations. Four nos. of thermal and five nos. of thermo-hydraulic tests were performed (Tables 3.1 and 3.2, chapter 3). The changes in the temperature, relative humidity, axial pressure, degree of saturation, dry density and water content are reported in Chapters 4 and 5. After the termination of each test the specimens were sliced in to 20 mm thick disks with 100 mm diameter. The disks were grinded to powder with a mortar and a pestle. The powder was kept in airtight containers and samples of each powder were used to perform the mineralogical analysis and the determination of the cations concentrations.

For the mineralogical analysis, three different conditions of the samples were used. Each sample was tested as undried, dried and magnesium saturated with glycerol solvation. The undried sample represents the powder taken from the crushed bentonite disks. The dried samples were the oven dried powder samples. For magnesium-saturated and glycerol solvated samples (i.e., Mg-saturated- glycerol solvated), 25 mL of 1 N $MgCl_2$ per 300 mg of clay was used. The sample was placed on a 0.45 μm membrane filter and 25 mL of deionized water used to rinse the sample. The sample was then removed from the filter with the aid of a rubber policeman and transferred to the surface

of a glass slide to air-dry. Once the air drying phase was completed, the sample was transferred on a 0.45 μm membrane filter mounted on a Buchner funnel. Sufficient quantity of glycerol (30%) was used to cover the Mg-saturated bentonite sample. The excess glycerol was removed by applying vacuum using the Buchner funnel. Once the sample was free from the excess glycerol, it was placed on a glass slide to air dry. The sample was then stored in glycerol desiccator until scanning was performed.

The procedure followed for XRD tests is described in section 3.2 (chapter 3). Two grams of bentonite sample was placed on a glass plate and inserted in the goniometer and was bombarded with X-rays (Ulery and Drees, 2008). The *c* axis spacing or the basal spacing (i.e., d_{001} spacing) and the relative peak intensities of the sample were recorded and compared for the relevant samples.

To prepare the samples for the cations exchange capacity determination, the ammonium acetate extraction method was used at a pH value of 7. Bentonite samples from each sliced disk were used (i.e., powdered and oven-dried samples). First, 25 ml of ammonium acetate was added to a sample of 5 g of bentonite powder. The mixture was shaken well intermittently for about 30 minutes. The solution was extracted by using a centrifuge and then preserved. A further 25 ml. of ammonium acetate was added to the sample mixture and left it for overnight and then the solution was extracted. This procedure was repeated two more times. The extracted solution was collated and considered for ICP-OS analysis to determine the type and amount of cations of Na^{+}, Ca^{2+}, Mg^{2+} and K^{+}.

The concentrations of cations measured from the Ion Chromatography (IC) and Inductively Couple Plasma Optimal Emission Spectroscopy (ICP-OES) were found out in mg/l of solution using. The concentrations of cations also presented in meq/100 g. The

concentration of soluble cations in bentonite were measured from the aqueous extract of solutions prepared with dry bentonite: water ratio of 1:10.

The method to convert the mg / l units into meq/100g of soil. The initial bentonite sample used for this test was 5 gram thus a multiplication by a factor of 20 is needed to upscale the values of cations for 100 g of soil. Then the conversion from milligrams to milliequivalent can be achieved with the following Equation 3. The valence and the atomic weight of the cations can be found in table 6.1

$$miliequivalent = {(miligrams \times Cation\ Valance)}/{Atomic\ Weight} \quad \text{(iii)}$$

Table 6.1 Atomic Weights and Valences of Cations

Cations	Atomic weight	Valence
Na^{+}	23	1
K^{+}	39	1
Ca^{2+}	40	2
Mg^{2+}	24.3	2

Triplicate measurements were performed on each sample to avoid error associated with the measurements. Additionally, duplicate samples were tested for each predetermined layers and the average measured values were considered for the presentation.

Table 6.2 presents the experimental program followed. The test results of two thermal tests and two thermo-hydraulic tests are considered in this chapter. The test

conditions cover both 85 and 150 °C. The selected tests were those with the longest testing period. The thermal tests had a duration of 160 days for an applied temperature of 85°C and 190 days at an applied temperature of 150°C. The durations of the two thermo-hydraulic tests was 285 days for the test with an applied temperature of 85 °C and 300 days for an applied temperature of 150 °C. The mineralogy and various cations of each sample was determined after termination of the thermal and thermo-hydraulic tests.

Table 6.2 Experimental program after termination of thermal and thermo-hydraulic tests

Type of test	Applied temperatures (°C) (Top-bottom)	Test duration (days)	Conditions of samples prior to XRD tests	List of cations analysed in using ammonium acetate and ICP-OS
Thermal	25-85 25-150	160 190	Undried, Dried, Mg saturated – glycol solvated	Na^+, K^+, Ca^{2+}, Mg^{2+}
Thermo-hydraulic	25-85 25-150	285 300	Undried, Dried, Mg saturated – glycol solvated	Na^+, K^+, Ca^{2+}, Mg^{2+}

6.4 Results and discussions

The XRD patterns of the compacted bentonite samples are presented in sections 6.4.1 to 6.4.4. The variations of cations concentration due to applied thermal and thermo-hydraulic gradients are presented in section 6.4.5.

6.4.1 XRD analysis of the compacted bentonite subjected to thermal gradient at temperature of 85 °C

The possible mineralogical changes of the compacted bentonite specimen upon subjected to an applied temperature of 85°C at the bottom and 25°C at the top was investigated after completion of the test. Powder samples from the predetermined sections along the full depth of each specimen were analysed with the aid of the x-ray diffraction technique to explore whether there were any changes in the mineralogical composition of the bentonite. Each powder sample was tested under three different treatment conditions, undried, dried and Mg-saturated-glycol solvated. The results for each type of test are demonstrated in the subsequent sections. For the sake of comparison the XRD pattern of the raw material under the same testing conditions (undried, dried and Mg-saturated-glycol solvated) is also presented.

Figures 6.1, 6.2 and 6.3 show the X-ray diffraction patterns of undried, dried and Mg-saturated-glycerol solvated samples at various predetermined depths of the bentonite specimens. In each of Figs. 6.1 to 6.3, three plots are shown, such as the XRD patterns of bentonite samples at various depths presented separately (Figs. 6.1a, 6.2a and 6.3a), the results obtained at each depth are superimposed in Figs. 6.1b, 6.2b, and 6.3b, and the superimposed XRD patterns are presented by considering a smaller x-axis scale in Figs. 6.1c, 6.2c, and 6.3c. The results obtained for the raw material are also shown in each case. The X-ray diffraction patterns presented in Figs 6.1 to 6.3 show the $d_{(001)}$ spacing of the samples in angstrom (Å) (10 Å = 1nm). The depths of bentonite specimens at which the XRD patterns were obtained are shown in the legend of each plot.

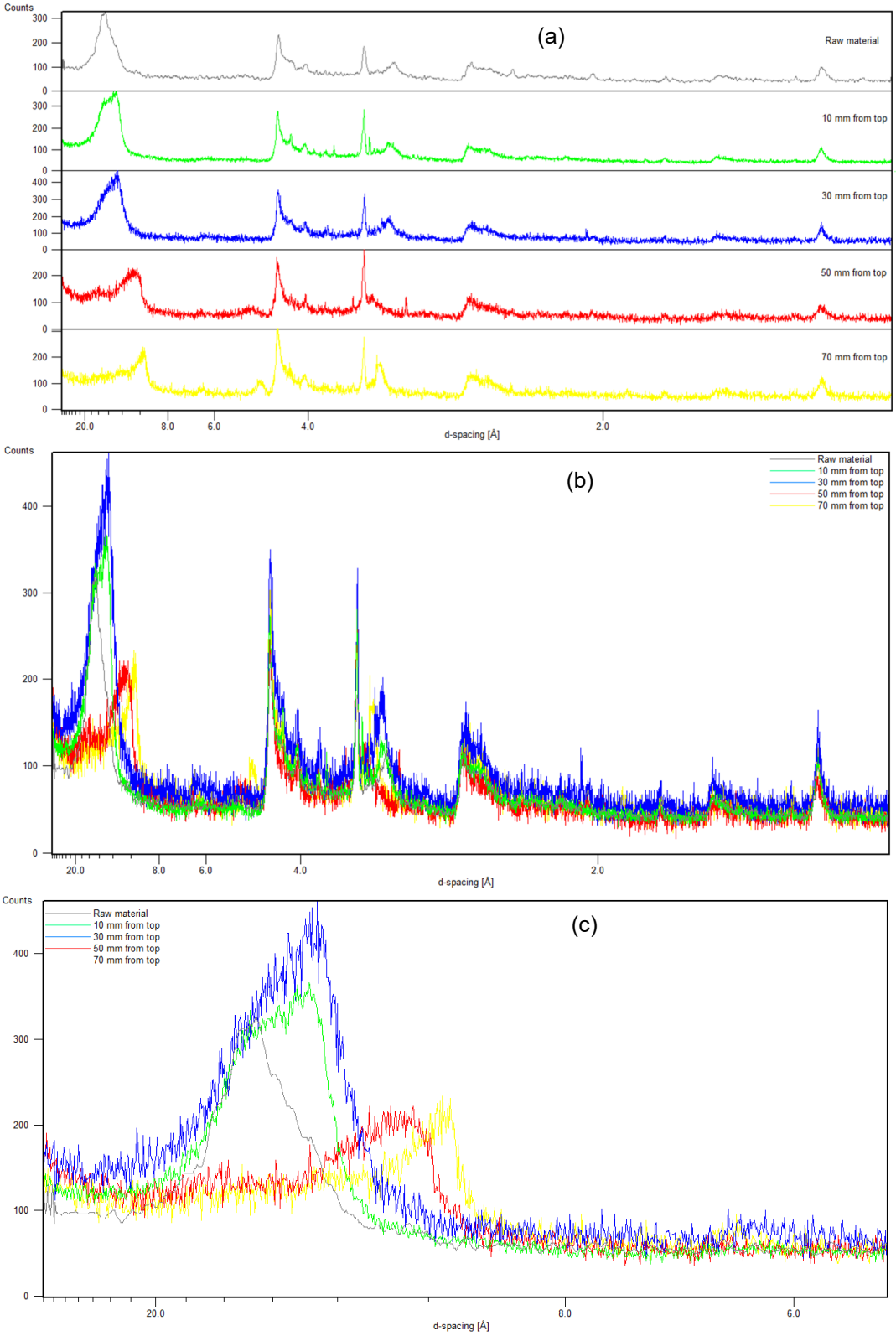

Figure 6.1 XRD patterns of undried samples after thermal tests conducted at 85 °C

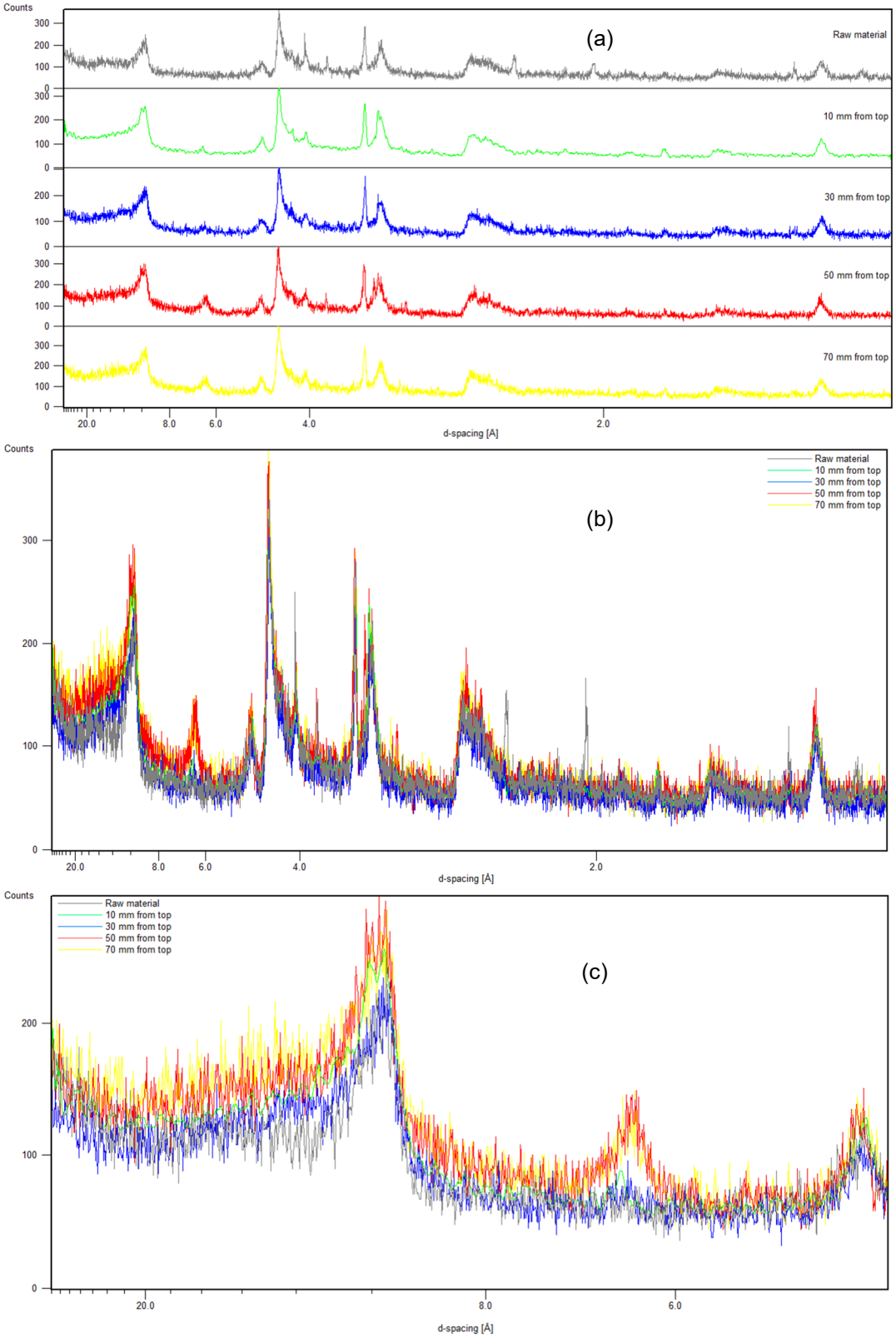

Figure 6.2 XRD patterns of oven-dried samples after thermal tests conducted at 85 °C

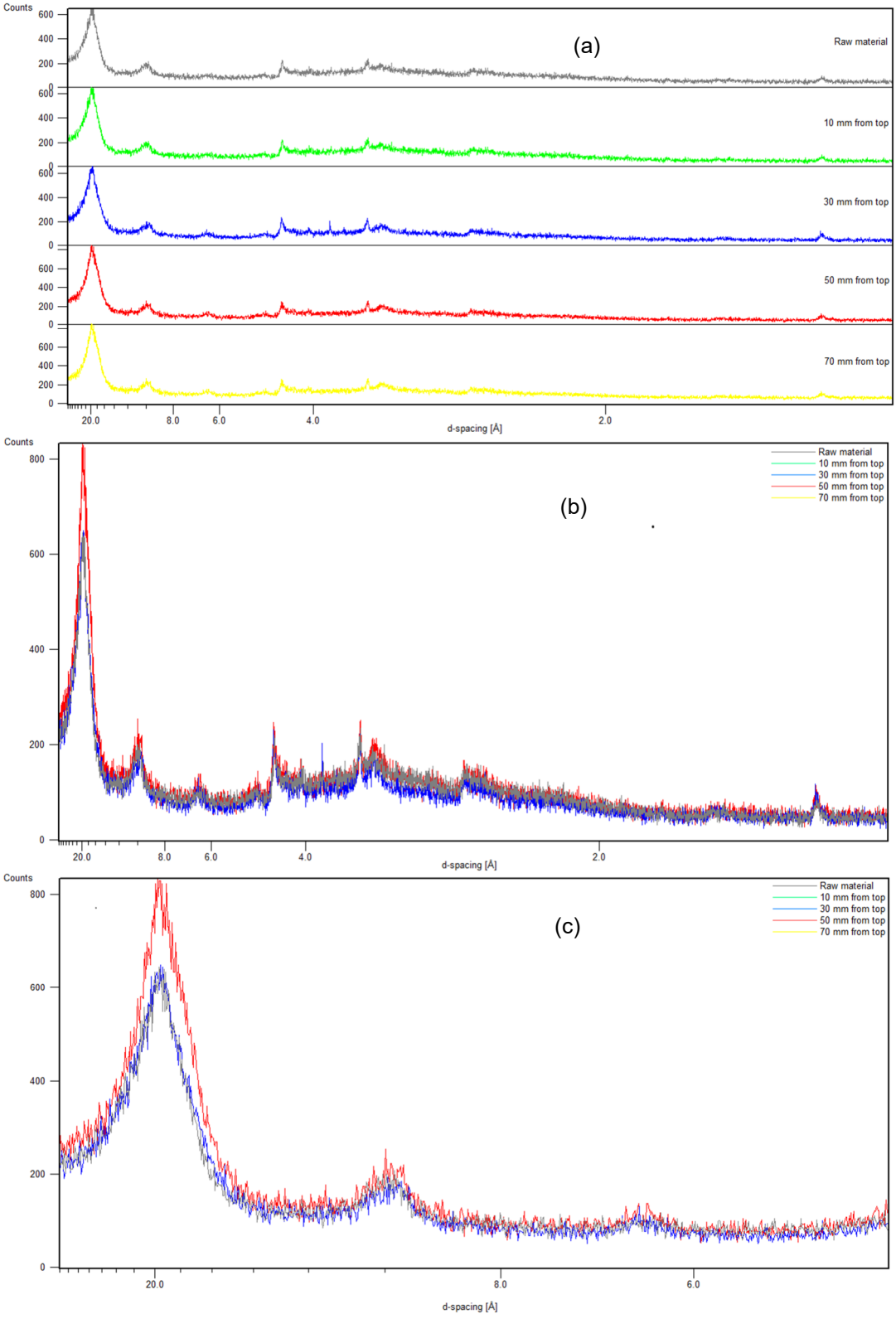

Figure 6.3 XRD patterns of Mg-saturated-glycerol solvated samples after thermal tests conducted at 85 °C

Figures 6.1 to 6.3 show that, in case of undried samples (Fig. 6.1), some variation of the XRD spectrum occurred between $d_{(001)}$ of 10 to 20 Å (i.e., 1.0 to 2.0 nm) and at all salient depths of the specimens considered, whereas in case of dried and Mg-saturated-glycerol solvated samples, the XRD patterns remained similar at all salient depths. In the latter cases, even the XRD patterns are found to be similar to the XRD pattern of the raw material.

Mitchell and Soga (2005) stated that for air dried montmorillonite the basal spacing (i.e., $d_{(100)}$ or c axis spacing) may remain between 12 to 15 Å, whereas after treatment with ethylene glycol or glycerol, montmorillonites expand to a $d_{(001)}$ value of 17 to 18 Å. Upon oven dried, $d_{(001)}$ decreases to about 10 Å as a result of the removal of interlayer water. Table 6.3 shows the $d_{(001)}$ spacing of montmorillonite at various initial conditions as obtained in this study for the raw material. The information presented in Table 6.3 were extracted from Figs. 6.1 to 6.3. It can be seen in Table 6.3 that, the $d_{(001)}$ spacing of montmorillonite agree very well with the data available in the literature.

Table 6.3 XRD patterns of as-received bentonite (raw material)

Conditions of samples prior to XRD tests	$d_{(001)}$ spacing (nm)
Undried	1.5
Oven-dried	1.0
Oven dried, Mg-saturated and glycerol solvated	2.0

Table 6.4 presents the $d_{(001)}$ spacing of undried samples at various predetermined depths of the bentonite specimen. The temperatures presented in Table 6.4 at various salient depths were obtained from temperature profile of the specimen as shown in Fig. 4.4. The d(001) spacing are based on the results presented in Fig. 6.1.

It can be seen in Table 6.4 that, the $d_{(001)}$ spacing increased from 0.95 nm at closer to the heat source to about 1.3 nm towards the cold end. An application of thermal gradient caused movement of water vapour from the heat source and towards the cold end. A change in the water content in the interlayer space is expected to cause a change in the $d_{(001)}$ spacing. The test results clearly indicates dehydration of the bentonite specimen at and near the heat source and hydration at the opposite end of heat source. An increase in the basal spacing towards the cold end is attributed primarily due to the hydration of exchangeable cations and surface of the mineral montmorillonite.

Table 6.4 $d_{(001)}$ spacing of montmorillonite as affected by an applied thermal loading of 85°C based on XRD pattern of undried sample (see Fig. 6.1)

Average distance from heat source (mm)	Temperature (°C) based temperature profile shown in Fig. 4.4	$d_{(001)}$ spacing (nm)
10	78	0.95
30	60	1.05
50	45	1.3
70	38	1.3

No variation in the c axis spacing was noted for the samples that were either oven dried or Mg-saturated-glycerol solvated. At all salient depths, the $d_{(001)}$ spacing remained at 1.0 nm (10 Å) for the oven dried samples (Fig. 6.2), whereas it remained at 1.8 nm (18 Å) for the Mg-saturated-glycerol solvated samples (Fig. 6.3). The results presented in Figs. 6.2 and 6.3 clearly show that, the treatment process (i.e., oven drying and treating samples with glycerol) prior to XRD tests eliminates the important information concerning the hydration/dehydration of montmorillonite minerals.

6.4.2 XRD analysis of compacted bentonite subjected to thermo–hydraulic gradient at temperature of 85 °C

The XRD test results of compacted bentonite specimens that were subjected thermal and hydraulic gradients simultaneously are presented in this section. The applied temperature was 85 °C at the bottom and 25 °C at top of the specimens, whereas water was supplied to the specimens at a pressure of 600 kPa from the top. The powder samples from the bentonite disks (20 mm thick and 100 mm dia.) were considered for the XRD tests. The samples were either undried or oven dried or even Mg-saturated-glycerol solvated. Figures 6.4, 6.5 and 6.6 show the XRD patterns of the samples for these conditions. Figures 6.4a, 6.5a and 6.6a present the XRD patterns of samples at various predetermined depths, Figs. 6.4b, 6.5b and 6.6b present the superimposed results, and Figs. 6.4c, 6.5c and 6.6c present the results with a smaller x-axis scale.

The following points emerged from the XRD patterns shown in Figs. 6.4 to 6.6 for the $d_{(001)}$ spacing of montmorillonite:

(i) Differences in the $d_{(001)}$ spacing of montmorillonite is noted for the undried samples (see Fig. 6.4); in this case, the basal spacing increased with an increase in the distance from the heat source (14 Å at 10 and 30 mm from the top, 12.5 Å at 50 mm from top and 11.5 Å at 70 mm from top). An increase in the basal spacing can be attributed due to the combined influence of movement of water vapour from the heat source and towards the cold end (25 °C) and water injection from the top end of the specimens. In general, there was an increase in the basal spacing for the specimens when subjected to thermo-

(ii) hydraulic gradient as compared to the results for the thermal tests (see Table 6.3).

(iii) The $d_{(001)}$ spacing is found to be similar for the samples that were oven-dried (Fig. 6.5); in this case, the impact of water movement and water injection was subdued, the basal spacing remained at about 10 Å.

(iv) Some differences in $d_{(001)}$ spacing were noted for the Mg-saturated-glycerol solvated samples; in this case, the basal spacing of montmorillonite remained between about 17 to 22 Å.

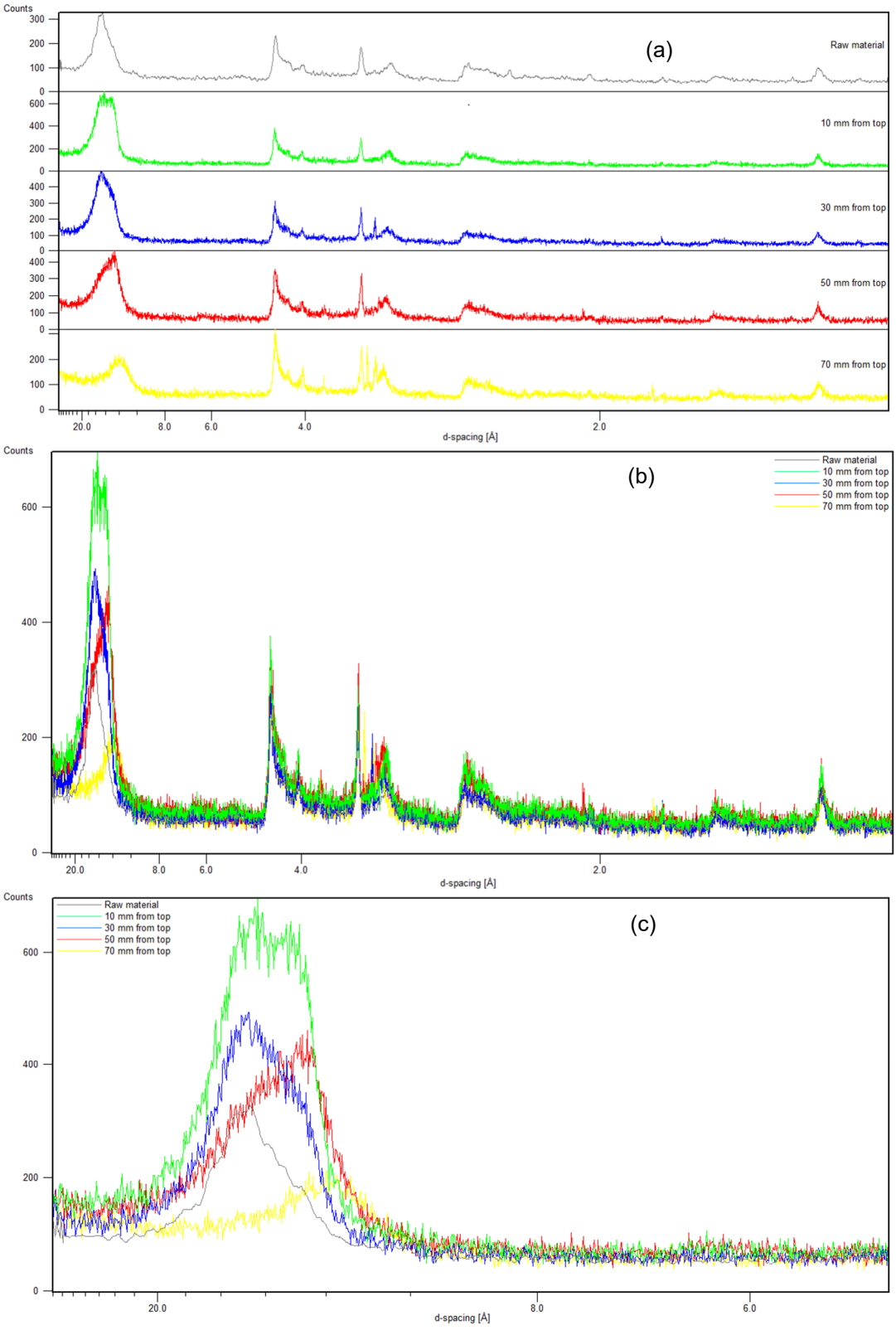

Figure 6.4 XRD patterns of undried samples after thermo-hydraulic tests conducted at 85 °C

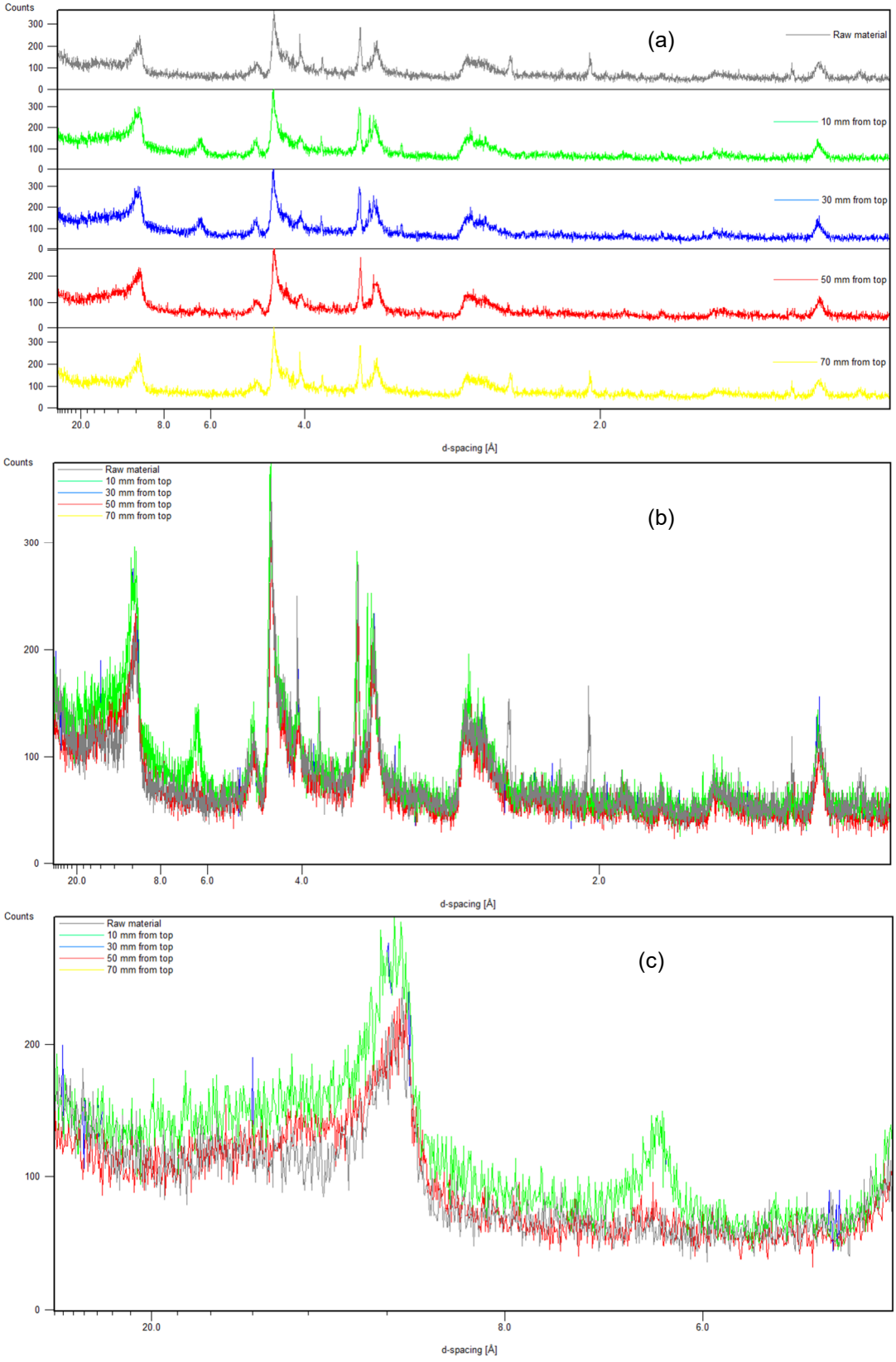

Figure 6.5 XRD patterns of oven-dried samples after thermo-hydraulic tests conducted at 85°C

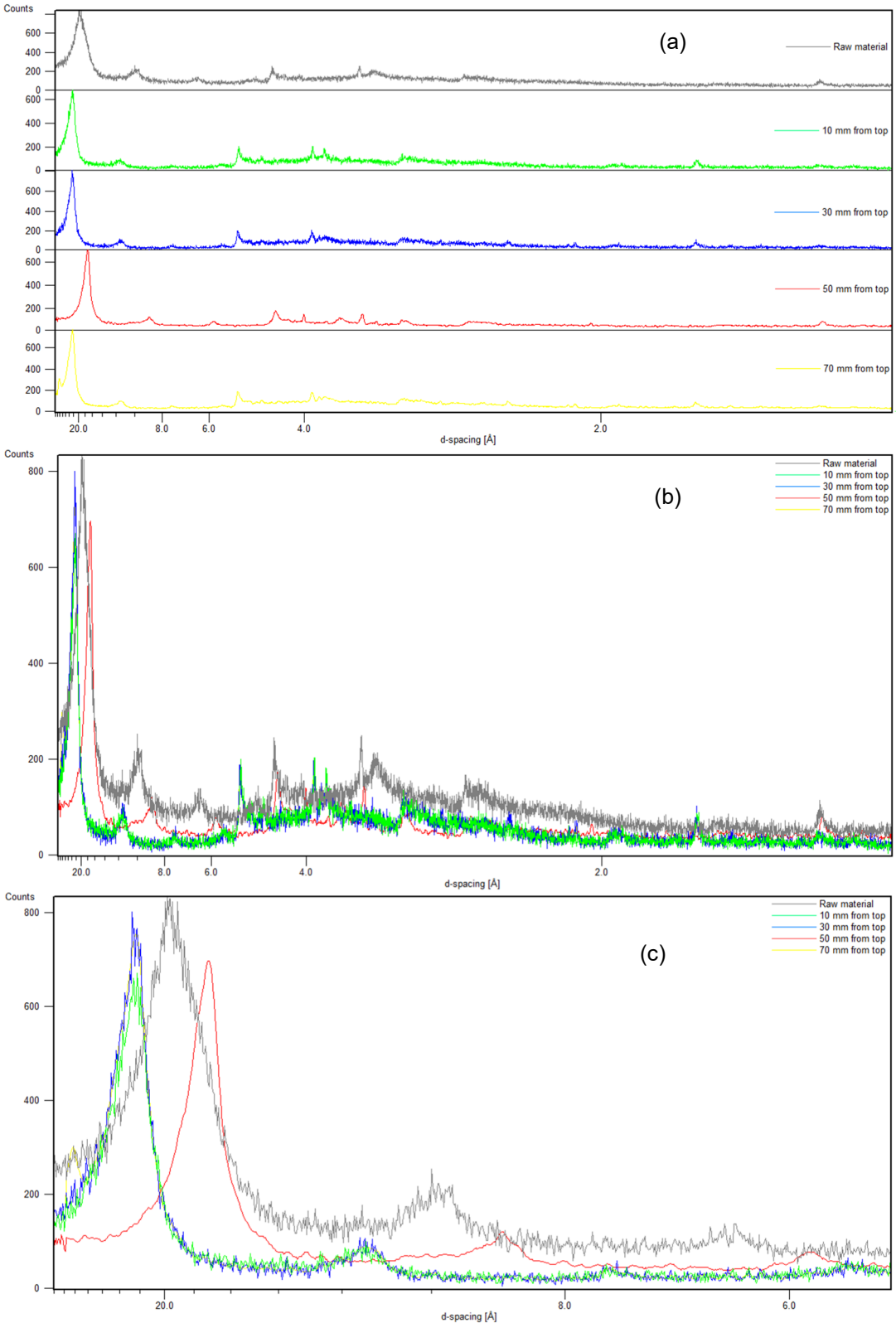

Figure 6.6 XRD patterns of Mg-saturated-glycerol solvated samples after thermo-hydraulic tests conducted at 85 °C

6.4.3 XRD analysis of the compacted bentonite subjected to thermal gradient at temperature of 150 °C

The compacted specimens tested at a temperature of 85 °C were 80 mm thick, whereas the specimens that were tested at 150 °C were 300 mm thick. Prior to the XRD tests, the 300 mm thick specimens were sliced into fifteen disks, each 20 mm thick and 100 mm dia. The bentonite disks were then pulverised and further the powder samples were prepared. The XRD tests on a sample corresponding to any predetermined depth of the specimens was repeated three times and for the three different treatment conditions mentioned earlier (undried, oven-dried and Mg-saturated-glycerol solvated).

Figure 6.7, 6.8 and 6.9 show the XRD spectra of the bentonite samples for the conditions of undried, oven-dried and Mg-saturated-glycerol solvated. In each case, three plots are presented, such as the XRD patterns of bentonite samples at various depths presented separately (Figs. 6.7a, 6.8a and 6.9a), the results obtained at each depth are superimposed in Figs. 6.8b, 6.8b, and 6.9b, and the superimposed XRD patterns are presented by considering a smaller x-axis scale in Figs. 6.7c, 6.8c, and 6.9c. The results obtained for the raw material are also shown in each case. The depths of bentonite specimens at which the XRD patterns were obtained are shown in the legend of each plot.

It can be seen in Fig. 6.7 that, the $d_{(001)}$ spacing of montmorillonite increased with an increasing distance from the heat source (see $d_{(001)}$ spacing between 8 and 20 Å). Table 6.5 presents the average distance from the heat source, the corresponding temperatures (obtained from Fig. 4.10) and the $d_{(001)}$ spacing. The basal spacing of montmorillonite remained similar to that of oven dried samples (i.e., 10 Å, see Table 6.3), whereas the basal spacing increased from the mid height of the specimen (i.e., 150 mm) and remained at about 12.5 Å towards the top end. This value is slightly smaller than that of the

specimen which was subjected to a temperature of 85 °C (see Table 6.4). Note that, the height of the specimens were smaller in case of applied temperature of 85 °C.

A variation of $d_{(001)}$ spacing of montmorillonite for the samples that were oven-dried and tested and that were Mg-saturated-glycerol solvated prior to testing was indistinct (Figs. 6.8 and 6.9). In case of the oven-dried samples, the basal spacing of montmorillonite remained at 10 Å (Fig. 6.8), whereas it remained between about 18 to 22 Å in case of the samples that were Mg-saturated-glycerol solvated prior to the XRD tests. The test results are similar to that of the specimens that underwent a thermal loading at 85 °C.

Table 6.5 $d_{(001)}$ spacing of montmorillonite as affected by an applied thermal loading of 150°C based on XRD pattern of undried sample (see Fig. 4.10)

Average distance from heat source (mm)	Temperature (°C) based temperature profile shown in Fig. 4.4	$d_{(001)}$ spacing (nm)
10	135	1.0
30	125	1.0
50	100	1.0
70	85	1.0
90	80	1.0
110	74	1.0
130	70	1.03
150	65	1.03
170	60	1.03
190	57	1.2
210	53	1.22
230	50	1.25
250	43	1.25
270	37	1.25
290	30	1.25

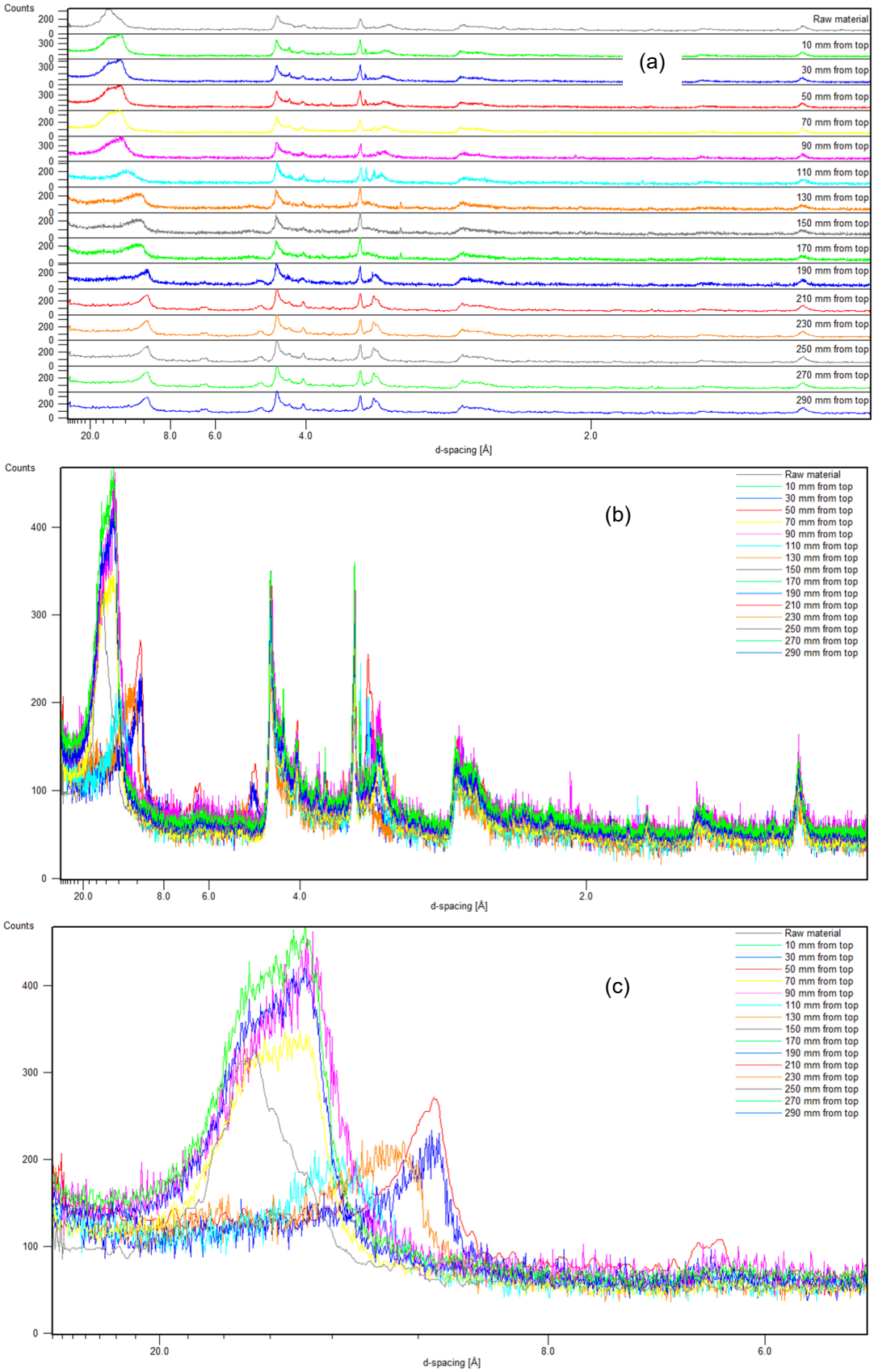

Figure 6.7 XRD patterns of undried samples after thermal tests conducted at 150 °C

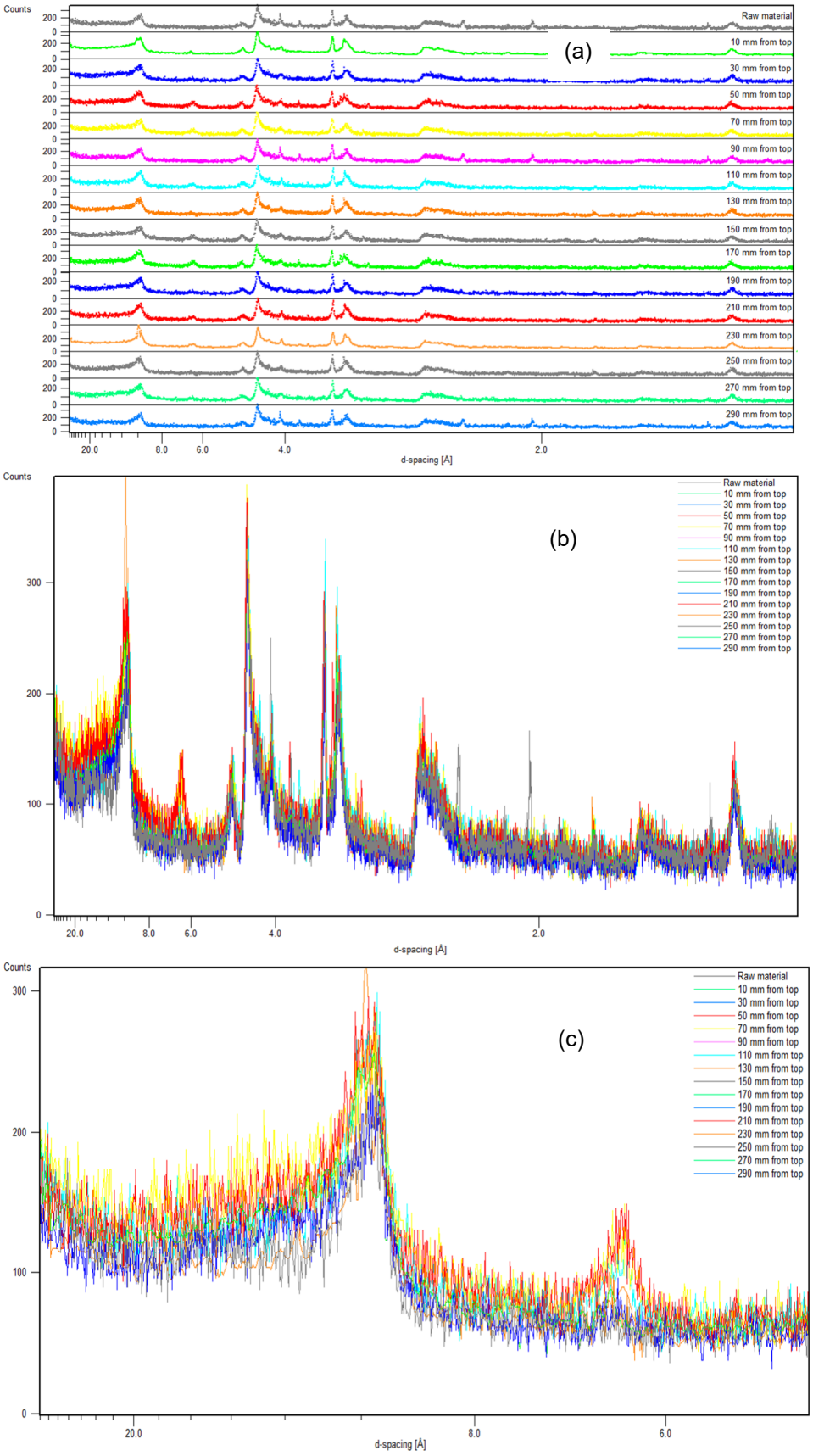

Figure 6.8 XRD patterns of oven-dried samples after thermal tests conducted at 150 °C

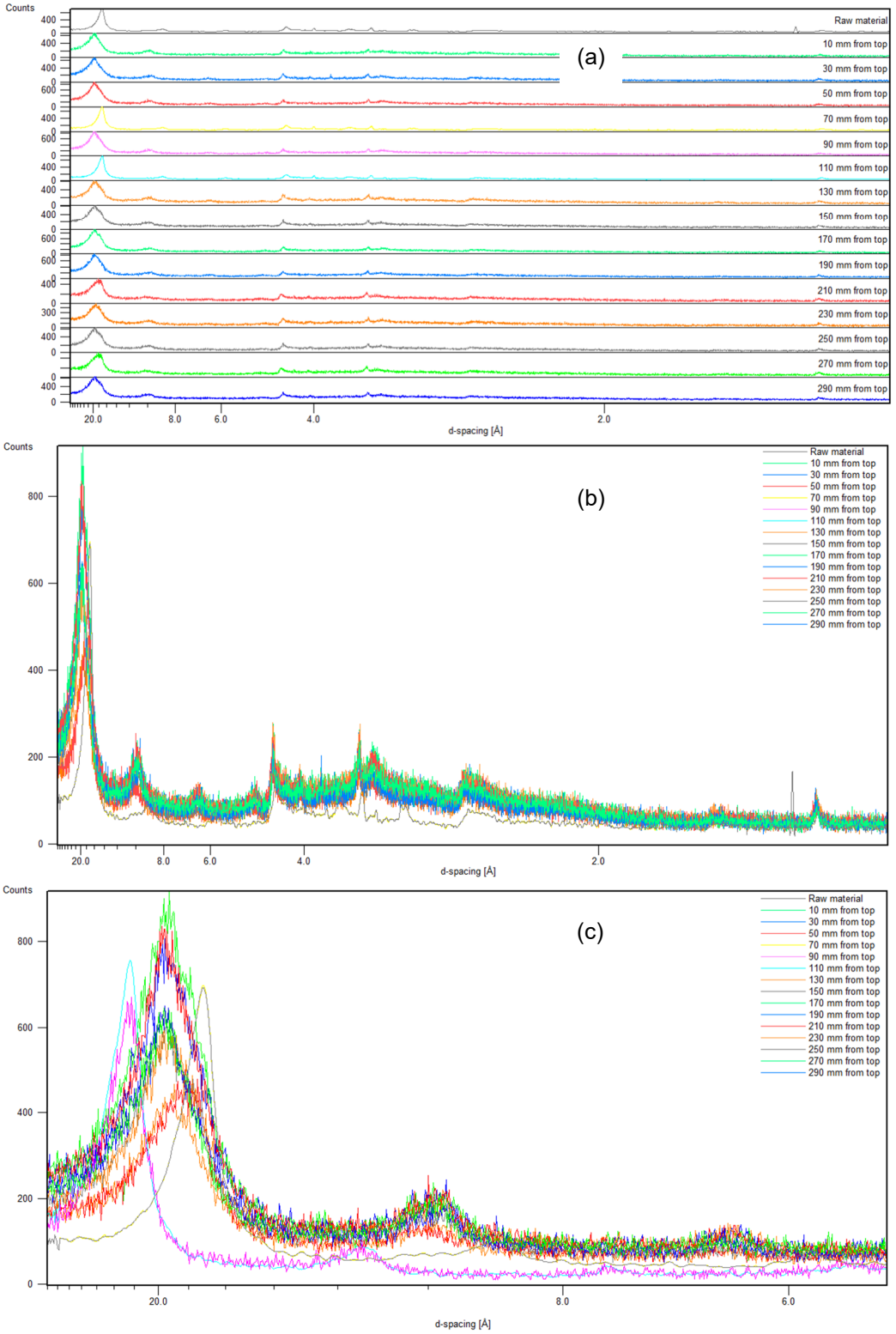

Figure 6.9 XRD patterns of Mg-saturated-glycerol solvated samples after thermal tests conducted at 150 °C

6.4.4 XRD analysis of compacted bentonite subjected to thermo-hydraulic gradient at 150 °C

Figures 6.10, 6.11 and 6.12 show the XRD patterns of the samples after the thermo-hydraulic tests (applied temperature = 150 °C and water injection pressure = 600 kPa) for sample conditions of undried, oven-dried and Mg-saturated-glycerol solvated, respectively. Figures 6.10a, 6.11a and 6.12a present the XRD patterns of samples at various predetermined depths, Figs. 6.10b, 6.11b and 6.12b present the superimposed XRD results, and Figs. 6.10c, 6.11c and 6.12c present the results with a smaller x-axis scale.

The following points emerged from the XRD patterns shown in Figs. 6.10 to 6.12 for the $d_{(001)}$ spacing of montmorillonite:

(i) Differences in the $d_{(001)}$ spacing of montmorillonite is noted for the undried samples (see Fig. 6.10); in this case, the basal spacing increased with an increase in the distance from the heat source (9.8 Å at 10 mm from the heat source to 14 Å at 290 mm from the heat source). An increase in the basal spacing can be attributed due to the combined influence of movement of water vapour from the heat source and towards the cold end (25 °C) and water injection from the top end of the specimens. In general, there was an increase in the basal spacing for the specimens when subjected to thermo-hydraulic gradient as compared to the results for the thermal tests (see Table 6.5).

(ii) The d(001) spacing is found to be similar for the samples that were oven-dried prior to XRD tests (Fig. 6.11); in this case, the impact of water movement and water injection was subdued, the basal spacing remained at about 10 Å,

(iii) Some differences in $d_{(001)}$ spacing were noted for the Mg-saturated-glycerol solvated samples; in this case, the basal spacing of montmorillonite remained at about 17.5 to 22 Å.

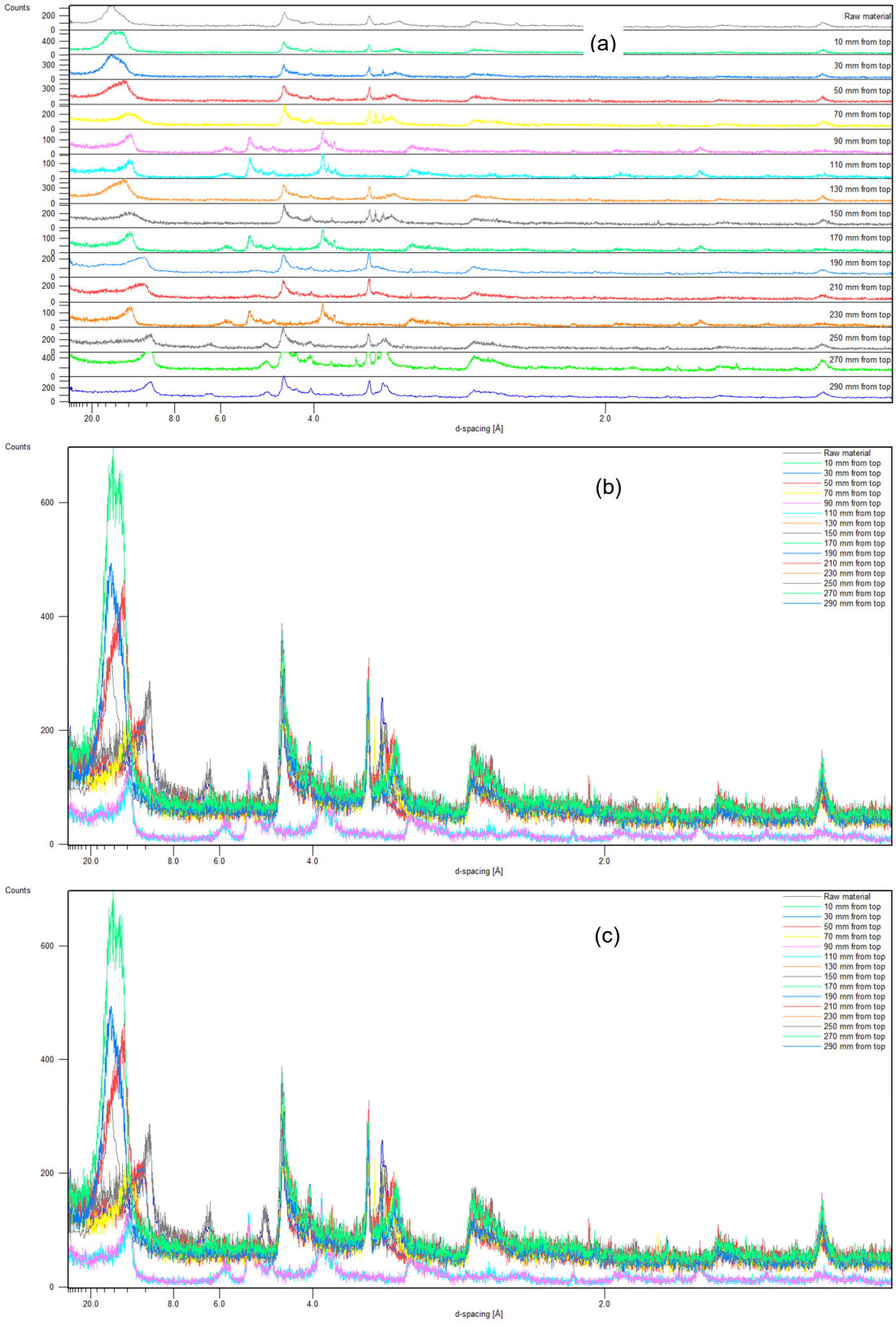

Figure 6.10 XRD patterns of undried samples after thermo-hydraulic tests conducted at 150°C

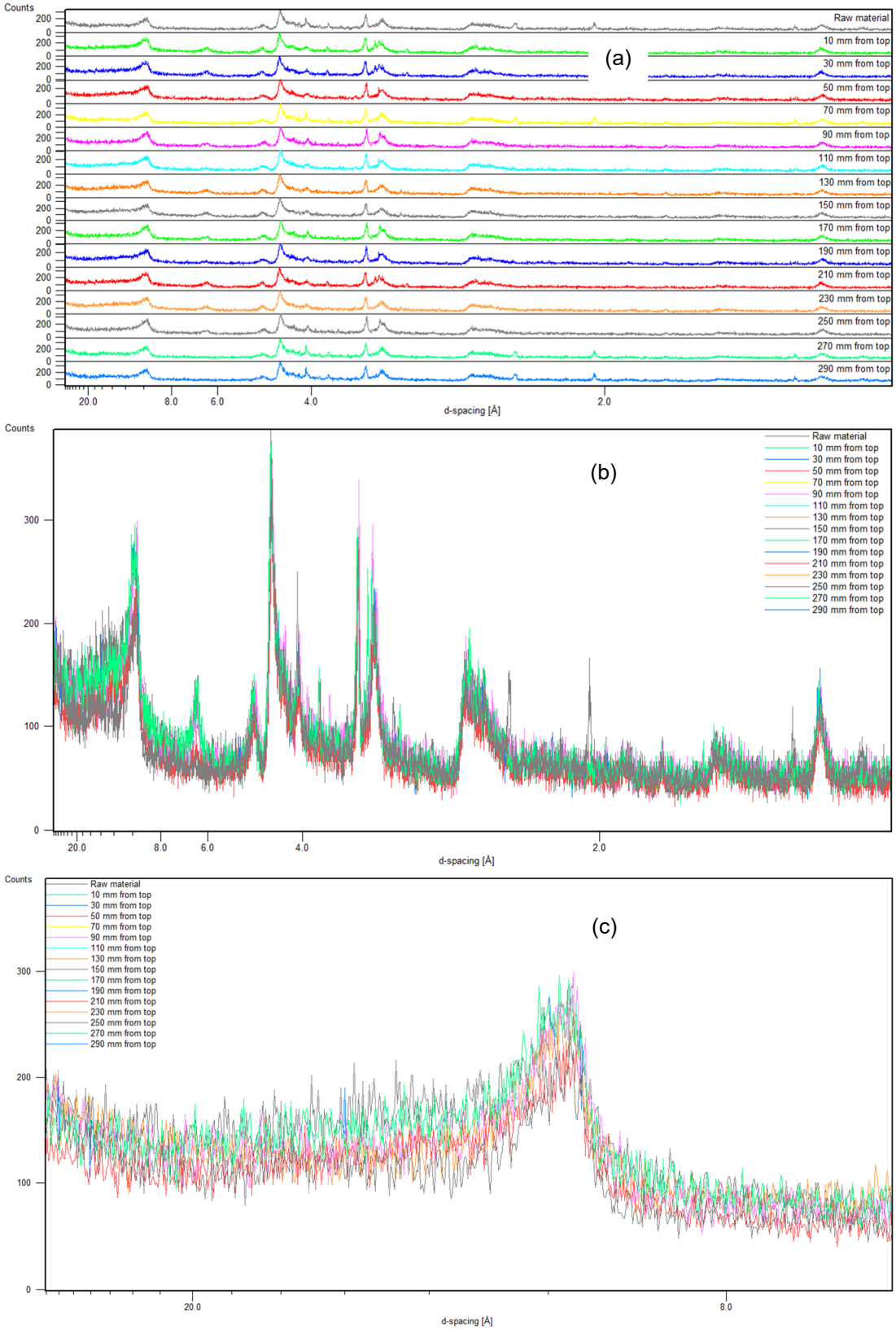

Figure 6.11 XRD patterns of oven-dried samples after thermo-hydraulic tests conducted at 150 °C

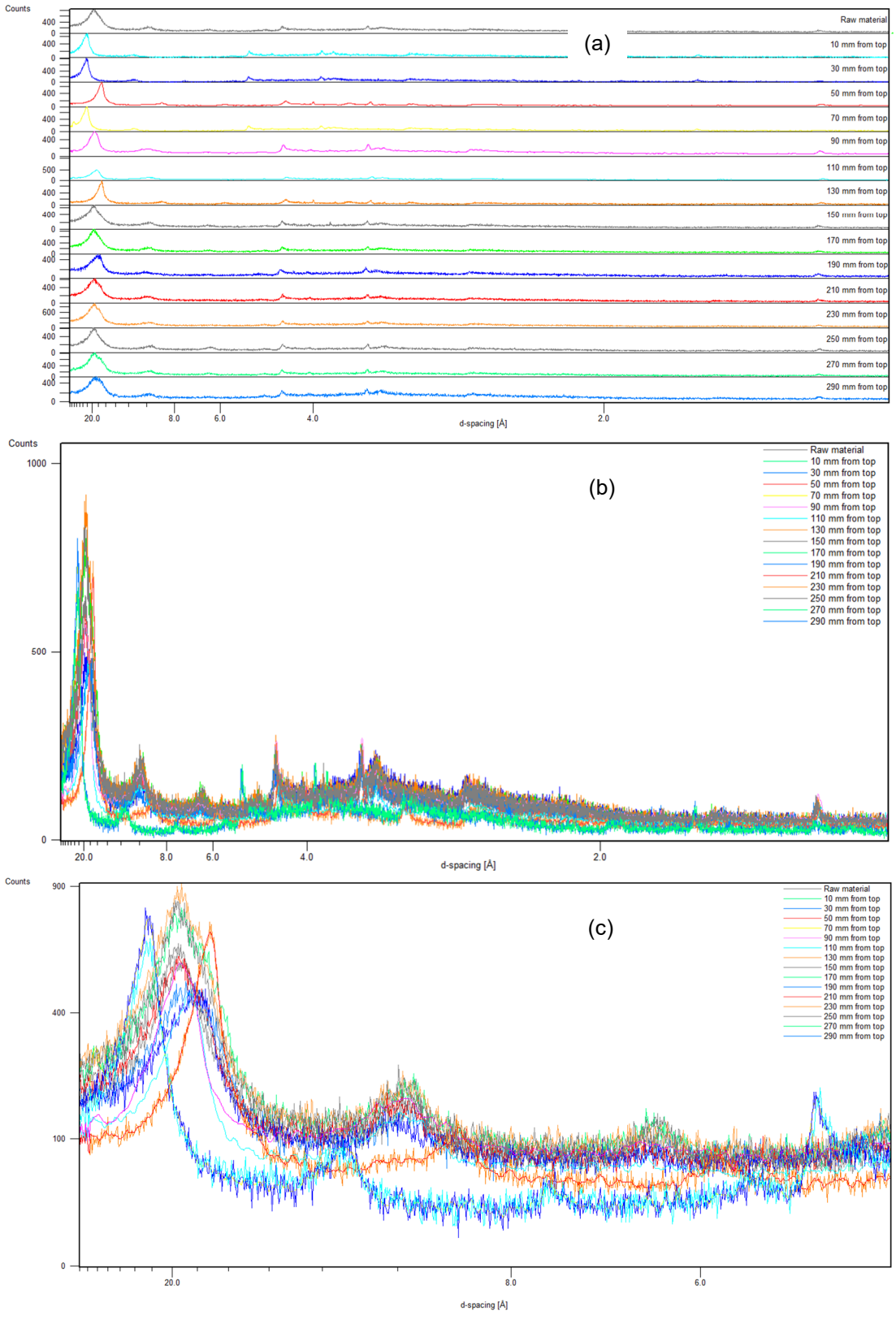

Figure 6.12 XRD patterns of Mg-saturated-glycerol solvated samples after thermo-hydraulic tests conducted at 150 °C

6.4.5 Solute transport due to applied thermal and thermo-hydraulic gradients

The non-isothermal tests in this study were carried out by applying temperatures of either 85 or 150 °C at the bottom and 25 °C at the top of the compacted bentonite specimens. During the thermo-hydraulic tests, in addition to the applied temperature conditions, water was supplied at a pressure of 600 kPa from the top of the specimens.

Figures 6.13 and 6.14 show the fractional cations values for Na^+, Mg^{2+}, Ca^{2+} and K^+ in the compacted bentonite specimens at various distances from the heat source. The values of cations represent the exchangeable cations and soluble ions. The compositions of the cations in the raw material (as-received) are shown in the corresponding plots.

The results presented in Fig. 6.13 shows that, for the thermal tests at 85 and 150 °C, the amount of Na^+ decreased slightly near the heat source, whereas it increased for the thermo-hydraulic tests. As compared to the raw material, a variation of Na^+ remained within about ± 11% for the entire heights of the specimens. The changes in the Mg^{2+} amount was about 66% at the heat source (Fig. 6.13b). In this case, the thermal loading caused an increase, whereas thermo-hydraulic loading caused a decrease in the amount of Mg^{2+} near the heat source. The amount of Mg^{2+} generally decreased as the distance from the heat source increased.

Figure 6.14 shows that, the amount of Ca^{2+} decreased near the heat source slightly as compared to the raw material. This occurred for all tests. However, no significant change is noted at distances away from the heat source. The amount of K^+ is found to be decreased (about 25%) for all cases.

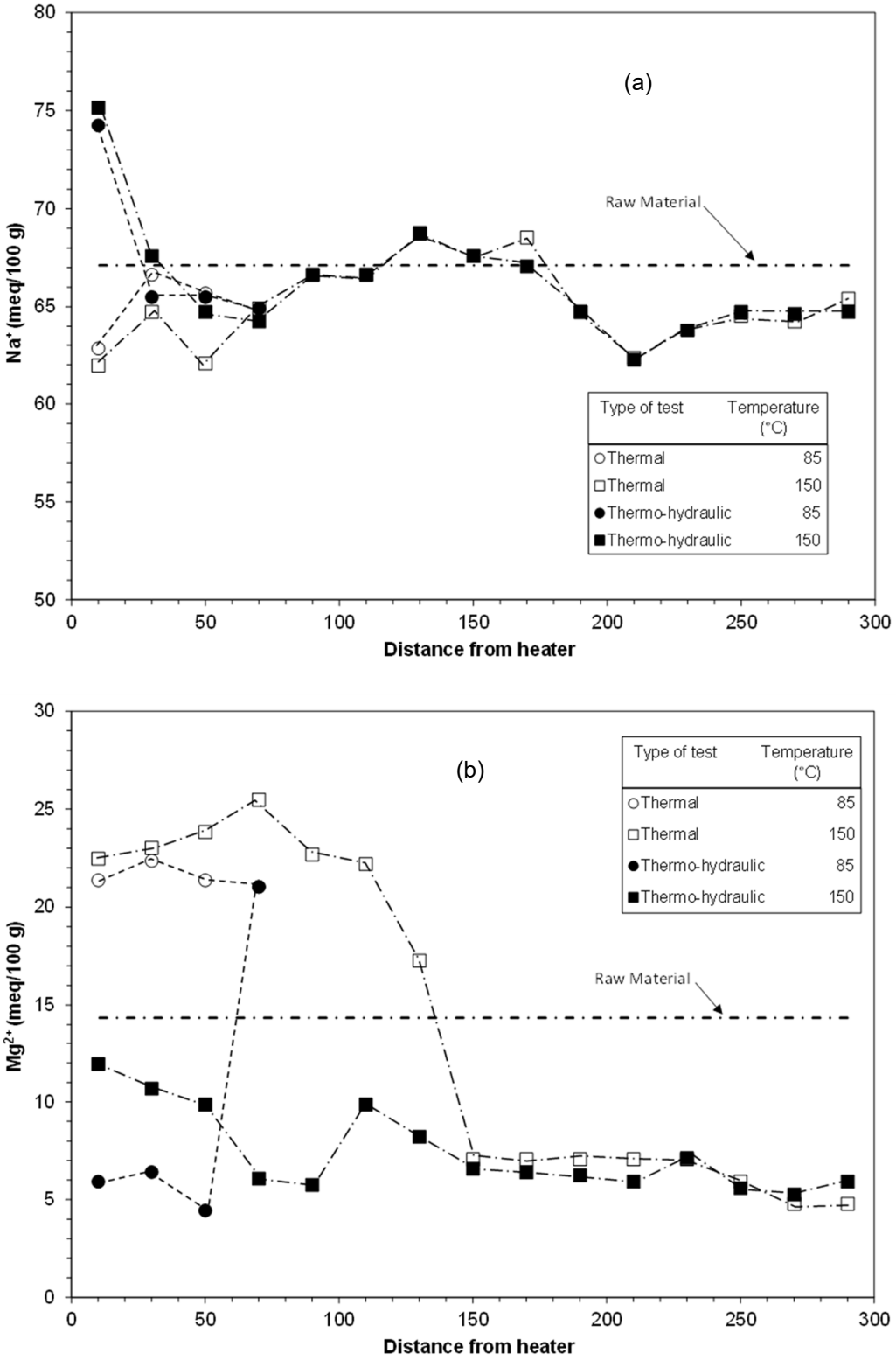

Figure 6.13 Values of cations in thermal and thermo-hydraulic tests at 85 and 150 °C for (a) Na^+ and (b) Mg^{2+}

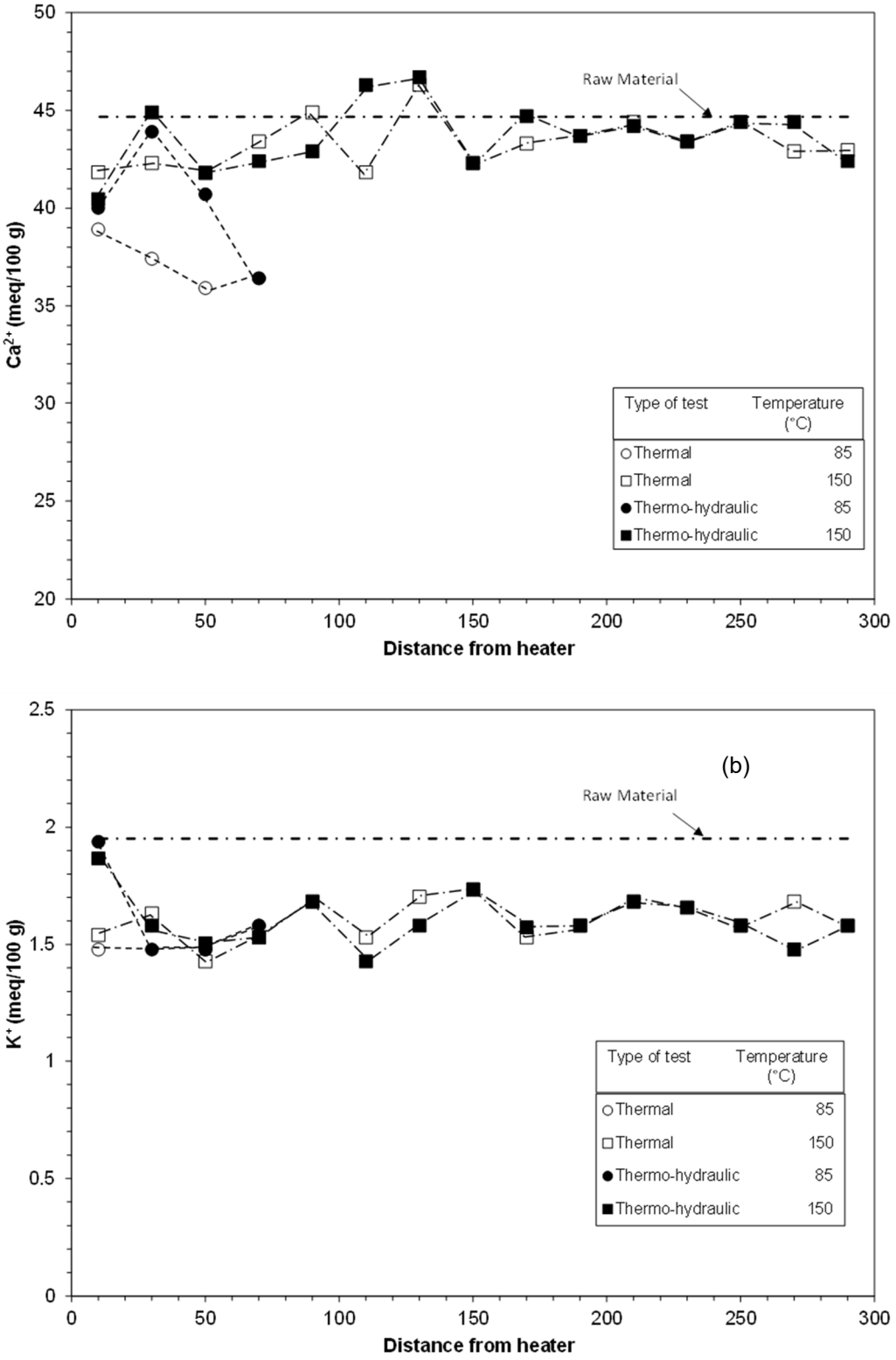

Figure 6.14 Values of cations in thermal and thermo-hydraulic tests at 85 and 150 °C for (a) Ca^{2+} and (b) K^{+}

Studies in the past have shown that cations exchange reactions occur in compacted bentonite due to thermal and thermo-hydraulic loadings, but structural degradation of smectite could not be identified (Dohrmann and Kaufhold 2014). Villar et al. (2008) stated that the amounts of Na^+ and Ca^{2+} decreased near the heat source, whereas the amounts of K^+ and Mg^{2+} increased. There was an increase in the amounts of Ca^{2+} and Na^+ near the hydration source, whereas no significant change was noted for K^+ and Mg^{2+}. Gomez - Espina and Villar (2010) stated that the amount of Na^+ near heat source decreased and it increased near the hydration source. The amounts of Ca^{2+} near the heat source increased, whereas it decreased near at the hydration source. The amounts of Mg^{2+} decreased near heater, whereas it increased near hydration end. No variation of K^+ was noted for such tests. Bag (2011) noted that the concentrations of Na^+ and Ca^{2+} near the heat source increased, whereas they decreased at the hydration source or at the cold end, both due to applied thermal and thermo-hydraulic gradients. The concentrations of Mg^{2+} generally increased at both heat source and hydration ends. The test results of Bag (2011) indicated no significant change in the concentration of K^+ occurred after thermal and thermo-hydraulic tests.

As can be seen, there are conjectural views concerning the variations of exchangeable/total cations both near and away from the heat source. The results in the current study showed some variations of cations, particularly near the heat source.

6.5 Summary

The investigation for any mineralogical changes due to thermal and thermo-hydraulic loadings is presented in this chapter. The samples from compacted bentonite specimens that were subjected to applied temperatures of 85 or 150 °C, and water injection pressure of 600 kPa or no water injection, were considered. X-ray diffraction (XRD) technique was used to investigate the mineralogical changes. Three different conditions of the samples were considered prior to the XRD tests.

The test results showed that thermal gradient and thermo-hydraulic gradient caused dehydration and hydration of interlayers of the mineral montmorillonite which was accompanied by a decrease or an increase in the basal spacing. The basal spacing variations were different for thermal and thermo-hydraulic loadings. A variation of the basal spacing due to a redistribution of water within compacted bentonites clearly indicates that illitisation (phase transformation from montmorillonite to illite) did not occur for the testing conditions considered in this study. Illite mineral generally tend to show a fixed basal spacing (10 Å) irrespective of changes in the testing procedure. The conditions of the samples prior to the XRD tests influenced the basal spacing. The test results agree very well to the findings reported by several researchers in the past (Inoue 1995, Pusch et al. 2003, Gómez-Espina and Villar 2010, Pusch et al. 2010, Gómez-Espina and Villar 2015). In 1982 Pytte introduced the empirical kinetic illitisation model.

$$-dS/dt = A \times \exp(E_a/RT) \times (K^+/Na^+) \times mS^n \qquad \text{(iv)}$$

where S is the mole fraction of the reaction product I/S, A is the pre-exponential factor, Ea is the activation energy, R the gas constant, T the temperature and m, n are coefficients depending on the K+/Na+ ratio and K+/Na+ are the concentrations in groundwater. Using

the above formula Wersin et al (2007) calculated that in a period of 200 years a bentonite specimen subjected to 150 °C will undergo a les that 5% illitisation.

The ion migration in bentonites due to thermal and thermo-hydraulic loading is presented in this chapter. Fractional total cations (both types and amount) were determined at various depths of compacted bentonite specimens after the thermal and thermo-hydraulic tests were terminated. Inductively Couple Optical Emission

Spectroscopy (ICP-OES) was used to measure the fractional exchangeable cations for sodium, calcium, magnesium and potassium.

A variation in the total cations was distinct for all the cations, particularly near the heat source. However, the trends for thermal and thermo-hydraulic loadings were inconclusive.

CHAPTER 7.
CONCLUSIONS

This thesis focused on the study of the coupled thermo-hydro-mechanical- behaviour of compacted MX80 bentonite under nuclear waste repository conditions (i.e., heavily compacted bentonites, high temperature, high fluid pressure, temperature isolation/thermal insulation). A commercially available MX80 bentonite was used in this study.

Standard laboratory tests were carried out to exploit the properties of the bentonite prior the actual testing. A device was fabricated to carry out the non-isothermal and non-isothermal hydraulic tests at a temperature of 150 °C, whereas a device already available was used to carry out the laboratory tests at a temperature of 85 °C. The new device enabled testing compacted bentonite specimens with dimensions, 100 mm dia. and 300 mm high, whereas the specimen size in the available device was 100 mm dia. and 80 mm high.

In total nine tests were performed with two different types of testing conditions, such as non-isothermal (four tests) and non-isothermal-hydraulic (five tests). For each type of test (non-isothermal and non-isothermal-hydraulic) two different thermal boundary conditions were considered. Compacted bentonite specimens were either subjected at a temperature of 150 °C or 85 °C at the bottom, whereas a temperature of 25 °C was maintained constant the top of the specimens. During the non-isothermal hydraulic tests, de-ionized water was supplied from the top of the specimens at a temperature of 25 °C. The hydraulic pressure for four specimens in thermo-hydraulic tests was 600 kPa, whereas a nominal water pressure of 5 kPa was considered for one test. The duration of the tests varied from 90 to 300 days (i.e., 3 to 10 months). The temperature and relative humidity were measured along the length of the compacted bentonite specimens, whereas the axial stress was measured at the opposite end of the heat source (i.e., from the hydration end).

Following the termination of the tests the bentonite specimens were dissected into smaller samples (i.e, slices of 20 mm thick). The samples were further used for determining the dry density, water content, and degree of saturation. The potential mineralogical changes in the compacted bentonite was investigated with the X-ray diffraction technique. The Inductively Coupled Plasma Optical Emission Spectroscopy (ICP-OES) was used to measure the concentration of the cations in the bentonite samples.

Some of the findings from the current study concerning the moisture transfer from regions of a high temperature to a low temperature and studies of the mineralogical and ion changes confirm the findings reported in the past by various researchers. The findings from the current study further emphasizes several novel aspects including the impacts of a change in boundary conditions from thermal to thermo-hydraulic, and within each boundary conditions, a change in the temperature from 85 to 150 °C on the thermo-hydro-

mechanical response of compacted bentonites. The characteristics of thermal insulation on its potential influence on the thermo-hydro-mechanical response of compacted bentonites is brought out in detail.

Based on the test results from the investigation reported in this thesis, the following conclusions are drawn.

Influence of non-isothermal loading:

1. The applied thermal gradient caused a decrease in the water content, relative humidity and degree of saturation, and an increase in the dry density at distances closer to the heat source indicating that compacted bentonites specimens underwent a shrinkage process. Opposite trends were observed at distances away from the heat source (an increase in the water content, relative humidity and degree of saturation, and a decrease in the dry density) indicating that compacted bentonite specimens underwent a wetting process. These findings are associated with moisture diffusion from hotter to cooler regions on account of applied thermal gradient and condensation occurring at cooler regions. These findings are in agreement with studies reported by several researchers in the past.

2. Due to an applied thermal gradient, a rise in the temperature within compacted bentonites was found to be dependent upon the characteristics of the thermal insulation surrounding the compacted bentonites. A use of a thicker insulation during the tests reduced the heat emission from compacted bentonites and caused an increase in the temperature, decrease in the relative humidity, and a decrease in the water absorption. A decrease in the relative humidity and water content in

this case is related to the thermodynamic effect at a constant water vapour since the vapour pressure in air decreases with an increase in the temperature.

3. Due to the applied thermal gradients, the axial stress increased and further decreased before attaining an equilibrium. The equilibrium axial stresses were found to be far smaller than the maximum axial stresses exhibited by the specimens. The development of maximum axial stress of different magnitudes, and similar axial stress for specimens at the equilibrium suggested that the equilibrium axial stress was independent of the applied thermal gradients under constant volume condition.

Influence of non-isothermal-hydraulic loading:

4. The applied thermo-hydraulic loading on a specimen with boundary temperatures 25 - 85 ℃ caused the increase of the water content and degree of saturation whereas the dry density and suction decreased. The findings come into an agreement with the studies performed from other researchers.

5. Comparing applied thermal and thermo-hydraulic loadings at same temperature (85 or 150 °C), the results showed that the applied thermo-hydraulic loadings reduced the drying effects at and near the heat source accompanied by an overall increase in the water content within compacted bentonites. A large portion of bentonite underwent the wetting process. At the same applied temperature (85 or 150 °C), the temperature profile did not alter significantly, whereas there was an overall increase in the relative humidity. A significant increase in the axial stress occurred due to a primarily increase

of the water content; however, the impact of higher applied temperature and water injection pressure did not significantly affect the magnitude of the axial stress in equilibrium.

6. Three equations for the temperature and relative humidity profiles derived from the experimental results of the non-isothermal and non-isothermal hydraulic tests. These equations used to model a previous work with similar boundary conditions and found similar profiles with those documented in the literature.

Influence of thermal and thermo-hydraulic loadings on mineralogy:

7. The conditions of the samples prior to the XRD tests influenced the basal spacing. The applied thermal and thermo-hydraulic gradients were found to cause dehydration (towards the hotter regions) and hydration (towards the cooler regions) of the interlayers as indicated by a decrease or an increase in the basal spacing of the mineral montmorillonite. A variation of the basal spacing (*c*-axis spacing) was found to be different for thermal and thermo-hydraulic loading conditions. The test results clearly showed that variations of the basal spacing was due primarily to the redistribution of water within compacted bentonites and no mineralogical phase changes took place for the maximum duration of the tests considered in this study (10 months).

8. Due to applied thermal and thermo-hydraulic gradients, a variation in the cations concentrations was noted, particularly near the heat source. However, any specific trend for the changes in the ion concentration for thermal and thermo-hydraulic loadings was inconclusive.

Suggestions for Further Works.

- Since there is a limited amount of studies in the literature for temperatures above the 100 °C it would be beneficial to replicate the tests conducted at 150 °C. It would be very useful to investigate whether tests running for longer periods could show any differences in the profiles.

- Another aspect that would be beneficial to be investigated is the radial swelling pressure generated from the expansion of the specimen. Also in the same terms it would be very interesting to capture in real time the potential shrinkage of the bentonite specimen during the heating period.

- The equations and generally the results derived from this study can be used to improve/optimize various existing numerical models that are used to study the coupled thermo-hydro-mechanical and chemical behaviour of unsaturated soils from research groups all around the globe.

- Finally large scale tests should be conducted to see how a buffer material reacts in real life conditions. As can be seen in section 2.7 there are several facilities around the world that can host a real size tests either in underground laboratories built in rock formations or in laboratories that use large scale equipment.

REFERENCES

Åkesson, M., Jacinto, A. C., Gatabin, C., Sanchez, M. and Ledesma, A. (2009). Bentonite THM behaviour at high temperatures: Experimental and numerical analysis. Geotechnique, 59(4), 307-318.

Al-Mukhtar, M., Qi, Y., Alcover, J.-F. and Bergaya, F. (1999). Oedometric and water-retention behaviour of highly compacted unsaturated smectites. Canadian Geotechnical Journal, 36(4), 675-684.

Alther, G. (2004). Some practical observations on the use of bentonite. Environmental & Engineering Geoscience, 10(4), 347-359.

Andrini, L., Toja, R. M., Gauna, M., Conconi, M., Requejo, F. and Rendtorff, N. (2017). Extended and local structural characterization of a natural and 800° C fired Na-montmorillonite–Patagonian bentonite by XRD and Al/Si XANES. Applied Clay Science, 137, 233-240.

ASTM-D (4943-08-2008). 4943-08-2008. Standard test methods for shrinkage factors of soils by the wax method. .

Bag, R. (2011). Coupled Thermo-Hydro-Mechanical-Chemical Behaviour Of MX80 Bentonite In Geotechnical Applications.Geoenvironmental Research Centre, Cardiff School of Engineering

Baille, W., Tripathy, S. and Schanz, T. (2010). Swelling pressures and one-dimensional compressibility behaviour of bentonite at large pressures. Applied Clay Science, 48(3), 324-333.

Bear, J. and Gilman, A. (1995). Migration of salts in the unsaturated zone caused by heating. Transport in porous media, 19(2), 139-156.

Birgersson, M. and Karnland, O. (2014). Flow and pressure repsonse in compacted bentonite due to external fluid pressure, SKB TR-14-28, Svensk kärnbränslehantering AB.

Bolt, G. (1956). Physico-chemical analysis of the compressibility of pure clays. Geotechnique, 6(2), 86-93.

Börgesson, L., Chijimatsu, M., Fujita, T., Nguyen, T., Rutqvist, J. and Jing, L. (2001). Thermo-hydro-mechanical characterisation of a bentonite-based buffer material by laboratory tests and numerical back analyses. International Journal of Rock Mechanics and Mining Sciences, 38(1), 95-104.

Bradbury, M. H. and Baeyens, B. (2003). Porewater chemistry in compacted re-saturated MX-80 bentonite. Journal of Contaminant Hydrology, 61(1), 329-338.

BS1377-2 (1990). Soils for civil engineering purposes. Part 2: Classification tests. British Standards Institution.

Bucher, F. and Müller-Vonmoos, M. (1989). Bentonite as a containment barrier for the disposal of highly radioactive wastes. Applied Clay Science, 4(2), 157-177.

Buil, B., Gómez, P., Peña, J., Garralón, A., Turrero, M., Escribano, A., Sánchez, L. and Durán, J. (2010). Modelling of bentonite–granite solutes transfer from an in situ full-scale experiment to simulate a deep geological repository (Grimsel Test Site, Switzerland). Applied Geochemistry, 25(12), 1797-1804.

Castellanos, E., Villar, M., Romero, E., Lloret, A. and Gens, A. (2008). Chemical impact on the hydro-mechanical behaviour of high-density FEBEX bentonite. Physics and Chemistry of the Earth, Parts A/B/C, 33, S516-S526.

Cho, W.J., Lee, J.O., Kwon, S., (2010) Analysis of thermo–hydro–mechanical process in the engineered barrier system of a high-level waste repository. Nuclear Engineering and Design.;240(6):1688-98.

Cleall, P., Seetharam, S. and Thomas, H. (2007). Inclusion of some aspects of chemical behavior of unsaturated soil in thermo/hydro/chemical/mechanical models. I: Model development. Journal of engineering mechanics, 133(3), 338-347.

Cleall, P. J., Singh, R. M. and Thomas, H. R. (2011). Non-isothermal moisture movement in unsaturated kaolin: an experimental and theoretical investigation.

Couture, R. A. (1985). Steam rapidly reduces the swelling capacity of bentonite. Nature, 318(6041), 50-52.

Cuevas, J., Villar, M., Martın, M., Cobena, J. and Leguey, S. (2002). Thermo-hydraulic gradients on bentonite: distribution of soluble salts, microstructure and modification of the hydraulic and mechanical behaviour. Applied Clay Science, 22(1), 25-38.

Delage, P., Howat, M. D. and Cui, Y. J. (1998). The relationship between suction and swelling properties in a heavily compacted unsaturated clay. Engineering Geology, 50(1-2), 31-48.

Delage, P., Marcial, D., Cui, Y. J. and Ruiz, X. (2006). Ageing effects in a compacted bentonite: a microstructure approach.

Dixon, D. A., Chandler, N, Graham, J. and Gray, M. N. (2002) Two large-scale sealing tests conducted at Atomic Energy of Canada's underground research laboratory: the buffer-container experiment and the isothermal test. Canadian Geotechnical Journal, 2002, 39:503-518.

Dixon, D. A., Graham, J. and Gray, M. N. (1999). Hydraulic conductivity of clays in confined tests under low hydraulic gradients. Canadian Geotechnical Journal, 36(5), 815-825.

Dohrmann, R. and Kaufhold, S. (2014). Cation Exchange and Mineral Reactions Observed in Mx 80 Buffer Samples of the Prototype Repository in Situ Experiment in Äspö, Sweden. Clays and Clay Minerals, 62(5), 357-373.

Dueck, A., & Nilsson, Ulf (2010). Thermo-Hydro-Mechanical properties of MX-80 Results from advanced laboratory tests. Sweden.

Ewen, J. and Thomas, H. (1987). The thermal probe—a new method and its use on an unsaturated sand. Geotechnique, 37(1), 91-105.

Ewen, J. and Thomas, H. (1989). Heating unsaturated medium sand. Geotechnique, 39(3), 455-470.

Fernández, A. M., Baeyens, B., Bradbury, M. and Rivas, P. (2004). Analysis of the porewater chemical composition of a Spanish compacted bentonite used in an engineered barrier. Physics and Chemistry of the Earth, Parts A/B/C, 29(1), 105-118.

Fernandez, A. M., Melon, A., Sanchez-Ledesma, D. M., Villar, M. V. and Cuevas, J. (2012). Lessons learned from the Febex in situ test: modifications at cation exchange positions by effect of a thermo-hydraulic gradient and the bentonite pore water.

Fernández, A. M. and Villar, M. V. (2010). Geochemical behaviour of a bentonite barrier in the laboratory after up to 8 years of heating and hydration. Applied Geochemistry, 25(6), 809-824.

Fernández, R., Torres, E., Ruiz, A. I., Cuevas, J., Alonso, M. C., García Calvo, J. L., Rodríguez, E. and Turrero, M. J. (2017). Interaction processes at the concrete-bentonite interface after 13 years of FEBEX-Plug operation. Part II: Bentonite contact. Physics and Chemistry of the Earth, Parts A/B/C.

Fredlund, D. G., Rahardjo, H. and Fredlund, M. D. (2012). Unsaturated soil mechanics in engineering practice. John Wiley & Sons,

Gatabin, C. and Billaud, P. (2005). Bentonite THM mock up experiments. Sensor data report. CEA, Report NT-DPC/SCCME 05-300-A.

Gens, A. and Alonso, E. (1992). A framework for the behaviour of unsaturated expansive clays. Canadian Geotechnical Journal, 29(6), 1013-1032.

Gens, A., Sánchez, M., Guimarães, L. D. N., Alonso, E. E., Lloret, A., Olivella, S., Villar, M. V. and Huertas, F. (2009). A full-scale in situ heating test for high-level nuclear waste disposal: Observations, analysis and interpretation. Geotechnique, 59(4), 377-399.

Goebel, I., Alheid, H. J., & Jockwer, N. (2006).Heater Experiment: Rock and bentonite Thermo-Hydro-Mechanical (THM) processes in the near field of a thermal source for development of deep underground high level radioactive waste repositories, EC report, 5th Euratom Framework Programme (1998–2002). Project FIS5-2001-00024.

Gens Solé, A., Vaunat, J., Garitte, B. and Wileveau, Y. (2007). In situ behaviour of a stiff layered clay subject to thermal loading: observations and interpretation. Géotechnique, 57(2), 207-228.

Gómez-Espina, R. and Villar, M. V. (2010). Geochemical and mineralogical changes in compacted MX-80 bentonite submitted to heat and water gradients. Applied Clay Science, 47(3-4), 400-408.

Gómez-Espina, R. and Villar, M. V. (2015). Effects of heat and humidity gradients on MX-80 bentonite geochemistry and mineralogy. Applied Clay Science, 109–110, 39-48.

Grim, R. E. (1968). Clay mineralogy. 2nd, McGraw - Hill, New York.

Grim, R. E. and Guven, N. (2011). Bentonites: geology, mineralogy, properties and uses. Elsevier,

Gurr, C., Marshall, T. and Hutton, J. (1952). Movement of water in soil due to a temeprature gradient. Soil Science, 74(5), 335-346.

Heilman, M., Carter, D. and Gonzalez, C. (1965). The Ethylene Glycol Monoethyl Ether (EGME) technique for determining soil-surface area. Soil Science, 100(6), 409-413.

Inoue, A. (1995). Formation of clay minerals in hydrothermal environments. Origin and mineralogy of clays, Springer: 268-329.

Karnland, O., Olsson, S., Nilsson, U. and Sellin, P. (2007). Experimentally determined swelling pressures and geochemical interactions of compacted Wyoming bentonite with

highly alkaline solutions. Physics and Chemistry of the Earth, Parts A/B/C, 32(1), 275-286.

Kaufhold, S., Stührenberg, D. and Dohrmann, R. (2009). Water redistribution between bentonite and salt at elevated temperature. Applied Clay Science, 46(3), 245-250.

Klute, A. (1986). Methods of soil analysis. Part 1. Physical and mineralogical methods. American Society of Agronomy, Inc.,

Komine, H., Yasuhara, K. and Murakami, S. (2009). Swelling characteristics of bentonites in artificial seawater. Canadian Geotechnical Journal, 46(2), 177-189.

Kozaki, T., Inada, K., Sato, S. and Ohashi, H. (2001). Diffusion mechanism of chloride ions in sodium montmorillonite. Journal of Contaminant Hydrology, 47(2–4), 159-170.

Laird, D. A. (2006). Influence of layer charge on swelling of smectites. Applied Clay Science, 34(1), 74-87.

Lee, O. J., Birch, K., Choi, J. H. (2014) Coupled thermal-hydro analysis of unsaturated buffer and backfill in a high-level waste repository, Annals of Nuclear Energy, Volume 72, 2014, Pages 63-75,ISSN 0306-4549

Li, X. L., Bastiaens, W., Van Marcke, P., Verstricht, J., Chen, G. J.,Weetjens, E., Sillen, X. (2010) Design and development of large-scale in-situ PRACLAY heater test and horizontal high-level radioactive waste disposal gallery seal test in Belgian HADES, Journal of Rock Mechanics and Geotechnical Engineering, Volume 2, Issue 2, Pages 103-110, ISSN 1674-7755,

Lloret, A. and Villar, M. V. (2007). Advances on the knowledge of the thermo-hydro-mechanical behaviour of heavily compacted "FEBEX" bentonite. Physics and Chemistry of the Earth, Parts A/B/C, 32(8–14), 701-715.

Lloret Morancho, A., Villar, M. V., Sanchez, M., Gens Solé, A., Pintado Llurba, X. and Alonso Pérez de Agreda, E. (2003). Mechanical behaviour of heavily compacted bentonite under high suction changes.

Lu, N. and Likos, W. J. (2004). Unsaturated soil mechanics. J. Wiley,

Madsen, F. (1998). Clay mineralogical investigations related to nuclear waste disposal. Clay Minerals, 33(1), 109-129.

Marcial, D., Delage, P. and Cui, Y. J. (2002). On the high stress compression of bentonites. Canadian Geotechnical Journal, 39(4), 812-820.

Martın, M., Cuevas, J. and Leguey, S. (2000). Diffusion of soluble salts under a temperature gradient after the hydration of compacted bentonite. Applied clay science, 17(1), 55-70.

Mesri, G. and Olson, R. E. (1971). Consolidation characteristics of montmorillonite. Geotechnique, 21(4), 341-352.

Mishra, M., Schanz, T. and Tripathy, S. (2008). A column device to study THM behaviour of expansive soils. 12th International Conference of International Association for Computer Methods and Advances in Geomechanics, Citeseer.

Mitchell, J. K. (1993). Fundamentals of Soil Behaviour. 2nd edition, John Wiley, New York.

Mitchell, J. K. and Soga, K. (2005). Fundamentals of soil behavior. 3rd edition, John Wiley, New York.

Montes-h, G., Duplay, J., Martinez, L. and Mendoza, C. (2003). Swelling–shrinkage kinetics of MX80 bentonite. Applied Clay Science, 22(6), 279-293.

Montes-Hernandez, G., Duplay, J., Géraud, Y. and Martinez, L. (2006). Several textural properties of compacted and cation-exchanged bentonite. Journal of Physics and Chemistry of Solids, 67(8), 1769-1774.

Nagaraj, T. and Murthy, B. S. (1985). Prediction of the preconsolidation pressure and recompression index of soils. Geotechnical Testing Journal, 8(4), 199-203.

Nassar, I. and Horton, R. (1989). Water transport in unsaturated nonisothermal salty soil: I. Experimental results. Soil Science Society of America Journal, 53(5), 1323-1329.

Olphen, H. V. (1977). An introduction to clay colloid chemistry, for clay technologists, geologists, and soil scientists. An introduction to clay colloid chemistry, for clay technologists, geologists, and soil scientists.,(2nd edition).

Oscarson, D. and Dixon, D. (1990). Effect of heating unsaturated bentonite on the swelling and hydraulic properties of subsequently saturated clay. Proceedings of the Annual Conference and 1st Biennial Environmental Speciality Conference of the Canadian Society of Civil Engineering, Hamilton, Ontario.

Pintado, X., Ledesma, A. and Lloret, A. (2002). Backanalysis of thermohydraulic bentonite properties from laboratory tests. Engineering Geology, 64(2), 91-115.

Pusch, R. (1980). Swelling pressure of highly compacted bentonite, SKB Technical report. TR-80-13.

Pusch, R. (1982). Mineral–water interactions and their influence on the physical behavior of highly compacted Na bentonite. Canadian Geotechnical Journal, 19(3), 381-387.

Pusch, R. (2000). On the effect of hot water vapor on MX-80 clay. SKB,

Pusch, R. (2001). The microstructure of MX-80 clay with respect to its bulk physical properties under different environmental conditions. SKB,

Pusch, R., Bluemling, P. and Johnson, L. (2003). Performance of strongly compressed MX-80 pellets under repository-like conditions. Applied Clay Science, 23(1–4), 239-244.

Pusch, R., Drawrite, A. B., Yong, R. N. and Nakano, M. (2010). Stiffening of smectite buffer clay by hydrothermal effects. Engineering Geology, 116(1–2), 21-31.

Pusch, R., Karnland, O. and Hökmark, H. (1990). GMM-a general microstructural model for qualitative and quantitative studies of smectite clays, Swedish Nuclear Fuel and Waste Management Co.

Pusch, R., Karnland, O., Lajudie, A. and Atabek, R. (1991). Hydrothermal Field Experiment Simulating Steel Canister Embedded in Expansive Clay-Physical Behavior of the Clay. MRS Proceedings, Cambridge Univ Press.

Pusch, R., Kasbohm, J. and Thao, H. T. M. (2010). Chemical stability of montmorillonite buffer clay under repository-like conditions—A synthesis of relevant experimental data. Applied Clay Science, 47(1–2), 113-119.

Pusch, R. and Yong, R. N. (2006). Microstructure of smectite clays and engineering performance. CRC Press,

Pytte, A., (1982). The kinetics of the smectite to illite reaction in contact metamorphic shales. M.A. thesis, Dartmouth College, 78 pp.

R Bag, S. T. H. R. T. (2010). Behaviour of compacted MX80 bentonite under thermo-hydraulic gradients. Proceedings of the Sixth International Congress on Environmental Geotechnics. Sixth International Congress on Environmental Geotechnics , 8-12 November 2010, Delhi, India, http://www.6iceg.org/.

Romero, E., Gens, A. and Lloret, A. (2003). Suction effects on a compacted clay under non-isothermal conditions. Géotechnique, 53(1), 65-81.

Saiyouri, N., Hicher, P. Y. and Tessier, D. (2000). Microstructural approach and transfer water modelling in highly compacted unsaturated swelling clays. Mechanics of Cohesive-Frictional Materials, 5(1), 41-60.

Samper, J., Juncosa, R., Navarro, V., Delgado, J., Montenegro, L. and Vázquez, A. (2000). Coupled Thermo-Hydro-Geochemical Models of Engineered Barrier Systems: The Febex Project. MRS Proceedings, Cambridge Univ Press.

Samper, J., Zheng, L., Montenegro, L., Fernández, A. M. and Rivas, P. (2008). Coupled thermo-hydro-chemical models of compacted bentonite after FEBEX in situ test. Applied Geochemistry, 23(5), 1186-1201.

Schanz, T., Khan, M. I. and Al-Badran, Y. (2013). An alternative approach for the use of DDL theory to estimate the swelling pressure of bentonites. Applied Clay Science, 83–84(0), 383-390.

Schanz, T., Nguyen-Tuan, L. and Datcheva, M. (2013). A Column Experiment to Study the Thermo-Hydro-Mechanical Behaviour of Expansive Soils. Rock Mechanics and Rock Engineering, 46(6), 1287-1301.

Schanz, T. and Tripathy, S. (2005). Soil-water characteristic curves of clays from physico-chemical concepts.

Schanz, T. and Tripathy, S. (2009). Swelling pressure of a divalent-rich bentonite: Diffuse double-layer theory revisited. Water Resources Research, 45(5).

Shainberg, I. and Kemper, W. (1966). Electrostatic forces between clay and cations as calculated and inferred from electrical conductivity. Clays & Clay Minerals Conference Proc.

Singh, R. M. (2007). An experimental and numerical investigation of heat and mass movement in unsaturated clays.School of Engineering, Cardiff University

Sparks, D. L., Page, A., Helmke, P., Loeppert, R., Soltanpour, P., Tabatabai, M., Johnston, C. and Sumner, M. (1996). Methods of soil analysis. Part 3-Chemical methods. Soil Science Society of America Inc.,

Sridharan, A., Rao, A. S. and Sivapullaiah, P. V. (1986). Swelling pressure of clays. ASTM Geotechnical Testing Journal, 9(1), 24-33.

Sun, D. a., Cui, H. and Sun, W. (2009). Swelling of compacted sand–bentonite mixtures. Applied Clay Science, 43(3), 485-492.

Swartzen-Allen, S. L. and Matijevic, E. (1974). Surface and colloid chemistry of clays. Chemical Reviews, 74(3), 385-400.

Tang, A.-M., Cui, Y.-J. and Le, T.-T. (2008). A study on the thermal conductivity of compacted bentonites. Applied Clay Science, 41(3–4), 181-189.

Thomas, H., Rees, S. and Sloper, N. (1998). Three-dimensional heat, moisture and air transfer in unsaturated soils. International journal for numerical and analytical methods in geomechanics, 22(2), 75-95.

Thomas, H. R., Yang, H. T., He, Y. and Cleall, P. J. (2003). A multi-level parallelized substructuring-frontal solution for coupled thermo/hydro/mechanical problems in unsaturated soil. International Journal for Numerical and Analytical Methods in Geomechanics, 27(11), 951-965.

Tripathy, S., Bag, R. and Thomas, H. R. (2015). Enhanced isothermal effect on swelling pressure of compacted MX80 bentonite. Engineering Geology for Society and Territory-Volume 6, Springer: 537-539.

Tripathy, S., Kessler, W. and Schanz, T. (2006). Determination of interparticle repulsive pressures in clays. Unsaturated Soils 2006: 2198-2209.

Tripathy, S. and Schanz, T. (2007). Compressibility behaviour of clays at large pressures. Canadian Geotechnical Journal, 44(3), 355-362.

Tripathy, S., Sridharan, A. and Schanz, T. (2004). Swelling pressures of compacted bentonites from diffuse double layer theory. Canadian Geotechnical Journal, 41(3), 437-450.

Tripathy, S., Thomas, H. R. and Bag, R. (2015). Geoenvironmental Application of Bentonites in Underground Disposal of Nuclear Waste: Characterization and Laboratory Tests. Journal of Hazardous, Toxic, and Radioactive Waste, D4015002.

Tripathy, S., Thomas, H. R. and Stratos, P. (2017). Response of Compacted Bentonites to Thermal and Themo-Hydraulic Loadings at High Temperatures. Geosciences 7 (3) , 53

Tsang, C.F., Barnichon, J.D., Birkholzer, J., Li, X.L., Liu, H.H., Sillen, X. (2012) Coupled thermo-hydro-mechanical processes in the near field of a high-level radioactive

waste repository in clay formations, international Journal of Rock Mechanics and Mining Sciences, Volume 49, 2012, Pages 31-44, ISSN 1365-1609

Ulery, A. L. and Drees, L. R. (2008). Methods of soil analysis: mineralogical methods. ASA-CSSA-SSSA,

Villar, M. V., Cuevas, J. and Martín, P. L. (1996). Effects of heat/water flow interaction on compacted bentonite: Preliminary results. Engineering Geology, 41(1–4), 257-267.

Villar, M. V., Fernández, A. M., Martín, P. L., Barcala, J. M., Gómez-Espina, R. and Rivas, P. (2008). Effect of Heating/Hydratation on Compacted Bentonite: Tests in 60-cm Long Cells, Centro de Investigaciones Energeticas Medioambientales y Tecnologicas (CIEMAT), Madrid (Spain).

Villar, M. V., García-Siñeriz, J. L., Bárcena, I. and Lloret, A. (2005). State of the bentonite barrier after five years operation of an in situ test simulating a high level radioactive waste repository. Engineering Geology, 80(3–4), 175-198.

Villar, M. V. and Gómez-Espina, R. (2008). Effect of temperature on the water retention capacity of FEBEX and MX-80 bentonites.

Villar, M. V., Gómez-Espina, R., Martín, P. L. and Barcala, J. M. (2013). Tests in Thermo-Hydraulic Cells to Simulate the Behavior of Engineered Barriers. Multiphysical Testing of Soils and Shales, Springer: 137-142.

Villar, M. V. and Lloret, A. (2004). Influence of temperature on the hydro-mechanical behaviour of a compacted bentonite. Applied Clay Science, 26(1–4), 337-350.

Villar, M. V. and Lloret, A. (2007). Dismantling of the first section of the FEBEX in situ test: THM laboratory tests on the bentonite blocks retrieved. Physics and Chemistry of the Earth, Parts A/B/C, 32(8–14), 716-729.

Villar, M. V. and Lloret, A. (2008). Influence of dry density and water content on the swelling of a compacted bentonite. Applied Clay Science, 39(1–2), 38-49.

Villar, M. V., Martín, P. L. and Barcala, J. M. (2005). Modification of physical, mechanical and hydraulic properties of bentonite by thermo-hydraulic gradients. Engineering Geology, 81(3), 284-297.

Villar, M.V.; Martin, P.L.; Bárcena, J.L, García-Siñeriz, R., Gómez-Espina, and Lloret, A (2012) Long-term experimental evidences of saturation of compacted bentonite under repository conditions, Engineering Geology, Volumes 149–150, 2012, Pages 57-69, ISSN0013-7952,

Villar, M.V.; Martin, P.L.; Romero, F.J (2014). Long-Term THM Tests Reports: THM Cells for the HE-E Test: Update of Results until February; CIEMAT Technical Report CIEMAT/DMA/2G210/03/2014, Long-Term Performance of Engineered Barrier Systems PEBS; CIEMAT: Madrid, Spain, 2014: 7 March 2014

Villar, M. V., Sánchez, M. and Gens, A. (2008). Behaviour of a bentonite barrier in the laboratory: Experimental results up to 8 years and numerical simulation. Physics and Chemistry of the Earth, Parts A/B/C, 33, Supplement 1(0), S476-S485.

Wang, M., Benway, J. M. and Arayssi, A. M. (1990). The effect of heating on engineering properties of clays. Physico-Chemical Aspects of Soil and Related Materials, ASTM International.

Wersin, P., Johnson, L. H. and McKinley, I. G. (2007). Performance of the bentonite barrier at temperatures beyond 100°C: A critical review. Physics and Chemistry of the Earth, Parts A/B/C, 32(8–14), 780-788.

Yong, R. (1999). Soil suction and soil-water potentials in swelling clays in engineered clay barriers. Engineering geology, 54(1), 3-13.